# Design of Experiments Optimization of *N*-acyl and *N*-alkyl Chitosan Synthesis and Application Investigations

Vivien Nagy

Thesis for the Degree of Philosophiae Doctor

December 2024

School of Health Sciences

FACULTY OF PHARMACEUTICAL SCIENCES

UNIVERSITY OF ICELAND

# Design of Experiments Optimization of *N*-acyl and *N*-alkyl Chitosan Synthesis and Application Investigations

Vivien Nagy

Thesis for the Degree of Philosophiae Doctor

Supervisor

Már Másson

Doctoral committee

Bergþóra Sigríður Snorradóttir
Christiaan Petrus Richter
Elvar Örn Viktorsson
Hélène Liette Lauzon

December 2024

School of Health Sciences
FACULTY OF PHARMACEUTICAL SCIENCES
UNIVERSITY OF ICELAND

# Hámörkun efnasmíða N-asýl og N-alkýl-kítósans og rannsóknir á notkun þeirra

Vivien Nagy

Ritgerð til doktorsgráðu

Leiðbeinandi

Már Másson

Doktorsnefnd

Bergþóra Sigríður Snorradóttir

Christiaan Petrus Richter
Elvar Örn Viktorsson
Hélène Liette Lauzon

Desember 2024

Heilbrigðisvísindasvið
LYFJAFRÆÐIDEILD
HÁSKÓLI ÍSLANDS

ISBN 978-9935-9689-5-1

ORCID: 0000-0002-4715-3106

Reykjavik, Iceland 2024

| | |
|---|---|
| Supervisor | Professor Már Másson<br>Faculty of Pharmaceutical Sciences<br>School of Health Sciences<br>University of Iceland |
| Doctoral Committee Members | Assistant Professor Bergþóra Sigríður Snorradóttir<br>Faculty of Pharmaceutical Sciences<br>School of Health Sciences<br>University of Iceland |
| | Professor Christiaan Petrus Richter<br>Faculty of Industrial Engineering, Mechanical Engineering and Computer Science |
| | Assistant Professor Elvar Örn Viktorsson<br>Faculty of Pharmaceutical Sciences<br>School of Health Sciences<br>University of Iceland |
| | Dr. Hélène Liette Lauzon<br>Director of Research & Development<br>Primex ehf., Iceland |
| Opponents | Dr. Luminita Marin<br>Head of Department at Petru Poni Institute of Macromolecular Chemistry<br>Iaşi, Romania |
| | Dr. Ögmundur Viðar Rúnarsson<br>Quality Control Manager<br>Alvotech, Iceland |

# Abstract

Chitosan, a biopolymer with broad applications, is valued for its antimicrobial, non-toxic, biocompatible, and biodegradable properties, making it particularly useful in healthcare. Chitosan derivatives, which have better solubility and enhanced properties, have been a key area of research. This thesis focuses on developing scalable and efficient processes for synthesizing *N*-alkyl and *N*-acyl chitosan derivatives and conjugates, using a Design of Experiments (DoE) approach to optimize the degree of substitution (DS) and improve biological properties for pharmaceutical and other medical applications.

For the synthesis of *N*,*N*,*N*-trimethyl chitosan (TMC), eight experimental designs were conducted, including sequential, fractional, and full factorial designs. Key parameters, such as alkylating agents, bases, molar ratios, solvents, temperature, base addition (BA) techniques, and reaction times were optimized. A one-step method for TMC synthesis was developed, achieving high degrees of trimethylation (DTM) without *O*-methylation. To manage viscosity issues, incremental BA and the introduction of a new base, *N*,*N*-diisopropylethylamine (DIPEA) were implemented. A new, low-viscosity method scalable for industrial production was established, yielding high DTM without *O*-methylation. Polyelectrolyte complex nanoparticles (NPs) were created using TMC and chondroitin sulfate. *In vitro* biocompatibility and cytotoxicity tests were conducted using human endothelial cells and ovarian cancer cell lines. The effects of DTM, molecular weight, and NP formation were studied.

The synthesis process of chitosan-hydroxycinnamic acid conjugates was investigated by performing analysis by DoE to a series of previously conducted experiments, that were analyzed manually at the time. Key factors were identified, and the biological properties of the conjugates, including antibacterial and antioxidant activities, were explored. The conjugates exhibited increasing antioxidant activity with increasing DS when using ferulic and caffeic acid. In contrast, the antibacterial activity against the tested pathogens decreased with increasing DS compared to unmodified chitosan.

Additionally, the synthesis of *N*-betaine chitosan was explored using HATU coupling, creating a simple, one-step process with high DS, avoiding the need for multistep synthesis. A full factorial design investigated the molar ratios of HATU and the base used in the reaction.

Overall, the work reported in this thesis developed a one-step synthesis method for TMC with up to 72% DTM, a selective synthesis of chitosan-hydroxycinnamic conjugates with DS up to 60%, and an efficient *N*-betaine chitosan synthesis method achieving up to 100% substitution. The DoE approach proved highly effective, offering a systematic way

to optimize chitosan derivative synthesis for improved pharmaceutical and medical applications.

Keywords:

Chitosan, *N,N,N*-trimethyl chitosan, *N*-betaine chitosan, Chitosan-hydroxycinnamic conjugates, Design of Experiments

# Ágrip

Kítósan er náttúruleg fjölliða með víðtækt notagildi. Hún er örveruhemjandi, óeitruð og hefur lífsamrýmanleika auk þess að vera niðurbrjótanleg. Þessir eiginleikar gera fjölliðuna áhugaverða til notkunar í lyfja- og læknisfræðilegum tilgangi. Rannsóknir á kítósani snúa að þróun afleiða með betri leysni sem og aðra betrumbætta eiginleika. Doktorsverkefnið fjallar um að þróa skilvirkar, hagkvæmar og uppskalanlegar aðferðir til að framleiða *N*-alkýl og *N*-asýl kítósan afleiður, með svokölluðum "Design of Experiments" (DoE) tilraunahönnnaraðferðum, og hámarka setni (e. *degree of substitution*; DS) fjölliðunnar ásamt því að betrumbæta líffræðilega eiginleika hennar með tilliti til notkunar í lyfja- og læknisfræði.

Fyrir efnasmíðar á *N*,*N*,*N*-trímetýlkítósan (TMC) voru framkvæmdar alls átta DOE tilraunir, annað hvort runubundnar, þrepaskiptar og fullþáttaðar hannanir. Lykilbreytur eins og alkýlerandi efni, basar, mólhlutföll, leysar, hitastig, aðferðir við bætingu basa, sem og hvarftímar voru hámarkaðar. Efnasmíð í einu skrefi fyrir TMC var þróuð með hárri setni af trímetýlhópum (e. *Degree of trimethylation*; DTM) án *O*-metýleringar. Til að bregðast við seigju vanda í hvörfum var notast við nýjan basa, *N,N*-díísóprópýletýlamín (DIPEA), með þrepaskiptri viðbætingu. Þessi nýja aðferð áætluð fyrir notkun á stærri iðnaðarskala gaf háar heimtur á DTM án *O*-metýleringar. Fjöljónanlegar fléttu nanóagnir(NPs) voru myndaðar á grunni TCM og kondríótín súlfats. *In vitro* prófanir á lífsamrýmandleika og frumudrepandi eituráhrifum voru framkvæmdar á mennskum þekjufrumum og krabbameinsfrumulínum með uppruna úr legi. Rannsökuð voru áhrif DTM, mólþyngdar og myndun NPs.

DoE greining fyrir röð áður framkvæmdra tilrauna á efnasmíðaferlum fyrir samtengdar kítósan-hýdroxýsinnamínsýru fjölliður var gerð. Borið var kennsl á lykilþætti ferlanna og líffræðilegir eiginleikar samtengdra fjölliða, þar á meðal andoxunar- og örveruhemjandi áhrif, voru rannsakaðir. Samböndin sýndu aukin andoxunaráhrif í samræmi við aukna setni þegar notast var við ferrulínsýru og kaffínsýru sethópa. Í samanburði minnkuðu örveruhemjandi áhrifin á þeim stofnum sem prófað var gegn með aukinni setni samanborið við óbreytt kítósan.

Einnig var framkvæmd efnasmíð á *N*-betaín kítósani með HATU miðluðu kúplunarhvarfi þar sem einfalt efnasmíðaferli var þróað með hárri setni í einu skrefi, án aðkomu verndarhópa. Fullþátta (e. *Full factorial*) hönnun var notuð til að rannsaka mólhlutföll HATU og þess basa sem notast var við í hvarfinu.

Í verkefninu var þróuð efnasmíð í einu skrefi fyrir TMC með allt að 72% DTM, sértæk efnasmíð á kítósan-hýdroxýsinnamínfjölliðum með allt að 60% DS sem og hagkvæm aðferð til efnasmíða á *N*-betaín kítósani með allt að 100% DS. DoE tilraunahönnun reyndist mjög árangursrík þar sem notast var við kerfisbundna leið til hámörkunar á smíði kítósan-afleiða með betrumbætta eiginleika fyrir notkun í lyfja- og læknisfræði.

Keywords:

Kítósan, *N,N,N*-trímetýlkítósan, *N*-betaín kítósan, kítósan-hýdroxýsinnamínsýruafleiður, hönnun tilrauna

# Acknowledgements

This study was performed at the Faculty of Pharmaceutical Sciences, School of Health Sciences, University of Iceland. Additional investigations were carried out at the Innovation Center of NanoMedicine (iCONM) in Kawasaki, Japan.

The research was funded by the University of Iceland Research Fund, the Rannis Student Innovation Fund, the Icelandic Research Fund (Rannis Grant No. 185188-053), the Icelandic Technology Development Fund as a part of the MariMed project (Rannis Grant No. 2112860-0611), the AVS Fund, and travel grants from the Scandinavia-Japan Sasakawa Fund, and the Watanabe Trust Fund. I received additional support from the Bergþóru og Þorsteins Scheving Thorsteinssonar Fund. These funds are gratefully acknowledged. The chitosan starting materials used in this study were kindly donated by Primex ehf. (Iceland).

I would like to express my sincere gratitude to all the people who have helped me on this journey. First and foremost, I would like to thank my supervisor, Prof. Már Másson, who has guided me since my MSc studies. He has been mentoring, teaching, and supporting me throughout all these years, always encouraging me, which has been a great motivation. I look forward to continuing my work with Prof. Már in the future, as we have established a joint startup company, Minamo.

I would like to thank the members of my doctoral committee Dr. Hélène Liette Lauzon, Dr. Elvar Örn Viktorsson, Dr. Bergþóra Sigríður Snorradóttir and Dr. Christiaan Petrus Richter for their support, insightful feedback, and valuable suggestions during my studies. Their guidance is greatly appreciated.

During my studies, I also had the opportunity to work at the Innovation Center of NanoMedicine (iCONM) in Kawasaki, Japan, under the supervision of Dr. Sabina Quader, in the laboratory of Prof. Kazunori Kataoka. I would like to thank them and everyone at iCONM for their support, guidance, and teaching me about Japanese culture.

I would also like to thank the co-authors of my research papers, Dr. Bergþóra Sigríður Snorradóttir, Dr. Hélène Liette Lauzon, Dr. Priyanka Sahariah, Dr. Sabina Quader, and Prof. Ásdís Hjálmarsdóttir for their help with the research as well as writing and editing. Furthermore, Dr. Sigríður Jónsdóttir for her help with NMR processing, Dr. Svetlana Solodova for the GPC training, and laboratory manager Árni Þorgrímur Kristjánsson for the technical support.

I would like to extend my gratitude to the Hagi students (past and present) Sankar, Amin, Sigga, Luca, Priyanka, Manisha, Alex, Maonian, Ellen, Goraksha, Oddny, Sebastian,

Erna, Suppakan, May, Ismael, Dagmar, Maia, Bria, Helena, Unnur, Natalia. I would also like to thank all faculty members: Solla, Inga, Guðrún, Unnur, Berglind, Elín Soffia, Palli, Helga, Freyja, Sveinbjörn, Lárus, Hákon, Arndís, Margret and Þorsteinn.

Finally, I would like to thank my family and friends for their patience and continuous support throughout these years. Special thanks to my feline friend Cosmo, who always enjoyed hearing about shrimp(-sourced chitosan).

# Contents

# List of Abbreviations

ACN: Acetonitrile
BA: Base addition
CCK-8: Cell Counting Kit-8
ChS: Chondroitin sulfate
COS: Chitooligosaccharide
DA: Degree of acetylation
DBN: 1,5-Diazabicyclo[4.3.0]non-5-ene
DBU: 1,8-Diazabicyclo[5.4.0]undec-7-ene
DCM: Dichloromethane
DD: Degree of deacetylation
DDM: Degree of *N,N*-dimethylation
DEA: *N,N*-Diethylaniline
DIPEA: *N,N*-Diisopropylethylamine
DLS: Dynamic light scattering
DMF: *N,N*-Dimethyl formamide
DMM: Degree of *N*-monomethylation
DMS: Dimethyl sulfate
DMSO: Dimethyl sulfoxide
DoE: Design of Experiments
DOM: Degree of *O*-methylation
DP: Degree of polymerization
DPPH: 2,2-Diphenyl-1-picrylhydrazyl
DQ: Degree of quaternization
DS: Degree of substitution
DtBP: 2,6-Di-*tert*-butylpyridine
DTM: Degree of *N,N,N*-trimethylation
EDC: 1-Ethyl-3-(3-dimethylaminopropyl) carbodiimide
EtOAc: Ethyl acetate
EtOH: Ethanol
FBS: Fetal bovine serum
FD: Factorial Design
GlcNAc: *N*-acetyl glucosamine
GPC: Gel permeation chromatography
HATU: 1-[Bis(dimethylamino)methylene]-1H-1,2,3-triazolo[4,5-b]pyridinium 3-oxid hexafluorophosphate)
HOBt: Hydroxybenzotriazole
HTCC: *N*-[(2-hydroxy-3-trimethyl ammonium) propyl] chitosan
HUVECs: Human umbilical vein endothelial cells
KOtBu: Potassium *tert*-butoxide
MeI: Methyl iodide
MIC: Minimum inhibitory concentration
MLC: Minimum lethal concentration
MLR: Multiple linear regression
MRSA: Methicillin-resistant *Staphylococcus aureus*
MSA: Methanesulfonic acid
Mw: Molecular weight
$M_w$: Weight-average molecular weight
N/A: Not applicable
NMP: *N*-methyl-pyrrolidone
NMR: Nuclear magnetic resonance
NPs: Nanoparticles
PBS: Phosphate-buffered saline
PDI: Polydispersity index
PLS: Partial least squares regression
RSD: Relative standard deviation
RT: Room temperature
TBDMS: *Tert*-Butyldimethylsilyl
TEA: Triethylamine
TFA: Trifluoroacetic acid
TMC: *N,N,N*-Trimethyl chitosan
UV: Ultraviolet

# List of Figures

# List of Schemes

# List of Tables

# List of Original Papers

This thesis is based on the following original publications*.

I. V. Nagy, B. S. Snorradóttir, H. L. Lauzon, M. Másson "Optimizing *N,N,N*-trimethyl chitosan synthesis: A design of experiments (DoE) approach" (*Carbohydrate Polymers,* 2024, 335, 122065)

II. V. Nagy, B. S. Snorradóttir, H. L. Lauzon, M. Másson "Design of Experiments optimization of *N,N,N*-trimethyl chitosan synthesis using *N,N*-diisopropylethylamine base" (*Carbohydrate Research*, 2024, 545, 109289)

III. V. Nagy, S. Quader, M. Másson "Fine-tuning the cytotoxicity profile of *N,N,N*-trimethyl chitosan through trimethylation, molecular weight, and polyelectrolyte complex nanoparticles" (*International Journal of Biological Macromolecules*, 2024, 281, Part 2, 135805)

IV. V. Nagy, P. Sahariah, M. Á. Hjálmarsdóttir, M. Másson "Chitosan-hydroxycinnamic acid conjugates: Optimization of the synthesis and investigation of the structure activity relationship" (*Carbohydrate Polymers*, 2021, 277, 118896)

* *The research papers are not presented in chronological order, but in a sequence that aligns with the progression presented in the thesis.*

List of other publications:

V. V. Nagy, M. Másson "Chitosan–Antioxidant Conjugates" (S. K. Kim (Editor) Encyclopedia of Marine Biotechnology 2, 2020, 1031-1050, Wiley) (book chapter)

# Declaration of Contribution

I hereby declare that the thesis entitled "Design of Experiments Optimization of *N*-acyl and *N*-alkyl Chitosan Synthesis and Application Investigations" submitted to obtain a Doctor of Philosophy degree has been based on work conducted in my PhD study at the Faculty of Pharmaceutical Sciences, University of Iceland. The project's central concept and general work plan were proposed by Prof. Már Másson (MM) at the Faculty of Pharmaceutical Sciences. Funding acquisition was done by MM.

The research was carried out in the period of 2019-2024. The main part of the research was carried out at the Faculty of Pharmaceutical Sciences, University of Iceland. Part of the research was carried out at the Innovation Center of NanoMedicine (iCONM) in Kawasaki, Japan.

NMR sample processing was conducted by Dr. Sigríður Jónsdóttir at the Science Institute, University of Iceland.

The aim of papers I&II was to optimize the synthesis process of *N,N,N*-trimethyl chitosan (TMC), using the Design of Experiments (DoE) method. The work was conceptualized by MM. The synthesis, experimental design, methodology, NMR characterization and formal analysis were done by me. The manuscripts were written by me and reviewed by all co-authors.

The aim of paper III was to investigate the cytotoxicity of TMC and TMC-chondroitin sulfate polyelectrolyte complex nanoparticles (NPs). The research was designed and supervised by MM and Dr. Sabina Quadar (SQ). The NP preparation and the cell studies were done at the iCONM in Kawasaki, Japan. The synthesis, the NP preparation, the GPC/SEC, and the NMR characterization were done by me. The *in vitro* cytotoxicity assays were done by me with supervision from SQ. The manuscript was written by me and reviewed by all co-authors.

The aim of paper IV was to synthesize hydroxycinnamic acid-chitosan conjugates and investigate their antibacterial and antioxidant properties. This research initially began as part of my MSc project at the University of Iceland, under the supervision of MM. Part of the results published in Paper I are reported in my MSc thesis entitled "*Chitosan-natural antioxidant conjugates: Synthesis, antimicrobial and antioxidant properties*". During my PhD studies, some data of the MSc research were re-analyzed. The antioxidant assay was revisited, and the data was re-fitted using Kaleidagraph software to obtain more accurate $EC_{50}$ values. Additionally, the manual DoE design used for synthesis optimization was input into MODDE software to gain a deeper understanding of the effects of different factors. The research was designed and supervised by MM. The synthesis, experimental design, analysis, the NMR characterization, and antioxidant assay were done by me. The antibacterial assay was done by me, supervised by Martha Á. Hjálmarsdóttir. The manuscript was written by me and reviewed by all co-authors.

The synthesis optimization of *N*-betaine chitosan was conducted as part of a collaborative research project with MSc. student Luca Protti (LP) from the University of Milano-Bicocca during his Erasmus visit to the University of Iceland. I carried out the preliminary experiments and their NMR characterization. The experimental designs, created using MODDE software, were also developed by me. LP conducted the syntheses according to these designs, as well as the NMR characterization of the resulting products. I was responsible for analyzing the experimental data from MODDE. These results have not yet been compiled into a manuscript, and we plan to by the end of 2024.

I have presented my research work at international conferences in Portugal, Japan, Iceland, Sweden and Austria. These travels were supported by travel grants provided by the University of Iceland Research Fund, the Scandinavia-Japan Sasakawa foundation and Watanabe Trust Fund.

During the preparation of this work, I used an AI tool, ChatGPT, to improve the grammar, syntax, and writing style of the text. Additionally, Figure 2 was generated by ChatGPT following my prompts. After using these tools, I reviewed and edited the content as needed and I take full responsibility for the content of this thesis.

Vivien Nagy

# 1 Introduction

## 1.1 Chitin and Chitosan

Chitin is the world's second most abundant biopolymer, following cellulose [1]. Chitin was first mentioned by the English scientist Charles Hachett, as a "*material particularly resistant to usual chemicals*" in the late 18th century reporting his experiments with crustacean shells [2]. Later, in the 19th century, the biopolymer was also discovered in fungal species by the French scientist, Henri Braconnot, who named the material "fungine" [3]. It was Auguste Odier, who first called the biopolymer "chitine" [4]. Chitin is a linear polymer, consisting of β-(1-4) linked *N*-acetyl glucosamine (GlcNAc) monomer units (Figure 1a). The structure is identical to cellulose, except that it has acetamido group (instead of hydroxyl) at the C-2 position. To date, chitin has been identified in the cell walls of fungi and yeast, in the exoskeleton of crustaceans and other arthropods, some sponge and squid species, and corals [5–7].

Chitosan is typically prepared from chitin by alkali *N*-deacetylation, resulting in randomly distributed GlcNAc and D-glucosamine monomer units linked through β-(1-4) glycosidic bonds (Figure 1b) [8]. In nature, chitosan is only found in some fungi (e.g. *Mucoraceae)* [9]. Chitosan contains three nucleophilic functional groups: a primary amino group at the C-2 position, a secondary hydroxyl group at the C-3 position, and a primary hydroxyl group at the C-6 position (Figure 1c).

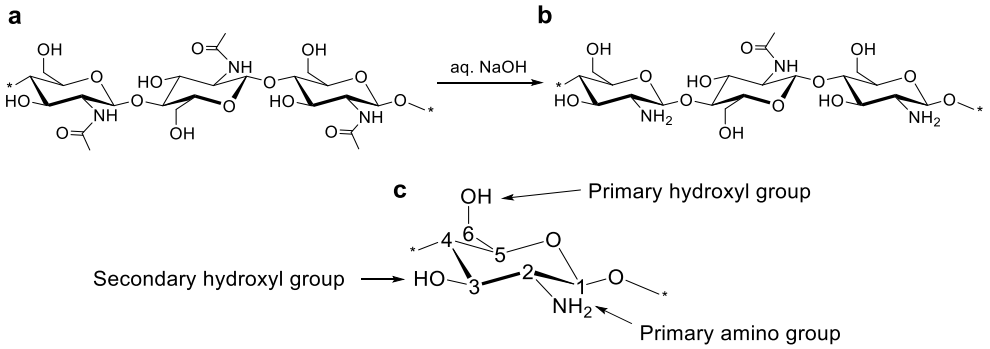


Figure 1. Chitin (a), chitosan (b), and the nucleophilic functional groups of chitosan (c).

The extent to which the chitosan monomers are deacetylated is expressed as the degree of deacetylation (DD). Alternatively, the term degree of acetylation (DA) is used to describe the average ratio of GlcNAc monomers in the polymer chain. While there is no commonly accepted definition, generally, the polymer is called chitosan, if the DA is below 30%. Above a DA of 30%, the polymer is considered to be chitin [10]. The DA

can be assessed using various techniques, such as titration, and Fourier-transform infrared spectroscopy (FT-IR). However, $^{1}$H NMR spectroscopy is widely regarded as the most precise and reliable method for determining the DA. A standard method for determining the DA of chitosan by $^{1}$H NMR spectroscopy has been reported by Lavertu *et al*. [11] and is approved by the American Society for Testing and Material International [12].

Chitosan is a highly valuable material owing to its wide range of beneficial properties, including biodegradability [13], biocompatibility [14], low toxicity [15,16], as well as its antibacterial [17], antifungal [18], anticancer [19] and mucoadhesive effects [20]. Furthermore, adsorption enhancing properties [21], wound healing [22,23], hemostatic [24], analgesic [25], and hypocholesterolemic [26] effects have been reported.

Whereas chitin is insoluble in most solvents and aqueous solutions, chitosan is soluble in an aqueous medium under acidic conditions (below pH 6), due to the protonation of its primary amino groups, resulting in a positively charged, water-soluble polyelectrolyte. This also means that the solubility is directly influenced by the DA. The solubility generally improves with an increase in the number of free amino groups; however, if the DD is too high, the material may become highly crystalline, rendering it insoluble [27]. The solubility and thus, subsequently the biological activities of chitosan are also influenced by the method of deacetylation used, the pattern of acetylation, the degree of polymerization, the polydispersity and the molecular weight (Mw) [8,28]. For chitosan to exhibit its biological properties, aqueous solubility is usually essential.

While there is no universal definition of chitosan Mw ranges, chitosan can be categorized as high Mw chitosan (>150 kDa), medium Mw chitosan (50-150 kDa), low Mw chitosan (<50 kDa) and chitooligosaccharides (COS, <10 kDa) [29]. The water-solubility improves with decreasing Mw [30]. There are various methods available for measuring the Mw of chitosan, including gel permeation chromatography (GPC), which is often also called size exclusion chromatography (SEC), and viscometry. These methods are interconnected through the Mark-Houwink-Sakurada equation, which states that the intrinsic viscosity of a polymer-solvent system at a given temperature is proportional to the Mw of the polymer. Viscosity measurements alone typically yield the viscosity-average molecular weight ($M_v$), providing limited insight compared to other methods like GPC, which gives a more comprehensive molecular weight distribution [31]. Unlike viscometry, where the average molecular weight is only based on how the polymer chains affect the viscosity of the solution, GPC distinguishes between different molecular weight fractions, enabling the calculation of number-average molecular weight ($M_n$), weight-average molecular weight ($M_w$), and the polydispersity index (PDI). $M_n$ is calculated from the mole fraction distribution of different sized molecules in a sample. $M_w$ takes into account both the size and mass of the polymer chains, with larger chains contributing more to the overall weight. $M_w$ is calculated from the weight fraction distribution of different sized molecules. The dispersity (or PDI) is a measure of the distribution of molecular weight in a polymer

sample. It is defined as the ratio of the $M_w$ to the $M_n$. The PDI value close to 1 indicates a narrow molecular weight distribution (monodisperse), while higher values indicate a broader distribution (polydisperse). Polymers with higher PDI values have more variation in chain length, affecting their physical properties.

Chitosan with varying chemical structures can be prepared by adjusting the reaction time, temperature, and concentration of the alkaline solution used in the deacetylation process. Chitin can be found in fungal and animal species [32]. The primary commercial sources for chitin are the exoskeletons of crustaceans, primarily shrimp and crab shells, which are the waste products of the food industry [33]. Recently, there has been increasing attention toward the production of chitosan from fungal [34] and insect sources [35].

Crustacean shell waste contains proteins (30-40%), calcium carbonate (30-50%), and chitin (20-30%), which is extracted through acid and alkaline treatments. This process often requires demineralization due to the high calcium carbonate content and the conversion of chitin to chitosan involves using a high alkali concentration under high heat, posing an environmental concern [36]. Fungal chitosan production offers advantages such as no demineralization step, absence of heavy metals or allergens, and better control over Mw and DA. However, fungal chitosan production is limited by lower biomass availability compared to crustacean sources and carries a risk of contamination from pathogenic fungi [37]. Chitosan production from insects is promising but under-researched, offering an alternative with fewer environmental impacts, though the process is not yet commercialized [35]. While reactive and solvent-friendly, squid-sourced chitosan remains commercially unexploited [38].

## 1.2 Chitosan derivatives and conjugates

Chemical modification can be applied to enhance the physicochemical and biological properties of chitosan. One significant limitation of chitosan is its poor aqueous solubility at physiological pH, which can be addressed through chemical modifications to introduce hydrophilic moieties. Various synthetic approaches are available for creating chitosan derivatives and conjugates, including direct modification (with or without chemical protective groups), enzymatic reactions, and chemical grafting. Chitosan possesses three reactive sites, which enable chemical reactions, namely a primary –OH group at the C-6 position, a secondary –OH group at the C-3 position and an -$NH_2$ group at the C-2 position (Figure 1c). The most commonly introduced groups are alkyl and aromatic groups, as well as cationic moieties.

Alkyl chitosan derivatives are commonly prepared by heating chitosan in the presence of alkyl halides and a base [39]. Materials produced using this method will often be heterogeneous, leading to both *N*- and *O*-modifications of chitosan. *N*-alkyl derivatives can be selectively synthesized by reductive alkylation. This involves the reaction with alkyl aldehyde in the presence of a reducing agent. This process generally occurs in two steps: the formation of a Schiff base followed by the reduction of the imine [40]. Chitosan can

be etherified with propylene epoxide under alkali conditions to prepare hydroxypropyl chitosan [41,42]. Reacting chitosan with glycidyl trimethylammonium chloride results in *N*-[(2-hydroxy-3-trimethyl ammonium)propyl] chitosan (HTCC) [43]. Depending on the method, *O*-alkylation can take place.

Quaternary chitosan derivatives can be synthesized by introducing quaternary ammonium groups to the amino or hydroxyl groups of chitosan. Examples of common quaternary derivatives include *N,N,N*-trimethyl chitosan (TMC) [44], *N*-betaine chitosan [45], and HTCC [43].

Alkyl or aromatic groups can be added to chitosan by acylation. This is usually carried out with the use of acyl chlorides [46], anhydrides [47] or carboxylic acids with carbodiimide-mediated synthesis, using 1-ethyl-3-(3-dimethyl-aminopropyl) carbodiimide (EDC) coupling reagent [48,49]. Reported *N*-acyl chitosan derivatives include chitosan-antioxidant conjugates, *N*-betaine chitosan, and other water-soluble and insoluble derivatives.

## 1.3 Antimicrobial properties

The broad-spectrum antimicrobial activity of chitosan is well-established [29]. However, the exact mode of action is still debated. Several different theories for the mode of action have been proposed. Most studies suggest that electrostatic interactions of the positively charged amino groups of chitosan with the negatively charged cell surface increase membrane permeability, ultimately leading to cell death [50]. Other theories include antibacterial activity due to the chelation binding of metal ions [51], inhibiting DNA replication and ultimately causing cell death [52], forming a polymeric membrane on the cell surface that blocks nutrients from entering the cell [53], or inhibits the growth of aerobic bacteria by acting as an oxygen barrier [54]. These mechanisms are not necessarily exclusive of one another. Not all are equally supported by experimental evidence. In a recent review, Másson examined the available experimental data on the subject [55] and concluded that the primary antimicrobial mechanism of chitosan and its derivatives is probably membrane disruption. Other proposed mechanisms, like effects on DNA or RNA or binding to teichoic acid, seem to be more speculative and not well supported by experiments. Although chitosan oligomers can cross into the cytosol, it's unclear if this causes harm to the organism. The exact way chitosan disrupts the membrane is not well understood but may involve the replacement of membrane-bound $Ca^{2+}$ or pore formation, similar to antimicrobial peptides.

Several factors influence the antimicrobial properties. Chitosan with low DA exhibits a more positive charge compared to chitosan with higher DA in the same acidic medium. A polymer with a higher positive charge will exhibit stronger electrostatic interactions with the negatively charged cell surface, thereby demonstrating enhanced antimicrobial activity. This structure-activity relationship has been demonstrated on pathogens such as *Escherichia coli*, *Listeria monocytogenes*, *Pseudomonas aeruginosa*, *Shigella*

*dysenteriae, Vibrio cholerae, Staphylococcus aureus*, *Enterococcus faecalis, Bacillus cereus*, and *Staphylococcus saprophyticus* [56–59]. Beyond the solubility and antimicrobial properties, the DA also influences the biodegradability [60], the biocompatibility [61], the hemostatic properties [62], and the mucoadhesion [20] of chitosan. Thus, along with the Mw, the DA is considered one of the most important parameters of chitosan. In recent years, investigating the pattern of acetylation and its effects on the physicochemical and biological properties has been a topic of interest. Chitosan produced by conventional methods generally possesses random-*N*-acetylation patterns. Production of chitosan with a non-random pattern of *N*-acetylation has been reported by enzymatic deacetylation using fungal chitin deacetylases [63]. In this case, the synthetic block-chitosan that was obtained exhibited stronger activity against Gram-negative *P. syringae* than chitosan with a random pattern of acetylation and similar DA.

Numerous studies have sought to clarify the relationship between Mw and antimicrobial activity. However, researchers have often arrived at divergent and sometimes conflicting conclusions. Some studies claim that low Mw chitosan exhibits greater antimicrobial activity. In a study [64], chitosan samples with Mw 55-155 kDa were investigated, and the authors claimed that low Mw chitosan exhibited higher activity against *E. coli* than the high Mw samples. According to some authors [65,66], the antimicrobial activities depend on the polymeric structure, reporting that COS exhibit significantly lower activity compared to its polymeric form. However, it has also been claimed that COS is more active than its polymeric counterparts [67]. Previous work, reported by our group, suggested the activity will increase with Mw until a maximum is reached and then there will be no further change in activity above this critical Mw (CMW) [68].

Some authors claim that the effects differ based on the pathogen species. In a study [69], chitosans with Mw >86 kDa demonstrated strong activity against Gram-positive bacteria (*B. subtilis, S. aureus*), whereas chitosans with Mw of 11-30 kDa showed the highest activity against Gram-negative bacteria (*E. coli, P. aeruginosa*). In another study [70], with a Mw range of 5-305 kDa, the activity against *E. coli* was enhanced with decreasing Mw, while against *S. aureus* the antimicrobial activity increased with increasing Mw of chitosan.

Recently, Másson analyzed 29 datasets from seven studies and proposed a bilinear equation (Eq. 1) to elucidate the relationship between Mw and the antimicrobial activity of chitosan and its derivatives [71].

Eq. 1 $$Log\left(\frac{1}{MIC}\right) = A_{Max} + \frac{(A_{Max} - A_{Min})}{CMW} \times Mw - Log\left(\frac{10^{\frac{A_{Max}}{CMW} \times Mw}}{10^{\frac{A_{Min}}{CMW} \times Mw}} + \frac{10^{A_{Max}}}{10^{A_{Min}}}\right)$$

The experimental input parameters are the minimal inhibitory concentration (MIC) and measured average Mw. The antimicrobial activity, represented as Log (1/MIC), and Mw (in kDa) and the shape of the curve is determined by three constants: $A_{Min,}$ which is the

Log (1/MIC) when the curve intersects the Y-axis; $A_{Max}$, the Log (1/MIC) value of the horizontal line that forms one segment of the bilinear curve; and the critical Mw for maximum activity (CMW), the Mw value at the intersection of the two lines.

A structure-activity investigation where the equation was fitted to the data in the 29 datasets revealed that the CMW values were mainly within 4-10 kDa. More interestingly, the relationship was consistent across Gram-positive and Gram-negative bacteria, and fungi. This seems to contradict the findings of some other publications in which a different structure-activity relationship, and thus, a different mode of action is proposed for different pathogens. The findings indicate that a common underlying mechanism is most likely, and it supports the theory that cell membrane disruption is the primary mode of antimicrobial action.

In addition to chitosan's well-established antibacterial properties, antifungal [72,73] and antiviral properties have also been reported [74], as well as the potential for the development of antiviral vaccines using chitosan, due to its adjuvant capabilities [75].

Numerous studies have documented that TMC exhibits enhanced antibacterial activity against both Gram-negative and Gram-positive bacteria compared to unmodified chitosan. This increased effectiveness is attributed to the polycationic structure of quaternized chitosan, which primarily interacts electrostatically with the anionic components of bacteria, especially anionic phospholipids in the cell membrane [17,76–78]. Research on the structure-activity relationship of TMC with varying degrees of trimethylation (DTM) against *P. aeruginosa, E. coli*, and methicillin-resistant *S. aureus* (MRSA) has demonstrated a linear increase in antibacterial activity with higher DTM at neutral pH. However, at pH 5.5, a plateau is observed, particularly within the 20–30% DTM range [79].

The antimicrobial activity of various *N*-betaine chitosan products against *E. coli* and *S. aureus* was studied [45]. At neutral conditions, the *N*-betaine chitosan products exhibited weaker activity compared to chitosan. However, in acidic media, their activity increased with decreasing degree of substitution (DS). In another study [79], *N*-betaine chitosan with DS of 17-88% was synthesized, and the antibacterial activity against *P. aeruginosa*, and MRSA was investigated at pH 7.4. A clear, linear correlation was observed against both bacterial strains. As the DS increased, so did the activity. The derivative with a DS of 88% showed a MIC of 265 µg/mL against *P. aeruginosa* and 64 µg/mL against MRSA. The same authors investigated the antibacterial activity against *S. aureus,* and *E. coli* at pH 7.2 and 5.5 [80]. At pH 7.2, the DS showed clear correlation with the activity, with higher DS leading to increased efficacy against both bacterial strains. The derivative with a DS of 88% showed a MIC of 64 µg/mL against both *S. aureus* and *E. coli*. However, when tested at pH 5.5, the antibacterial activity diminished compared to TMC or the unmodified chitosan. Several studies also report enhanced antibacterial activity of the chitosan-antioxidant conjugates [81–84].

## 1.4 Biocompatibility

Both chitin and chitosan exhibit good biocompatibility and are considered non-toxic. Despite partial degradation by gastrointestinal enzymes, neither chitin nor chitosan is absorbed (in the upper part of the digestive system) when orally administered [85]. The positively charged amino groups in chitosan have been investigated for their ability to bind with dietary fats, creating complexes that are resistant to absorption. This interaction underlies the use of chitosan as a dietary supplement for weight management [86]. In a study [85] chitosan had an $LD_{50}$ (dose of a substance required to kill 50% of a test population) of around 16 g/kg, comparable to salt and glucose in mice, with toxicity influenced by the DD. Chitosan with DD above 35% showed low toxicity, while chitin with a DD below 35% exhibited dose-dependent toxicity. Additionally, the authors claimed that the Mw did not impact toxicity. Huang *et al*. reported that decreasing the DD decreases the toxicity evaluated against the A549 cells, with minimal effects of the Mw [87]. In a different study [88], chitosan membranes containing 250 mg chitosan showed cytocompatibility in chondrocytes and keratinocytes. Another study [61] reported cytocompatibility of chitosan films containing 1.25 g chitosan with keratinocytes and fibroblasts. It has also been reported in a study [89] that while chitosan exhibited anticancer activity against SCC Ca9-22 cells (53.3 ± 5.2% cell viability at 800 µg/mL), it exhibited minimal toxicity toward non-cancer keratinocyte HaCaT cell lines (89.7 ± 16.6% cell viability at 800 µg/mL). In a study [90], nitrosalicylimine-chitosan hydrogels were prepared. The hydrogels showed an *in vitro* cytotoxicity of 60% against HeLa human cancer cell line. However, *in vivo* biocompatibility assessments, conducted via subcutaneous administration in rats, revealed no significant alterations in blood parameters, biochemical profiles, or immune system responses.

TMC is a commonly reported derivative, however, its cytotoxic effects on human and mammalian cells have not been studied as much as unmodified chitosan. Additionally, literature on the effects of DTM and Mw on cytotoxicity is lacking. Thanou *et al*. reported that TMC remains non-toxic even at high DTM. The toxicity of TMC with DTM values of 20%, 40%, and 60% was evaluated using intestinal Caco-2 cell monolayers. The study [91] showed that all TMC samples were non-toxic at the tested concentration of 1% (w/v), leading to the conclusion that TMC is a safe absorption enhancer for nasal and intestinal epithelia. In contrast, Kean *et al*. observed a general trend of increasing toxicity with higher DTM levels (ranging from 36% to 93%) in COS-7 (African green monkey kidney fibroblast-like cells) and MCF-7 (human breast epithelial cells). However, this trend plateaued once the DTM exceeded 76% [92]. A different study [93] investigated the effects of TMC (DTM ranging from 33% to 76%) on the viability of Caco-2 cells, and reported that as DTM increased, there was a corresponding rise in both cytotoxicity and membrane permeability. In another publication [94], the importance of the ratio between the degree of dimethylation (DDM) and the DTM was highlighted. The study found that when the DDM to DTM ratio exceeded 1, cytotoxicity began to decrease, ultimately becoming completely non-toxic toward a mouse connective tissue fibroblast cell line

when the ratio reached 3:1. TMC with a relatively high DDM showed reduced solubility and mucoadhesion, which contributed to a decrease in cytotoxicity. However, the impact of DDM was deemed insignificant when quaternization exceeded 40%, where cytotoxicity was primarily influenced by the DTM. Mao *et al*. conducted a study examining the cytotoxicity of TMC samples with varying Mw (ranging from 5 to 400 kDa) and observed that all polymers exhibited dose- and Mw-dependent toxicity against mouse connective tissue fibroblast cells (L929). The highest Mw TMC (400 kDa) was found to be particularly toxic, with an $IC_{50}$ of 15 µg/mL, whereas the TMC with a Mw of 5 kDa was completely non-toxic ($IC_{50}$>1 mg/mL) [95]. The cytotoxicity associated with TMC is largely attributed to its permanent positive charge, which can interact electrostatically with the negatively charged components of cell membranes, potentially leading to membrane disruption [96].

## 1.5 Antioxidant properties

Chitosan's antioxidant activity has not been as extensively studied as its antimicrobial properties, as it is not considered one of its primary attributes. However, chitosan does possess an amino and two hydroxyl groups, which could react with free radicals, giving chitosan a scavenging ability [97]. A study [98] reported that the antioxidant activity of chitosan is closely linked to its Mw, with activity increasing as Mw decreases. COS exhibited the highest antioxidant activity, whereas high Mw chitosan showed no activity against superoxide and hydroxyl radicals. This is because shorter chains are less likely to form intramolecular hydrogen bonds, leaving more hydroxyl and amino groups activated and available for radical scavenging. Some authors [48,49,99] reported that native chitosan had no reducing power and insignificant scavenging ability against DPPH radicals, thus chitosan had no antioxidant activity in *in vitro* tests.

Therefore, the extent to which chitosan can function as an antioxidant remains inconclusive, and it is unclear if its specific physicochemical properties allow effective antioxidant activity to be detected by radical scavenging testing. However, by conjugating chitosan with well-known antioxidants, its antioxidant activity can be significantly enhanced. In a study [100], it was reported that unmodified chitosan (Mw 200 kDa, DD 90%) exhibited a 41.4% DPPH scavenging ability. When grafted with ferulic acid, this scavenging ability increased to 96.6%. Eom *et al*. studied eight different phenolic acid-conjugated COS with Mw of 3-5 kDa and found that, while native COS exhibited weak antioxidant activity, the derivatives showed enhanced activity [101]. Pasanphan *et al*. investigated the activity of gallic acid-conjugated chitosan. While native chitosan (Mw 950 kDa, DD 95%) showed no reducing ability against the DPPH radical at a concentration of 1200 µM, one of the conjugates demonstrated an 87.3% reduction at the same concentration [48]. In a different study [102], native chitosan (Mw 100 kDa, DD 90%) showed no inhibition against DPPH and hydroxyl radicals. However, the synthesis of four new phenolic conjugates resulted in significantly enhanced activities. In another study [103], caffeic acid-conjugated chitosan maintained a DPPH radical scavenging

activity comparable to that of caffeic acid alone, achieving over 90% scavenging activity at a concentration of 1 mg/mL.

## 1.6 Applications

The beneficial properties of chitosan and its derivatives make them suitable for a broad range of applications across many fields, such as the pharmaceutical, medical, cosmetic and food industries, as well as agriculture and water treatment. The United States Food and Drug Administration (US-FDA), the European Union (EU), Japan, and South Korea have approved chitosan for use in dietary supplements, and as wound dressings [104–108]. The potential applications of chitosan and chitosan derivatives are estimated to be over 200 [109]. The global chitosan market was valued at USD 10.88 billion in 2022 and is expected to grow at a compound annual growth rate (CAGR) of 20.1% from 2023 to 2030 [110]. This growth is driven by the rising demand for naturally sourced products and their widespread use in wastewater treatment, agriculture, pharmaceutical and cosmetic applications.

### 1.6.1 Biomedical applications

#### *1.6.1.1 Wound treatment*

Wound treatment is one of the more promising applications of chitosan and its derivatives. Chitosan serves as a non-protein matrix that supports 3D tissue growth and activates macrophages for tumoricidal activity. It promotes cell proliferation and the organization of tissue architecture. As a hemostat, chitosan triggers natural blood clotting and blocks nerve endings to reduce pain. Over time, chitosan depolymerizes, releasing *N*-acetyl-β-D-glucosamine, which stimulates fibroblast proliferation, orderly collagen deposition, and increases natural hyaluronic acid synthesis at the wound site. These properties contribute to faster wound healing and scar prevention [111]. Chitosan and its derivatives have been applied as: bandages [112], fibers [113], nanofibers [114,115], hydrogels [116–119], and membranes [120]. Commercially available chitosan-based wound dressings include brands such as ChitoCare®, Opticell™, HemCon®, Chitodine®, Trauma-DEX®, and more [121,122].

#### *1.6.1.2 Dietary supplement*

Chitosan and chitosan derivatives have been used as dietary supplements based on their fat-binding and anticholesteremic properties, which help contribute to weight management and to maintain healthy cholesterol levels. Chitosan has the ability to inhibit fat digestion in the gastrointestinal tract, which contributes to this beneficial effect [123]. The proposed mechanism is the following: In the stomach, chitosan dissolves in the acidic gastric juice, where it acts as an emulsifier on fat globules and combines with fat to form an emulsion. When this emulsion moves into the intestine, the chitosan transforms into an insoluble gel-like substance that traps the fat, preventing it from being broken down

by enzymes like pancreatin or other intestinal enzymes. Consequently, this leads to an increase in fat excretion through feces. For chitosan to effectively block fat absorption, it must be present in the digestive system at the same time as the fat [124]. Chitosan-based dietary supplements on the market include LipoSan Ultra®, ChitoSlim®, and ChitoRich™, among others [125,126].

The use of chitosan NaCl as a substitute product for regular table salt has been marketed as Symbiosal® to reduce blood pressure and, thus, reduce the risk of hypertension [127]. It has also been proposed that chitosan, as ProChitosan® (among other measures) should be taken after mercury exposure since it has chelating abilities [128].

#### *1.6.1.3 Drug delivery system*

Another important biomedical application of chitosan is in the development of drug delivery systems, including nanoparticles (NPs), hydrogels, microspheres, films, and tablets [129]. Pharmaceutical applications include nasal, oral, ocular, parenteral as well as transdermal drug delivery. The most important characteristics of chitosan for pharmaceutical applications include purity, DA and Mw. Aqueous solubility at physiological pH is essential for most pharmaceutical applications. In drug delivery, an ideal vehicle prolongs the duration of drug activity, improves therapeutic efficiency, and reduces the side effects.

There is a rapidly growing global interest in nanotechnology, particularly in its applications within the pharmaceutical industry [15]. Properties of NPs may differ from their native bulk material, due to their small size, significantly larger surface-to-volume ratio, and changed polydispersity. As particles decrease in size, a greater percentage of their atoms reside on the surface, offering new biological properties [130]. NPs are small particles ranging from 1 to 100 nm in size, though the term is sometimes applied to larger particles in pharmaceutical contexts. When active substances are encapsulated within NPs, they are shielded from the external environment and can be more efficiently delivered to targeted areas, depending on the surface characteristics of the NPs. Chitosan in NP formulations is particularly notable due to its mucoadhesive properties, positive surface charge, and its ability to open tight junctions between cells [131,132].

Due to its cationic nature, chitosan and its quaternized derivatives can react with polyanions, forming polyelectrolyte complexes. Preparing NPs with chitosan and its derivatives provides improved stability, enhanced mucoadhesion, and permeation capabilities, and facilitates active targeting [133]. Chitosan NPs have been studied as oral drug carriers for proteins, because they can protect against enzymatic degradation in the gastrointestinal system and enhance mucoadhesion to the intestinal mucus layer [134]. Chitosan NPs have the potential for ocular-targeted drug delivery. In an *in vivo* study [135] the NPs were able to penetrate the corneal and conjunctival epithelia. Additionally, cell survival 24h after incubation with the chitosan NPs was high, with nearly 100% viability in the recovered cells. It has been reported that chitosan NPs are able to deliver

drugs over the blood-brain-barrier [136]. Chitosan NPs may also be used for virus DNA mucosal vaccines. *In vivo* immunization demonstrated that specific pathogen-free chickens immunized with Newcastle disease virus DNA encapsulated in chitosan NPs exhibited stronger immune responses and prolonged release of plasmid DNA compared to those immunized with the control plasmid [137]. Chitosan NPs are considered a promising tool for targeted cancer therapy [138] as well as for targeted delivery of markers for bio-imaging [139].

One limitation of chitosan to be used as a nanocarrier is its low solubility above pH 6. Thus, chitosan derivatives can be used in applications that require higher pH. Quaternized chitosan derivatives offer a valuable alternative for applications in a broader pH and concentration range [140].

TMC NPs have been reported in combination with various drugs, including the following examples: polyelectrolyte complexation with insulin [141], and cisplatin-hyaluronate [142], ionic gelation with curcumin [143], paclitaxel [144], lactosyl-norcantharidin [145], docetaxel [146], ovalbumin [147] and capsaicin [148], and ionic crosslinking with low molecular weight heparin [149]. Chondroitin sulfate (ChS) is an anionic heteropolysaccharide composed of repeating disaccharide units of D-glucuronic acid and *N*-acetyl-D-galactosamine, with sulfate groups attached at various carbon positions [150]. It is a key structural element in connective tissues and cartilage. ChS is recognized for its antioxidant, anti-inflammatory, neuroprotective, anti-thrombotic, anticancer, and immunoregulatory effects [151–154]. Young *et al.* previously reported on novel hydrophilic TMC-chondroitin sulfate (TMC-ChS) NPs with a cell viability assay conducted using human umbilical vein endothelial cells (HUVECs) [155]. The results indicated that the TMC-ChS NPs were not cytotoxic to HUVECs, with 80% cell viability observed after 24h of incubation at the tested concentrations (3.5-56 µg/mL). However, the study did not explore the effects of DTM and Mw of the TMC, nor did it provide a direct comparison of the cytotoxicity between TMC and TMC-ChS NPs.

#### *1.6.1.4 Other biomedical applications*

The use of chitosan and its derivatives is also explored in tissue engineering. Regenerative tissue engineering proposes the use of scaffolds to support and organize damaged tissue, as three-dimensional matrices offer a more favorable environment for cellular behavior. Chitosan scaffolds are particularly promising for tissue engineering systems due to their low immunogenicity, controlled biodegradability, and porous structure [156–158]. Chitosan's physical and chemical properties allow for the creation of various scaffold types, including molded macroporous, fiber-based, hydrogel microspheres, and 3D-printed scaffolds tailored for specific treatments requiring unique characteristics [159]. In recent years, 3D-printed chitosan-based scaffolds have garnered increasing attention, as this technique enables the biofabrication of patient-specific scaffolds with highly complex geometries [160,161].

### 1.6.2 Other applications

Chitin, chitosan and their derivatives can be used in different body sites such as skin, hair, gums and teeth [162]. Chitosan and its derivatives are widely used in various hair products, including shampoos, rinses, hair sprays, colorants, and styling lotions, among others [163]. Chitosan is also used in skincare [164].

Chitosan provides a variety of applications in the food industry, such as preserving foods from microbial spoilage, forming biodegradable films, and recovering materials from food processing waste [129]. Chitosan and its derivatives have found numerous applications in agriculture as biopesticides, and fungicides, offering an eco-friendly alternative to chemical pesticides by enhancing plant resistance to diseases and pests. Chitosan also acts as a growth promoter, stimulating seed germination, root development, and overall plant growth [165–168].

Chemical contamination of water by various toxic substances, including metals, dyes, detergents, grease, aromatic compounds, pesticides and bacteria poses a significant environmental threat due to their potential toxicity to humans. The use of low-cost polymers like chitin and chitosan for removing these water pollutants is of considerable interest [129,169].

Chitosan and its derivatives have gained attention in the textile industry, particularly in the development of eco-friendly and functional fabrics. Due to its natural antibacterial and antifungal properties, chitosan is used as a bio-coating for textiles to inhibit microbial growth, thus enhancing the hygiene and longevity of garments [170].

While it is widely recognized that the biological activity and suitability of chitosan materials for the applications mentioned above are strongly linked to the DA and Mw, it is less clear how the chemical structure of chitosan derivatives affects biological activity and general applicability. This is in part due to the fact that many reported chitosan derivatives have poorly defined structures, and the synthesis methods lack selectivity and reproducibility. Thus, it is of utmost importance to carefully consider the synthesis methods that are used to produce derivatives for scientific study.

## 1.7 Synthesis processes for chitosan derivatives and conjugates

The synthesis of chitosan derivatives and conjugates is not necessarily regio-selective and often results in heterogeneous, partially *N*- and *O*-modified products. The modification of groups not targeted for modification (one of the -OH groups or the -$NH_2$ group) is more difficult to avoid as the DS for the derivatization increases. Thus, it is challenging to repeat the synthesis and obtain precisely the same structure, leading to variations in the biological properties. Low efficiency in the reaction can be a further issue, resulting in low DS and requiring a large excess of the reagent. This can be mitigated by using a protection group strategy (Scheme 1). The protection of the C-6 hydroxyl group to enable selective *N*-acylation of the amino groups can be achieved by using triphenylmethyl (trityl

or Tr) protection. Thus, 6-*O*-triphenylmethylchitosan can be synthesized by *N*-phthaloylation of chitosan, reaction with TrCl and finally hydrazine to remove the phthaloyl groups [171,172]. This intermediate is the starting material for selective *N*-acylation reactions followed by treatment by acid to remove the trityl group [173].

Silyl ether protection strategy has also been used in the synthesis of chitosan derivatives [174]. Rúnarsson *et al*. developed a simple approach to protect both the hydroxyl groups of chitosan with *tert*-butyldimethylsilyl (TBDMS) groups. In their method, the TBDMS moiety is introduced to the mesylate salt of chitosan in a single step, resulting in 100% 3,6-*O*-TBDMS protected chitosan. The resulting product demonstrated good solubility in organic solvents such as *N*-methyl-pyrrolidone (NMP), dichloromethane (DCM), and ethanol (EtOH), facilitating efficient modification of the polymer [175,176]. Silyl ether protection groups can be removed by treatment with strong acid or $F^-$.

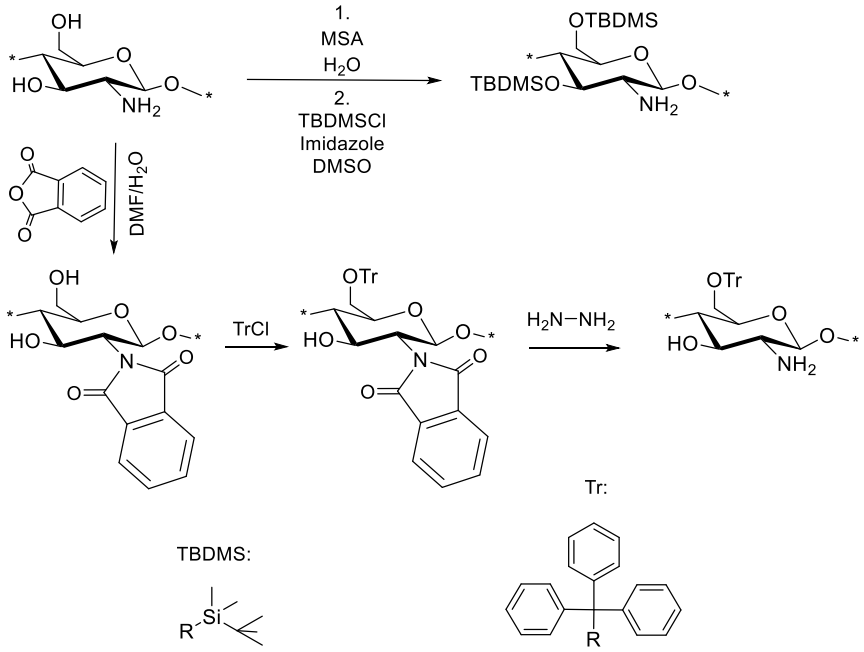


Scheme 1. Synthesis of 3,6-*O*-TBDMS chitosan [175] and 6-*O*-triphenylmethylchitosan [171,172], common precursors in the synthesis of chitosan derivatives and conjugates.

### 1.7.1 *N,N,N*-trimethyl chitosan (TMC)

One of the most studied *N*-alkyl chitosan derivatives is TMC (Scheme 2, next page), commonly prepared by a reaction with methyl iodide (MeI) in the presence of sodium hydroxide (NaOH) base and potassium iodide (KI) as a catalyst and using NMP as a solvent. This method is also referred to as the Domard methylation [177]. Materials produced using this method will be heterogeneous, leading to *N,N,N*-trimethyl-, *N,N*-dimethyl-, *N*-monomethyl-, 6-*O*-methyl-, and 3-*O*-methyl modifications of chitosan. The *O*-methylation is undesirable because it decreases the water solubility of the polymer [178].

Consequently, the derivative's effectiveness as a mucosal permeation enhancer is diminished when the pH rises above 6.5 [179]. Moreover, although a high degree of *N,N,N*-trimethylation (DTM) enhances aqueous solubility, dimethylation and monomethylation negatively impact it [94]. Additionally, the synthesis might require repetitions to obtain a high DTM. Alternatively, *O*-methyl free TMC can be synthesized by reductive alkylation. With this method, initially, mono- and dimethyl chitosan is prepared using formaldehyde and reduced by sodium borohydride or formic acid, followed by methylation in the subsequent step with MeI, resulting in up to 75% DTM [44,93]. However, this requires long reaction times. Later, this process was modified to achieve up to 82% DTM [180]. Still, the reaction time remained lengthy, requiring 118h to prepare *N,N*-dimethyl chitosan, and an additional 110h to synthesize TMC, excluding the work-up process. This extended duration poses a challenge for the scale-up of this process. Rúnarsson and colleagues devised a process similar to the Domard method, which produced *O*-methyl-free TMC without the use of a catalyst. They implemented a DMF:$H_2O$ solvent system and achieved up to 85% DTM. However, reaching high DTM levels required multiple iterative methylation steps [175]. Alternatively, selective *N*-alkylation can be accomplished using a protection group strategy, resulting in fully quaternized TMC homopolymer via *O*-silylation using TBDMSCl, followed by the application of the MeI methylating agent, and subsequent deprotection using tetrabutylammonium fluoride (TBAF) [181]. A drawback of this method is its lengthy and complex multistep reaction process. The use of an alternative alkylating agent to MeI, specifically dimethyl sulfate (DMS), has also been documented [182]. The use of DMS seems more cost-effective, as it is less expensive than MeI and does not require a solvent for the reaction. However, unwanted *O*-methylation and rapid degradation at elevated temperatures remain inevitable challenges. The use of dimethyl carbonate has been reported as a greener alternative to MeI and DMS [183]. While resulting in an *O*-methyl free product, the DTM is very low (9%), and dimethylation is predominant, which negatively affects the aqueous solubility. Another approach involves the etherification of chitosan dissolved in aqueous lithium hydroxide/potassium hydroxide/urea solutions, achieving up to 48% DTM [184]. However, this method results in unwanted *O*-methylation. An approach to TMC synthesis that is gaining attention involves enzymatic methods. In particular, the use of lipase combined with dimethyl carbonate has been reported to produce selectively *N*-methylated chitosan [185]. Despite its potential, this method results in a low DTM of only 15% and demands a prolonged reaction time of 96h.

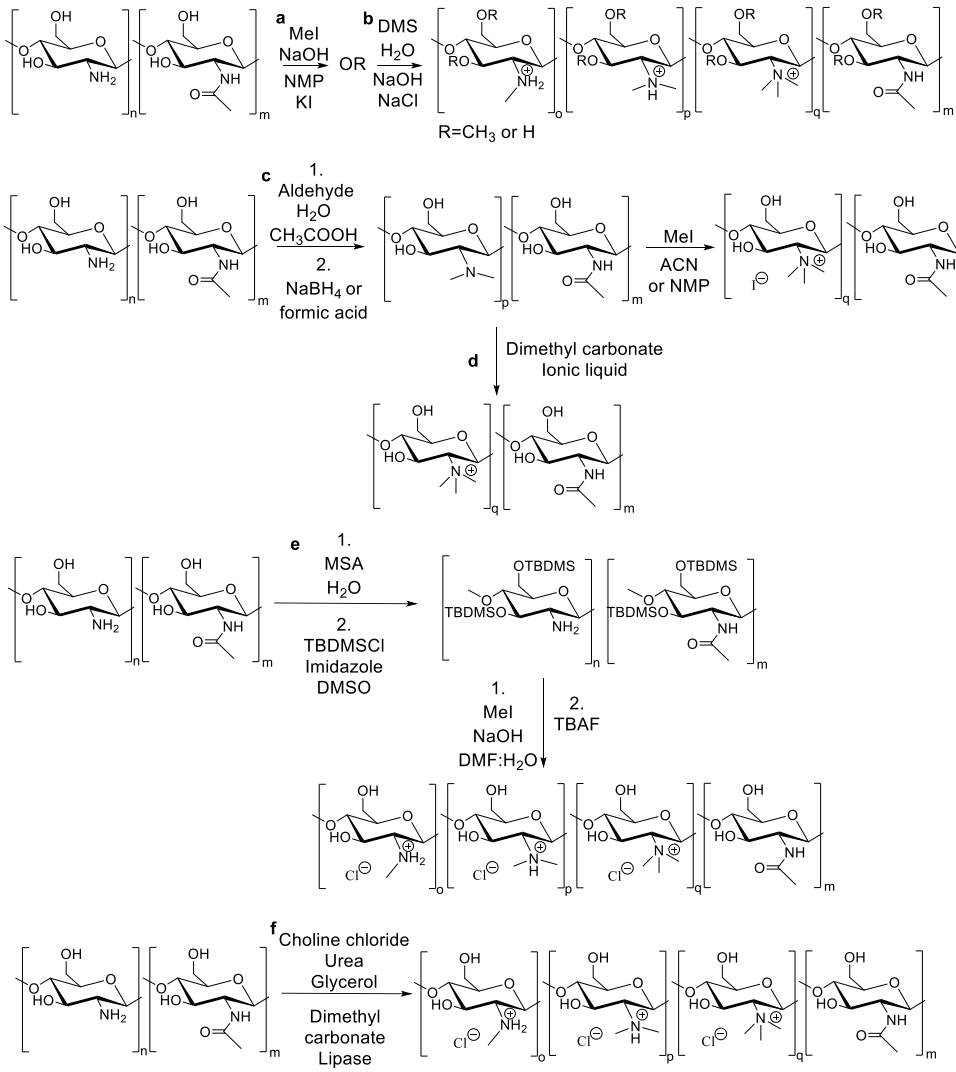


Scheme 2. Synthesis methods for the production of TMC. a. [177], b. [182], c. [44,93], e. [181], f. [185].

In summary, while the previously published methods successfully produce TMC with high DTM and, in some cases, no *O*-methylation, they also present several drawbacks. Achieving high DTM often requires repeated reagent additions, precipitation, and re-dissolution, leading to very long reaction times, usually spanning several days. Additionally, a substantial excess of methylating agents is required, and in some cases, the reproducibility of the procedure is inconsistent. These conditions are not ideal for the economical production of TMC, highlighting the need for an improved and optimized method.

### 1.7.2 *N*-betaine chitosan

*N*-betaine chitosan (also named *N*-(*N*,*N*,*N*-trimethyl ammonium)-2-acetyl chitosan) is a quaternary *N*-acyl derivative of chitosan but less studied than TMC. Both derivatives contain quaternary *N*,*N*,*N*-trimethyl groups, but in the case of *N*-betaine chitosan it is separated from the polymer backbone by a two-carbon *N*-acetyl spacer. The synthesis has been reported using *N*-phthaloylation protection strategy, introducing a phthaloyl group (derived from phthalic anhydride to the amino groups of chitosan) and 6-*O*-triphenylmethylation (or tritylation, which involves the protection of the hydroxyl groups at the C-6 position of chitosan by attaching a trityl group) protection strategy, followed by the addition of *N*-chlorobetainyl chloride [173]. Full *N*-substitution was obtained using 4 eq of *N*-chlorobetainyl chloride. This five-step method was later utilized to synthesize *N*-betaine chitosan with up to 85% DQ [186]. The synthesis method for *N*-betaine chitosan was further developed, and a more efficient TBDMS protection strategy was implemented, resulting in a fully *N*-substituted chitosan and COS, without prior protection of the amino groups [176]. The synthesis of *N*-betaine has also been reported using 2-ethoxy-1-ethoxycarbonyl-1,2-dihydroquinoline (EEDQ) in aqueous media both with COS ($M_w$=4.7 kDa, DA=5%) and chitosan ($M_w$=90 kDa, DA=20%) [187]. Up to 60% DQ was obtained using COS starting material and a molar ratio of 1:2:4 of COS:betaine:EEDQ. With chitosan, up to 50% DQ was achieved with a ratio of 1:2:6. However, increasing DQ also led to an increase in *N*-ethoxycarbonylation (DS of 25% and 30% for chitosan and COS, respectively). The preparation of betaine HCl and chitosan derived bio-sourced poly(aprotic/protic) ionic liquids with enhanced antibacterial activity against *E. coli* and *S. aureus* has also been reported [188].

Although employing the *N*-phthaloylation/tritylation protection strategy for synthesizing *N*-betaine derivatives achieves full substitution, the process is time-consuming, requiring several steps and taking up to six days. Consequently, a more straightforward and quicker method is needed to synthesize *N*-betaine chitosan with a high DS.

### 1.7.3 Chitosan-antioxidant conjugates

Alongside chemical modifications through the addition of functional groups to the chitosan backbone, chitosan-based conjugates have often been reported in recent years. Chitosan-phenolic compounds have gained significant attention as chitosan-antioxidant conjugates. Three conjugation methods have been commonly described in the literature. The activated ester-mediated synthesis is one of the most reported approaches to obtain *N*-acyl antioxidant conjugates, as it is claimed that it can be used to form amide bonds without needing *O*-protection. The synthesis processes have been described using 1-ethyl-3-(3-dimethyl-aminopropyl) carbodiimide (EDC) coupling reagent in combination with *N*-hydroxysuccinimide (NHS) [48], with hydroxy benzotriazole (HOBt) [189], and *N,N*-dicyclohexylcarbodiimide/HOBt [190]. The main drawback of this experimental method is low DS. This might be due to the highly reactive intermediate, which can lead to

hydrolysis instead of the formation of the conjugate. Nevertheless, one study [191] reported up to 70% DS, using EDC and 4-dimethylaminopyridine. However, the molar ratio of reagents was not reported. Another commonly described method is the enzyme-mediated synthesis. Advantages of the approach include targeted functionalization and being eco-friendly, however, undesired byproducts can form in the process. The synthesis has been reported with laccase [192], tyrosinase [193], and peroxidase [194]. These methods resulted in low DS (<15%). Chitosan-antioxidant conjugates have also been prepared by free radical grafting, most commonly using ascorbic acid with $H_2O_2$ [195–198]. The drawback of the process is that the covalent insertion of the antioxidant can happen on the amino group of chitosan at the C-2 position, or on its hydroxyl groups at the C-3 or C-6 position. Additionally, the literature is often lacking in reporting the DS.

Although chitosan-antioxidant conjugates have been studied for various applications [199], the impact of the DS and structural variations on biological activities remains poorly understood. In some previous studies, structural characterization was limited to IR spectroscopy, so the DS values were not clearly defined. Additionally, it is often unclear whether the chemical or enzymatic method used to graft antioxidant moieties onto the polymer is sufficiently selective to produce the intended conjugate structure [84,200].

Thus, an improved method for the efficient synthesis of chitosan-antioxidant conjugates with high DS is desired.

## 1.8 Design of Experiments (DoE) process optimization

In the pharmaceutical and fine chemical industries, there is a continuous demand for the development of new products and the improvement of existing ones, all while meeting increasingly stringent quality and standard requirements. The conventional approach to process development typically relies on a trial-and-error method, varying only one factor at a time. This approach can be time-consuming, costly, and often lacks reproducibility.

Design of Experiments (DoE) is a systematic and statistical approach to planning, conducting, analyzing, and interpreting controlled tests to evaluate the factors (the independent variables or conditions that are systematically varied during the experiment) that may influence a particular response (outcome) [201]. DoE helps researchers and engineers optimize processes, improve product quality, and gain a deeper understanding of the relationships between different variables. By systematically varying the inputs and analyzing the corresponding outputs, DoE allows for the identification of key factors that significantly impact the performance of a system or process. Furthermore, DoE is a powerful tool in optimization. For instance, in product development, DoE can be used to fine-tune formulations by adjusting the proportions of ingredients, temperature, and other variables to achieve the highest product quality or performance. In industrial processes, DoE can help minimize waste, reduce costs, and increase efficiency by pinpointing the most significant factors that influence process outcomes [202].

One of the primary benefits of DoE is its ability to evaluate multiple factors simultaneously, rather than one at a time. The key stages of DoE are screening, optimization, and robustness testing [203]. Screening identifies which experimental factors and interactions significantly affect the responses. Optimization refines the key factors from screening to find the best settings for the desired responses. Robustness testing assesses how well a process or method performs when subjected to slight variations in key factors. Different designs such as full factorial, fractional factorial, D-optimal, Plackett-Burman, or Box-Behnken designs can be employed depending on the stage of the experimentation, the number of factors, and the objective [204].

Full Factorial Designs (FDs) are a comprehensive approach to experimental design where all possible combinations of factors and their levels are considered (Figure 2A). This method ensures that the effects of each factor and their interactions are thoroughly examined. In a full FD, if there are $k$ factors, each with $n$ factor levels, the total number of experiments required is $n^k$. For example, with three factors, each with two levels (e.g., high and low), a full FD would require $2^3$, a total of 8 experiments. This exhaustive exploration provides a complete picture of how each factor influences the outcome, both individually and in combination with other factors. The primary advantage of full FDs is their ability to capture all interaction effects, making them ideal when understanding these interactions is crucial to the process or product being studied [205].

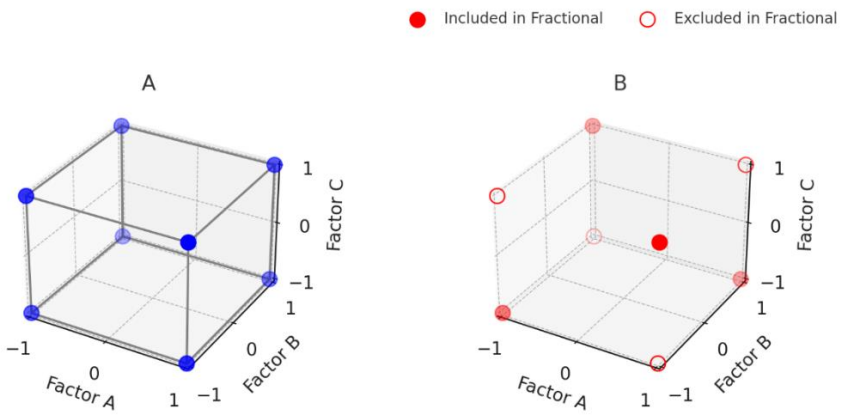


Figure 2. Factorial Designs with three factors on two levels. A: Full Factorial Design. All factor combinations are included in the design. B: Fractional Factorial Design. Filled spheres represent the experimental runs included in the design, while unfilled spheres represent the runs that are not part of the design. *(This image was generated by ChatGPT with the following prompts: "visual representation of a full factorial and a fractional factorial design, each with three factors on two levels".)*

However, the main drawback of full FDs is that they can become impractically large and resource intensive as the number of factors and levels increases. For example, a full FD with five factors, each at three levels, would require $3^5$=243 experiments. This can be

time-consuming and costly and, thus, does not offer a clear advantage over the traditional trial-and-error method.

Fractional FDs offer a more efficient alternative to full FDs by reducing the number of experiments needed while still providing valuable insights into the main effects and lower-order interactions. In a fractional FD, only a subset or fraction of the full factorial experiments is conducted (Figure 2B). This approach assumes that higher-order interactions (interactions involving three or more factors) are negligible, allowing the experimenter to focus on the most important effects [206].

In a fractional FD, instead of running all $2^3$=8 experiments for three factors at two levels, only four experiments (a half-fraction) might be run to estimate the main effects and some interactions. This reduction in the number of experiments makes fractional FDs more practical for large-scale studies, especially when time and resources are limited and when it is reasonable to assume that higher-order interactions are minimal.

The disadvantage with fractional factorial designs is that some information about interactions may be lost, and the remaining interactions may be "confounded" or combined with others. This means that the design might not fully differentiate between certain interaction effects. However, the efficiency gained often outweighs this limitation, especially when dealing with many factors at the early stages of process development.

The DoE approach has not been widely used in the synthesis of chitosan derivatives. A search on Google Scholar using the terms "chitosan derivative" "synthesis" and "design of experiments" together resulted in only 116 publications in September 2024. It should be noted that some of these papers were focused on the optimization of another material, but the process included the use of a chitosan derivative (e.g. a chitosan derivative was a component in a NP formulation, where the ratio of different components was optimized, not the synthesis of the chitosan derivative). The papers focusing on the DoE synthesis optimization of a chitosan derivative are much fewer. In contrast, searching for research papers on "chitosan derivative" and "synthesis" resulted in 11,700 publications.

### 1.8.1 DoE process optimization of chitosan derivatives

The production of TMC has been previously explored using DoE. In a study [207], TMC was synthesized in NMP solvent, with NaOH, sodium bromide, and an excess of MeI as the alkylating agent, at rt. A $2^3$ full FD was employed to examine the effects of reaction time, NaOH concentrations, and the molar ratio of MeI. The highest DTM achieved was 67% after 24h, using a molar ratio of MeI/chitosan 36:1 and 40% (w/v) NaOH. While this study provided valuable insights for improving the synthesis in a single step, it also resulted in significant *O*-methylation (60% $DOM_3$ and 50% $DOM_6$), and the use of 36 eq of MeI is not considered economically viable. Another study [208] explored the effects of reaction time (3 vs 6h), temperature (25°C vs 50°C), and the addition of NaCl as a base (no base vs a 1:3 molar ratio for chitosan/NaCl) using a $2^3$ FD, with DMS as the

alkylating agent. They achieved up to 41% DTM and reported that increasing the temperature had a negative impact on DTM, while the addition of NaCl and variations in reaction time had minimal effects. *O*-methylation could not be avoided with this method.

The synthesis optimization of a common chitosan derivative, carboxymethyl chitosan (a highly water-soluble polyelectrolyte derivative) has been reported in a couple of studies [209,210]. The synthesis of hydroxypropyl trimethyl ammonium chloride chitosan (HTCC) has been optimized with the objective of obtaining a high DQ by varying three factors, namely reaction time, temperature and the epoxypropyl trimethyl ammonium chloride/chitosan molar ratio [211]. In a different study [212], the synthesis of *N,N*-dimethyl *N*-ethyl chitosan was optimized with a $2^2$ FD. The investigated factors were the NaOH and MeI amounts, with the DQ as the response. Up to 52% DQ was obtained by using 2 mL NaOH (30% (w/v) solution) and 5 mL MeI. In another study, [213], *N,N*-dimethyl *N*-ethyl chitosan with up to 79% DQ was obtained from *N,N*-dimethyl chitosan by varying the concentration of NaOH and ethyl iodide on two levels in a FD.

Using the DoE method for the synthesis of *N*-acyl chitosan derivatives is lacking in the literature. During the literature review, only one paper [214] was identified that focused on optimizing the synthesis process of *N*-succinyl chitosan. The effects of three factors on three levels, namely the ultrasonic radiation power, the mass ratio of succinic anhydride to chitosan, and ultrasonic radiation time were investigated on the DS. Up to 75% DS was obtained with the optimized method.

# 2 Aims

The project aimed to develop efficient and scalable production processes for *N*-alkyl and *N*-acyl derivatives of chitosan with improved biological properties that are suitable for pharmaceutical and other medical applications. Successful process developments were to be accomplished by using the Design of Experiments (DoE) approach to optimize the synthesis process and investigate the relationship between various reaction conditions and the resulting degree of substitution.

The following sub-aims were defined to achieve the stated goals:

I. Develop an economical and efficient one-step synthetic method for *N*-alkyl TMC with high DTM, along with a shortened reaction time, reduced reagent usage, lower costs, and minimal *O*-methylation.

II. Optimize a scalable method for the synthesis of TMC, enabling implementation from batch processing to industrial processing, utilizing factorial DoE.

III. Establish the effects of Mw and DTM on the biocompatibility and cytotoxicity of TMC.

IV. Develop polyelectrolyte complex NPs with TMC and an anionic polyelectrolyte, mitigating the cytotoxic limitations of TMC, and enabling pharmaceutical and other medical applications.

V. Develop a production process for chitosan-hydroxycinnamic conjugates using TBDMS protection strategy, optimizing the method with DoE, and investigating their antioxidant and antibacterial activities.

VI. Develop a one-step production process for synthesizing *N*-betaine chitosan with HATU coupling and optimize the method with DoE.

# 3 Materials and Methods

## 3.1 Materials

Food grade chitosan I derived from *Pandalus borealis* shrimp shells was obtained from Primex ehf., Iceland, with $M_w$=136 kDa*, polydispersity index (PDI)=2.6 and DA=12%, as determined by GPC and NMR.

Food grade chitosan II derived from *Pandalus borealis* shrimp shells was obtained from Primex ehf., with $M_w$=270 kDa*, polydispersity index (PDI)=2.6 and DA=18%, as determined by GPC and NMR.

Food grade chitosan oligosaccharide (COS) was obtained from Qingdao Hehai Biotech (China) with $M_w$=340-1630 Da and DA=9%, as determined by the manufacturer. DA=6% determined by NMR.

*Measured by GPC, following a previously published procedure by Rathinam *et al.* [80].

Methyl iodide (MeI), dimethyl sulfate (DMS), sodium hydroxide (NaOH), sodium bicarbonate ($NaHCO_3$), triethylamine (TEA), potassium *tert*-butoxide (KOtBu), 1,8-diazabicyclo[5.4.0]undec-7-ene (DBU), 2,6-di-tert-butylpyridine (DtBP), *N,N*-diethylaniline (DEA), 1,5-diazabicyclo[4.3.0]non-5-ene (DBN), cinnamic acid, *p*-coumaric acid, caffeic acid, ferulic acid, L-ascorbic acid, tert-butyldimethylsilyl chloride (TBDMSCl), imidazole, thionylchloride ($SOCl_2$), cinnamoyl chloride, 1-ethyl-3-(3-dimethylaminopropyl)carbodiimide (EDC), *N*-hydroxysuccinimide (NHS), *N,N*-dicyclohexylcarbodiimide (DCC), *N,N*-dimethylformamide (DMF), dimethyl sulfoxide (DMSO), dichloromethane (DCM), acetonitrile (ACN), ethyl acetate (EtOAc), methanol (MeOH), *N*-methyl-2-pyrrolidone (NMP), hydrochloric acid (HCl), methanesulfonic acid (MSA), trifluoracetic acid (TFA), sodium chloride (NaCl), deuterium oxide ($D_2O$), deuterium chloride solution 35 wt. % in $D_2O$ (DCl), acetic acid-$d_4$, DMSO-d6, chloroform-d ($CDCl_3$), sodium sulfate ($Na_2SO_4$), 2,2-diphenyl-1-picrylhydrazyl (DPPH), Dulbecco's modified Eagle's medium – high glucose (DMEM), and acetone puriss. were purchased from Sigma Aldrich, Germany. *N,N*-diisopropylethylamine (DIPEA), hydroxybenzotriazole (HoBt), 1-[bis(dimethylamino)methylene]-1H-1,2,3-triazolo[4,5-b]pyridinium3-oxidhexafluoro-phosphate) (HATU), and betaine anhydrous were purchased from TCI Europe, Belgium. Ethanol (EtOH) 96% was purchased from Gamla Apótekid, Iceland. Chondroitin sulfate A sodium salt (average Mw 10-50 kDa) was purchased from Biosynth, USA. Endothelial Cell Growth Medium-2 (EGM-2, SingleQuots) and RPMI 1640 Medium were purchased from Lonza, USA. Cell Counting Kit-8 (CCK-8) was purchased from Dojindo Laboratories, Japan. Mueller Hinton broth and Mueller

Hinton Agar were obtained from Oxoid Ltd., United Kingdom. Spectra/Por Standard RC dialysis membranes (Mw cutoff 3.5 kDa) were purchased from Repligen, USA.

## 3.2 Methods and characterization

### 3.2.1 NMR spectroscopy

$^1$H NMR samples underwent analysis using Bruker AVANCE 400 instrument (Bruker Biospin GmbH, Germany) at 400 MHz and 298 K. For the chitosan/chitosan derivative samples, the *N*-acetyl peak (HAc, 2.08 ppm) was used as the internal reference with $D_2O$, $D_2O$/DCl, $D_2O$/acetic acid $d_4$, or $CDCl_3$ as the solvent. The sample concentrations varied between 6-15 mg/mL. Hydroxycinnamic acids were analyzed in $CDCl_3$ and $DMSOd_6$ solvents. The sample concentrations varied between 10-17 mg/mL. *Topspin* software (Bruker, Germany) was used to analyze the spectra.

The following methods were used to determine the DS values of the chitosan and chitosan derivatives.

DS for acetylation of chitosan (DA):

The H2-H6 protons (chitosan backbone) are present between 3.0-4.5ppm. The integral of H2 is defined as 1. Next, the H3-H6 and *N*-acetyl (HAc, 2.08 ppm) can be determined by integration, and the DA can be calculated.

$$DA(\%)=[(\int HAc/\int[H2\text{-}H6]) \times (6/3)]x100$$

The Mesylate/$NH_3^+$ ratio in the mesylate salt of chitosan:

$$Ratio(\%)=[(\int CH_3S/\int H2) \times (1/3)]x100$$

$CH_3S$ represents the protons of the mesylate methyl group at 2.83 ppm.

DS of di-TBDMS protection of chitosan:

$$DS_{TBDMS}(\%)=(\int[(CH_3)_3Si]/\int[H1\text{-}H6] \times (7/18))x100$$

$(CH_3)_3Si$ represents the protons (18H) of two *tert*-butyl groups of the TBDMS at 0.99 ppm.

DS for cinnamic acid of chitosan-cinnamic acid conjugate:

$$DS_{cin}(\%)=[(\int H_{cin}/\int[H2\text{-}H6]) \times (6/7)]x100$$

$H_{cin}$ represents the protons (7H) corresponding to the hydrogens in the cinnamoyl moiety, in the region of 6.7-8.0 ppm.

DS for *p*-coumaric acid of chitosan-coumaric acid conjugate:

$$DS_{coum}(\%)=[(\int H_{coum}/\int[H2\text{-}H6]) \times (6/6)]x100$$

$H_{coum}$ represents the protons (6H) corresponding to the hydrogens in the coumaroyl moiety, in the region of 6.4-7.6 ppm.

DS for ferulic acid of chitosan-ferulic acid conjugate:

$DS_{fer}(\%)=[(\int H_{fer}/\int H2) \times (1/5)]x100$

$H_{fer}$ represents the protons (5H) corresponding to the hydrogens in the feruloyl moiety, in the region of 6.5-7.5 ppm. Only the H2 proton of chitosan is used, because the protons corresponding to the methoxy group of ferulic acid overlap with the H3-H6 chitosan protons.

DS for caffeic acid of chitosan-caffeic acid conjugate:

$DS_{caf}(\%)=[(\int H_{caf}/\int [H2\text{-}H6]) \times (6/5)]x100$

$H_{caf}$ represents the protons (5H) corresponding to the hydrogens in the caffeoyl moiety, in the region of 6.1-7.5 ppm.

DS for *N*-betaine chitosan:

$DS_{bet}(\%)=[(\int H_{bet}/\int [H2\text{-}H6]) \times (6/9)]x100$

$H_{bet}$ represents the protons (9H) corresponding to the $N^+$-methyl groups of the betaine moiety, at 3.3 ppm.

DS for trimethylation (DTM, DDM, DMM):

The tri-, di- and monomethyl peaks were observed at chemical shifts of 3.3, 3.0, and 2.8 ppm, respectively (Figure 3, next page). The H2-H6 peaks of the chitosan backbone were observed in the chemical shift range of 4.6-3.4 ppm [178]. The integral values were used to calculate the percentages of the degrees of tri-, di- and monomethylation of the derivatives, using the integral of the tri- (∫TM), di- (∫DM) and monomethyl (∫MM) peaks. These calculations were carried out with the assumption that the total DS for mono-, di-, and trimethylation added up to 100%. *N*-acetylated monomers were excluded in the calculation of DS in this case.

$\int TM=\int (N(CH_3)_3^+)$ trimethyl peak at 3.3 ppm

$\int DM=\int (NCH_3)_2$ dimethyl peak at 3.0 ppm

$\int MM=\int NH(CH_3)$ monomethyl peak at 2.8 ppm

$A = ((\int TM/9)+(\int DM/6)+(\int MM/3))$

DS for *N,N,N*-trimethylation:

$DTM(\%)=((\int TM)/9)/A\ 100\%$

DS for *N,N*-dimethylation:

DDM(%)=((∫DM)/6)/A×100%

DS for *N*-monomethylation:

DMM(%)=((∫MM)/3)/A×100%.

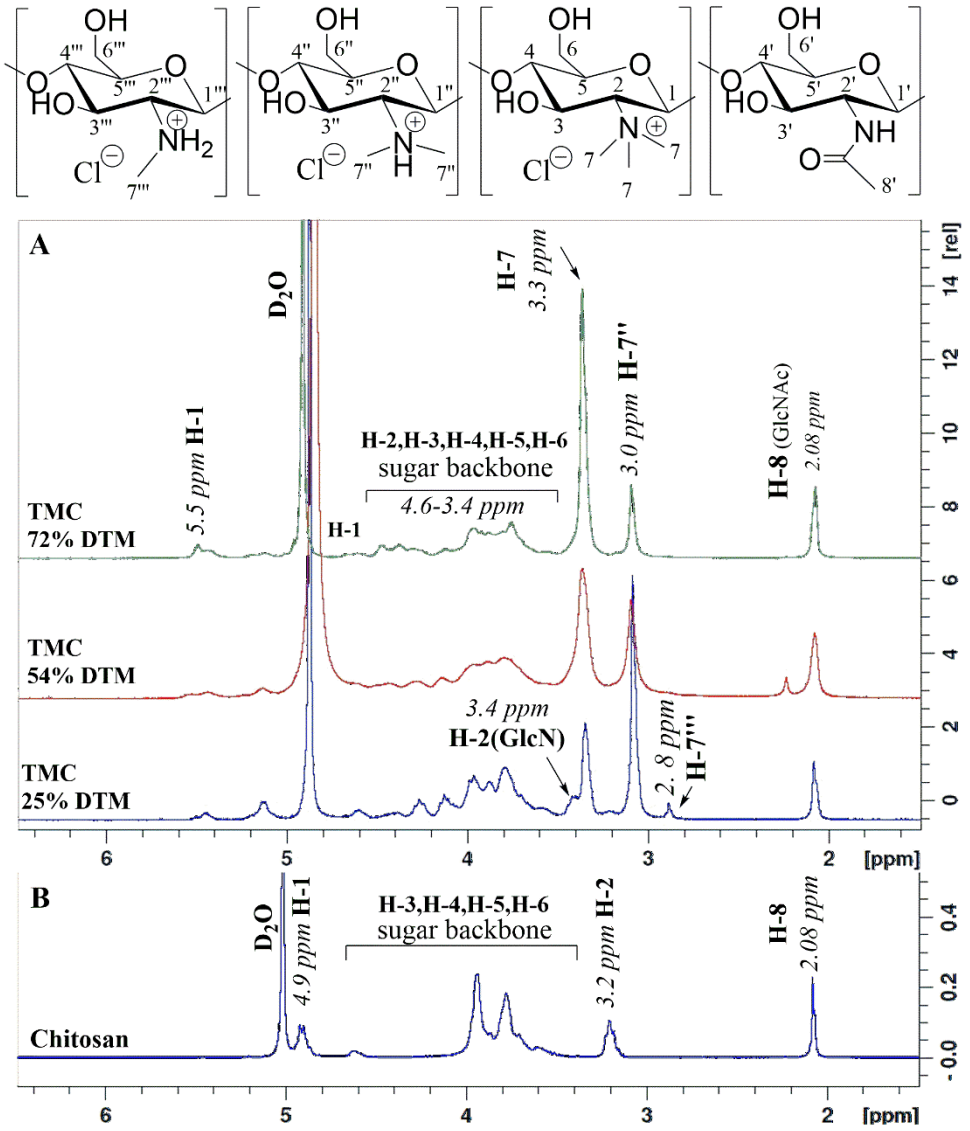


Figure 3. A: $^1$H NMR spectra of three TMC samples with varying degrees of trimethylation. B: $^1$H NMR spectrum of unmodified chitosan.

In the event of *O*-methylation ($OCH_3$), distinct sharp singlet peaks are typically observed

at 3.5 ppm and 3.4 ppm, corresponding to 3-*O*-methyl and 6-*O*-methyl groups, respectively [215]. It is important to note that if only a multiplet is observed at 3.4 ppm, it is assigned to the H2 proton of the glucosamine unit.

DS for *O*-methylation:

$DOM(\%)=[(\int OCH_3)/(H2\text{-}H6) \times 6/6)]x100\%$

### 3.2.2 Gel Permeation Chromatography (GPC)

Weight-average molecular weight ($M_w$) and polydispersity index (PDI) determination of the chitosan starting material and the chitosan derivatives were performed using gel permeation chromatography (GPC). The GPC measurements were carried out using the Polymer Standards Service (PSS GmbH, Germany) SECcurity2 GPC System, SECcurity2 Inline Degasser and TCC 6500 Column Oven (PSS GmbH), Infinity II 1260 Iso Pump (Agilent, USA), Infinity II 1260 Vialsampler (Agilent), Infinity II 1260 refractive index detector (Agilent), ETA-2010 viscometer and MALLS detector (PPC SLD 7100) from PSS GmbH. WINGPC Unity 8.31 software (PSS GmbH) was used for the data collection and processing. A series of three columns from PSS GmbH [PSS Novema Max 10 µ precolumn (50 x 8 mm), PSS Novema Max 10 µ 30 Å (300 x 8 mm) and PSS Novema Max 10 µ 1000 Å (300 x 8 mm)] were used. Calibration was performed using ReadyCal-Kit Pullulan standards with $M_p$ (180 – 1 020 000 Da) from PSS GmbH. 0.1 M NaCl/0.1% TFA solution was used as the eluent. The samples were dissolved in the eluent at a concentration of 1 mg/mL and allowed to dissolve at rt for 24h before injection. They were filtered prior to analysis with syringe filter (PTFE membrane, pore size 0.45 µm, PHENEX). The dn/dc was equal to 0.150. Each sample had an injection volume of 100 µL and a retention time of 30 min. Flowrate: 1 mL/min. Column Oven: 40°C. All the measurements were done in triplicates, and the $M_w$ and PDI were calculated.

### 3.2.3 Viscosity measurements

The apparent viscosity of chitosan solutions was measured with a Brookfield rotational viscometer, model DV-I+ (Brookfield, Canada). The samples were measured at 60°C, with 12 rpm speed, using spindle SC02. The viscosity was recorded 30 min after the addition of the respective base. The viscosity values were reported in centipoises (cP). The instrument's measurement range was up to 300 cP. Samples with viscosity levels exceeding the measurement range are indicated as >300 cP in the thesis. Each measurement represents the average of three readings.

### 3.2.4 Particle size and polydispersity measurements by dynamic light scattering (DLS) method

The average hydrodynamic diameter (Z-average) and polydispersity index (PDI) of the NPs were measured using the dynamic light scattering (DLS) technique at 25°C. A

Zetasizer Nano Ultra (Malvern Instruments, UK) was employed, operating at a detection angle of 173° with a 633 nm He-Ne laser, utilizing a ZEN2112 Low Volume Quartz Batch Cuvette. The results were analyzed with ZS Xplorer 2.1.0.15 software using the General Purpose Analysis model.

### 3.2.5 Antibacterial assay

The minimum inhibitory concentration (MIC) and minimum lethal concentration (MLC) measurements were performed according to the CLSI standard [216]. For the MIC test, Mueller Hinton broth was used (adjusted to pH 5.5 with HCl). Mueller Hinton agar was used for the MLC test. The samples were dissolved in 5% (v/v) DMSO in $H_2O$ at a concentration of 8192 µg/mL. Next, 50 µL of broth was added to wells 2-12 of a microtiter plate, then 50 µL of sample solution was added to the first two wells, and a twofold dilution series was prepared from well 2-10. Bacterial solutions of *E. coli* (ATCC 25922) and *S. aureus* (ATCC 29213) were prepared at 0.5 MacFarland (approximately $1\text{-}2*10^8$ bacteria/mL) and then diluted 100 times (approximately $10^6$ bacteria/mL). 50 µL of the diluted bacterial solution was added to wells 1-11. A viable cell count was conducted to verify the number of bacteria present in the tests. Gentamicin was used as performance control, broth without conjugates served as the growth control (well 11), and broth without bacteria or conjugates was used as the sterility control (well 12). The microtiter trays were incubated at 36°C for 24h. The MLC measurement was performed after determining the MIC. Following the determination of the MIC, 10 µL from each dilution showing inhibition was subcultured onto Mueller Hinton agar plates. These plates were incubated overnight at 36°C, after which the colony-forming units (CFU) were counted to determine the MLC.

### 3.2.6 Antioxidant assay

The DPPH radical scavenging activity was evaluated following a previously reported method with minor modifications [99]. DPPH (2,2-diphenyl-1-picrylhydrazyl) free radical was used. The chitosan-antioxidant conjugates' scavenging abilities were determined in terms of DPPH-reducing for each conjugate. The samples were dissolved in a 1:1 mix of 1% (v/v) acetic acid solution in $H_2O$ and MeOH solvent system by stirring for 12h (chitosan: 11232 µg/mL, hydroxycinnamic acids and conjugates: 5616 µg/mL). The samples were diluted with MeOH to give dilution series in test tubes with a twofold dilution interval between samples. A volume of 2500 µL of DPPH solution (0.1 mM in MeOH) was added to 500 µL of each sample, vortexed, and then left to stand in the dark at rt for 1h. L-ascorbic acid was used as positive control. The absorbance was recorded at 512 nm using an Ultrospec 2000 pro UV/Visible spectrophotometer. The solvent was used as the blank without DPPH. Solvent with DPPH was used as the control. The scavenging activities were expressed as the percentage inhibition of DPPH and were calculated using the following equation:

$$\text{Inhibition}(\%) = (1-(Abs_1-Abs_2)/Abs_0)x100$$

In this equation, $Abs_1$ represents the absorbance of the corresponding sample, $Abs_2$ is the absorbance of the sample without DPPH solution, and $Abs_0$ is the absorbance of the control. The absorbance values were plotted against the logarithmic concentration on a semi-logarithmic graph using Kaleidagraph 4.5.4 (Synergy Software, USA) and the half-maximal effective concentration ($EC_{50}$) values were determined.

### 3.2.7 *In vitro* cell viability assay with HUVECs

The *in vitro* cell viability of five TMC samples and TMC-ChS NPs was assessed using HUVEC cells cultured in sterile endothelial growth medium (EGM-2) with growth supplements, including heparin, human recombinant epidermal growth factor, hydrocortisone, gentamicin sulfate amphotericin-B, human recombinant vascular endothelial growth factor, ascorbic acid, recombinant long R3 insulin-like growth factor-1, human fibroblast growth factor-B, penicillin, streptomycin (final concentration 0.1 mg/mL), and fetal bovine serum (FBS). ChS was used as a non-toxic control. The cells (6000 per well) were incubated at 37°C for 24h on collagen-coated 96-well microtiter plates, then exposed to the TMC samples and TMC-ChS NPs at final concentrations ranging from 800 to 1.56 µg/mL and 250 to 0.49 µg/mL, respectively. After 24h of incubation, the cells were washed with phosphate-buffered saline (PBS, pH 7.4), and cell viability was measured using the Cell Counting Kit-8 (CCK-8, Dojindo Laboratories, Japan) with a Tecan Infinite M1000Pro microplate reader (Tecan, Switzerland) at 450 nm.

The relative cell viability percentage was calculated using the following equation:

$$\text{Cell viability}(\%)=[(A_{sample}-A_{media})/(A_{100\%}-A_{media})]x100$$

In this equation, $A_{sample}$ represents the mean absorbance of the treated sample, $A_{media}$ corresponds to the mean absorbance of cell culture media, and $A_{100\%}$ is the mean absorbance of the positive control (100% cell viability).

The data was analyzed, and curve fitting was performed using Kaleidagraph 4.5.4 (Synergy Software, USA) for result plotting.

### 3.2.8 *In vitro* cytotoxicity assay against human ovarian cancer cell lines SKOV-3 and OVISE

The *in vitro* cytotoxicity of five TMC samples and TMC-ChS NPs was assessed using two human ovarian cancer cell lines, OVISE and SKOV-3.

OVISE: Cells were cultured in RPMI-1640 medium containing L-glutamine, sodium bicarbonate, 10% FBS, 1% penicillin and streptomycin (final concentration 0.1 mg/mL).

SKOV-3: Cells were cultured in DMEM medium supplemented with glucose, L-glutamine, sodium pyruvate, sodium bicarbonate, 10% FBS, 1% penicillin and streptomycin (final concentration 0.1 mg/mL).

For both OVISE and SKOV-3 cell lines, the experimental procedure was as follows: Cells (OVISE: 3000 per well, SKOV-3: 4000 per well) were incubated at 37°C for 24h on 96-well microtiter plates. The cells were then treated with the TMC samples and TMC-ChS NPs at final concentrations ranging from 800 to 1.56 µg/mL for the TMC samples and 250 to 0.49 µg/mL for the TMC-ChS NPs. After 24h of incubation, the cells were washed with PBS (pH 7.4), and cytotoxicity was assessed using the CCK-8 kit (Dojindo Laboratories, Japan). Absorbance was measured at 450 nm using a Tecan Infinite M1000Pro microplate reader (Tecan, Switzerland). The $IC_{50}$ (50% inhibitory concentration) was calculated using Kaleidagraph 4.5.4 (Synergy Software, USA), based on the following equation:

$$Y(\%)=m_1+(m_2-m_1)/[1+(x/m_3)^{m4}]$$

Where $m_1$ is the $Y_{min}$ value (the minimum value of the response observed in the dataset), $m_2$ is the $Y_{max}$ value (the maximum value of the response observed in the dataset), $m_3$ is the X value at mid-point of Y ($IC_{50}$), and $m_4$ is the slope of the curve at midpoint. This equation models the dose-response curve to determine the $IC_{50}$ value.

## 3.3 Synthesis

### 3.3.1 Synthesis of mesylate salt of chitosan

The synthesis method described by Benediktsdóttir *et al*. was used with some modifications for the synthesis of chitosan mesylate [181].

Chitosan (1 g) was weighed into a beaker and MSA (9.7 mL, 25 eq corresponding to the eq of $-NH_3$ groups in the polymer) was slowly added while stirring the suspension at 0 °C. Next, $H_2O$ was added dropwise until a clear, homogenous solution was achieved. The reaction mixture was stirred for 1h at rt, followed by the addition of cold EtOH, resulting in a white precipitate in the solution. The solid material was washed on a sintered funnel with plenty of EtOH and acetone. The obtained salt precipitate was then redissolved in $H_2O$, stirred for 1h, re-precipitated with acetone, filtered on a sintered funnel, and finally washed with acetone. The obtained mesylate salt was vacuum-dried for 9h and powdered in a mortar (exp A1). The salt formation was confirmed by $^1$H-NMR.

$^1$H NMR (400 MHz, $D_2O$) $\delta$ ppm: 2.08 (HAc, s), 2.83 ($CH_3S$, s, 3H), 3.20 (H2, s, 1H), 3.48–4.08 (H3-H6, m, 5H), 4.87 (H1, partially overlapped with the solvent peak, s, 1H).

### 3.3.2 Synthesis of 3,6-*di*-TBDMS-chitosan

The mesylate salt of chitosan (1 g) was weighed into a round bottom flask ($RBF_1$) and 15 mL dry DMSO was added under $N_2$. In a separate round bottom flask ($RBF_2$), TBDMSCl (2.9 g, 5 eq) and imidazole (4.5 g, 17 eq) were stirred in 15 mL of dry DMSO under $N_2$ for 1h, until a white turbid solution was formed. Next, the content of $RBF_2$ was slowly added to $RBF_1$ with a syringe. The reaction mixture was stirred overnight, resulting in a

gel-like material in the reaction mixture, which was subsequently filtered on a sintered funnel, and washed with plenty of $H_2O$, followed by washing with ACN until a powder-like material was obtained. The compound was vacuum-dried at 40°C for 9h and powdered in a mortar (exp A2). The synthesis was confirmed by $^1$H-NMR. The full TBDMS protection can be confirmed by free solubility in chloroform or DCM solvents, and it can be calculated from the NMR spectrum.

$^1$H NMR (400 MHz, $CDCl_3$) $\delta$ ppm: 0.16 ($(CH_3)_2$Si, s, 12H), 0.99 ($(CH_3)_3$C, s, 18H), 2.81 (H2, s, 1H), 3.19-4.82 (H1-H6, m, 6H).

### 3.3.3 General procedure for TMC

The synthesis of TMC materials (exp 1-84) was carried out following several procedures, with some variations in the solvents and reagents used. Here a general method is described.

The starting material (chitosan II/mesylate salt of chitosan) was dissolved in the relevant solvent (DMF/DMF:$H_2O$/DMSO/NMP) and acid (HCl/MSA) at different concentrations. Next, the alkylating agent (MeI/DMS) was added, and the reaction mixture was stirred for 30 min, followed by the base (NaOH/$NaHCO_3$/DIPEA/TEA/DEA/KOtBu /DtBP/DBU or DBN) addition dropwise. In the case of solid materials, the base was added as a 1M solution in $H_2O$. The respective base was added with vigorous stirring several different ways, at given times. The reaction was carried out for a set time at the given temperature, then the product was precipitated with cold EtOH, filtered on a Buchner funnel, and washed with acetone. The solid samples were then re-dissolved and ion-exchanged (9% (w/v) NaCl solution), then re-precipitated, filtered, and washed with acetone. Lastly, the samples were dissolved in a 1M HCl solution and dialyzed (Mw cutoff=3.5 kDa) against $H_2O$ for five days, followed by freeze-drying for four days at -60°C (Scanvac CoolSafe, LagoGene, Denmark). The synthesis was confirmed, and the DS was calculated by $^1$H-NMR. Several sequential and factorial designs were utilized to optimize the TMC synthesis (Designs 1-8).

$^1$H NMR (400 MHz, $D_2O$/DCl) $\delta$ ppm: 2.08 (HAc, s), 2.8 (MM, s), 3.0 (DM, s), 3.2 (H2 glucosamine and glucosamine substituted, m), 3.3 (TM,s), 4.6–3.4 (H2-H6 m, 6H), 4.9–5.1 (H1, partially overlapped with the solvent peak, m).

### 3.3.4 TMC-ChS NP preparation

The TMC sample (exp 78, 50% DTM) and the ChS were each dissolved in $H_2O$ at a concentration of 1.5 mg/mL and stirred for 48h. The solutions were filtered through a 0.44 µm syringe filter. An initial evaluation was performed to explore the NP formation ability of TMC and ChS independently at this concentration. Subsequently, various TMC/ChS weight ratios (1:12, 1:6, 1:3, 1:2, 1:1, 1.1:1, 1.2:1, 1.3:1, 1.4:1, 1.5:1, 2:1, 3:1, 6:1, 12:1)) were tested for NP formation. In all cases, the TMC solution was added to the

ChS solution and briefly vortexed.

### 3.3.5 Synthesis of TBDMS-hydroxycinnamic acids (exp A3-A5)

The hydroxyl groups of *p*-coumaric acid, ferulic acid and caffeic acid required protection. This was accomplished by using the same strategy as with chitosan, simplifying the removal of protective groups in the final stages of the synthesis. Thus, TBDMSCl and imidazole were employed for protection, yielding a crude product of the corresponding acid, which was further purified in subsequent steps. A previously published method was used for the synthesis of 4-*O*-tert-butyldimethylsilylcoumaric acid (exp A3), 4-*O*-tert-butyldimethylsilylferulic acid (exp A4), and 3,4-*O*-tert-butyldimethylsilylcaffeic acid (exp A5) [217]. The TBDMS protection step was unnecessary for cinnamic acid, as its aromatic core lacks hydroxyl groups.

### 3.3.6 Synthesis of TBDMS-chitosan-hydroxycinnamic acid conjugates (exp A6-A27)

In the first step, cinnamic acid and the TBDMS-protected hydroxycinnamic acids (exp A3-A5) were refluxed with $SOCl_2$ (8 eq) in DCM for 5h. Afterwards, the mixture was concentrated *in vacuo* to yield crude cinnamoyl chloride or TBDMS-coumaroyl/feruloyl/caffeoyl chloride. The resulting chloride (0.25 eq) was then reacted with 3,6-*di*-TBDMS-chitosan (prepared from chitosan I, 1 eq, exp A2) using varying amounts of TEA in DCM, with varying reaction times. The aim was to control the DS of the conjugates, targeting DS values of 25% and 50%. The initial reactions followed the methodology of Okamoto *et al.*, where the molar ratio of amine to TEA was 1:7.6 [218]. The obtained crudes were worked up by evaporating the solvent, re-dissolved in DCM followed by concentrating again, then washed with $H_2O$ and ACN. The obtained products were dried in a vacuum oven at 40°C for 8h.

### 3.3.7 Deprotection

The deprotection was done by stirring in a 2M HCl solution in MeOH for 48h, followed by ion exchange in a 10% (w/v) NaCl solution and dialysis against $H_2O$. The deprotected and purified materials were freeze-dried at -60°C (Scanvac CoolSafe, LagoGene, Denmark), resulting in the final products, cinnamic acid- (exp 85-97), *p*-coumaric acid- (exp 98-100), ferulic acid- (exp 101-103) and caffeic acid (exp 104-106) conjugated chitosan. The synthesis was confirmed, and the DS was calculated by $^1$H-NMR. A full FD design was used to optimize the method (Design 9).

Chitosan-cinnamic acid conjugate: $^1$H NMR (400 MHz, $D_2O$, acetic acid-$d_4$) $\delta$ ppm: 2.08 (HAc, s), 3.23 (H2, s, 1H), 3.48–4.08 (H3-H6, m, 5H), 4.89 (H1, partially overlapped with the solvent peak, s, 1H), 6.74-8.08 ($H_{cin}$, m, 7H).

Chitosan-*p*-coumaric acid conjugate: $^1$H NMR (400 MHz, $D_2O$, acetic acid-$d_4$) $\delta$ ppm: 2.08 (HAc, s), 3.21 (H2, s, 1H), 3.48–4.08 (H3-H6, m, 5H), 5.06 (H1, partially overlapped with the solvent peak, s, 1H), 6.58-7.59 ($H_{coum}$, m, 6H).

Chitosan-caffeic acid conjugate: $^1$H NMR (400 MHz, $D_2O$, acetic acid-$d_4$) $\delta$ ppm: 2.08 (HAc, s), 3.05 (H2, s, 1H), 3.17–4.02 (H3-H6, m, 5H), 4.91 (H1, partially overlapped with the solvent peak, s, 1H), 6.20-7.46 ($H_{caf}$, m, 5H)

Chitosan-ferulic acid conjugate: $^1$H NMR (400 MHz, $D_2O$, acetic acid-$d_4$) $\delta$ ppm: 2.08 (HAc, s), 3.20 (H2, s, 1H), 3.32–4.24 (H3-H6, m, 5H), 3.77 (O-$CH_3$, overlapping with chitosan peaks) 4.94 (H1, partially overlapped with the solvent peak, s, 1H), 6.71-7.66 ($H_{fer}$, m, 5H)

*The synthesis of TBDMS-hydroxycinnamic acids (exp A3-A5), TBDMS-chitosan-hydroxycinnamic acid conjugates (exp A6-A27), and their subsequent deprotection (exp 85-106) were carried out as part of my MSc project. These synthesis methods are included in this thesis to provide necessary background information, as the DoE optimization of the synthesis process is discussed later in the thesis.*

### 3.3.8 Synthesis of *N*-betaine chitosan

The synthesis of *N*-betaine chitosan materials (exp 107-123) was carried out following several procedures, with some variations. Here a general method is described. The synthesis was carried out based on a previously published method with slight modifications [219]. Betaine (and in some cases, cinnamic acid) was added to DMSO solvent under $N_2$, followed by the addition of HATU and HOBt. Next, chitosan (Chitosan II), MSA (4.5 eq) and base (DIPEA/TEA) were added, stirred at rt/60°C with varying reaction times. The reaction mixture was dialyzed (Mw cutoff=3.5 kDa) against 10% (w/v) NaCl solution (1 day) and $H_2O$ (4 days), followed by freeze-drying for four days at -60°C (Scanvac CoolSafe, LaboGene, Denmark). The synthesis was confirmed, and the DS was calculated by $^1$H-NMR. DoE was utilized to optimize the *N*-betaine chitosan synthesis (Design 10).

$^1$H NMR (400 MHz, $D_2O$/DCl) $\delta$ ppm: 2.08 (HAc, s), 3.2 (H2 glucosamine and glucosamine substituted, m) 3.35 ($H_{bet}$, s, 9H), 4.6–3.4 (H2-H6 m, 6H), 4.9–5.1 (H1, partially overlapped with the solvent peak, m), 6.74-8.08 ($H_{cin}$, m, 7H).

## 3.4 Experimental design and statistical analysis

### 3.4.1 Sequential designs – TMC (Designs 1-5, exp 1-20)

A series of five simple sequential designs (Designs 1-5) was performed as the initial optimization of the TMC synthesis. In each of these designs, the optimal reaction conditions served as the starting point of the following design. The optimization was performed without the use of software.

### 3.4.2 Fractional Factorial Design – TMC (Design 6, exp 21-32)

A fractional FD (Design 6) in screening mode was conducted to examine the main effects of four factors in the TMC synthesis: the molar ratio of MeI/chitosan, the molar ratio of $NaHCO_3$/chitosan, temperature, and reaction time, each tested at three levels (-1, 0, and 1) on the DTM (%) response. The experimental design was generated using MODDE 12.1 software (Sartorius GmbH), with the goal of maximizing the DTM response. The software recommended an L9 (9-run design) fractional FD, which was selected, resulting in a total of 12 experiments (exp 21-32) (Linear+Quadratic mode). The independent variables and factor levels of the screening design are shown in Table 1.

Table 1. Fractional FD (Design 6) for the synthesis of TMC with four factors (molar ratio of MeI/chitosan, molar ratio of $NaHCO_3$/chitosan, temperature, and reaction time) on three levels ($3^4$).

| Factors | | Symbol | Level 1 | Level 2 | Level 3 |
|---|---|---|---|---|---|
| MeI (eq) | | $X_1$ | 3 (-) | 6 (0) | 12 (+) |
| $NaHCO_3$ (eq) | | $X_2$ | 1.5 (-) | 3 (0) | 6 (+) |
| Temperature (°C) | | $X_3$ | 60 (-) | 80 (0) | 100 (+) |
| Time (h) | | $X_4$ | 6 (-) | 20 (0) | 40 (+) |
| Exp | Run order | $X_1$ | $X_2$ | $X_3$ | $X_4$ |
| 21 | 3 | - | - | - | - |
| 22 | 5 | - | 0 | 0 | 0 |
| 23 | 2 | - | + | + | + |
| 24 | 7 | 0 | - | 0 | + |
| 25 | 11 | 0 | 0 | + | - |
| 26 | 1 | 0 | + | - | 0 |
| 27 | 12 | + | - | + | 0 |
| 28 | 9 | + | 0 | - | + |
| 29 | 4 | + | + | 0 | - |
| 30 | 10 | 0 | 0 | 0 | 0 |
| 31 | 8 | 0 | 0 | 0 | 0 |
| 32 | 6 | 0 | 0 | 0 | 0 |

For the analysis of Design 6, multiple linear regression (MLR) was applied to fit the following equation.

$$Y=\beta_0 +\beta_1X_1 +\beta_2X_2 +\beta_3X_3 +\beta_4X_4 +\beta_{11}(X_1)^2 +\beta_{22}(X_2)^2+\beta_{33}(X_3)^2 +\beta_{44}(X_4)^2$$

In this equation, Y corresponds to the response variable. $X_1$, $X_2$, $X_3$, and $X_4$ are the four factors (the molar ratio of MeI/chitosan, the molar ratio of $NaHCO_3$/chitosan, temperature, and reaction time, respectively), each at three levels (-1, 0, and 1). $\beta_0$ represents the intercept or the constant term in the model. $\beta_1$, $\beta_2$, $\beta_3$, and $\beta_4$ represent the main effects of the factors; $X_1$, $X_2$, $X_3$ and $X_4$, respectively. $\beta_{11}$, $\beta_{22}$, $\beta_{33}$, and $\beta_{44}$ are

the quadratic effects (square terms) of the factors.

## 3.4.3 Full Factorial Designs

### *3.4.3.1 Full Factorial Design – TMC (Design 7, exp 33-44)*

Following the fractional FD (Design 6), a full factorial interaction model (Design 7), with three center points was carried out to further investigate two factors, (the $NaHCO_3$ base addition (BA) and the temperature), each tested on three levels (-1, 0, and 1) on the DTM (%) response in the synthesis of TMC. The experimental design was generated using MODDE 12.1 software (Sartorius GmbH), with the goal of maximizing the DTM response. The independent variables and the factor levels of Design 7 are displayed in Table 2 (next page).

Table 2. Full FD (Design 7) for the synthesis of TMC with two factors (the $NaHCO_3$ base addition (BA) and the temperature) on three levels ($3^2$). *The BA (base addition) refers to the amount of increments the 4 eq $NaHCO_3$ was divided into. Gradual addition: the $NaHCO_3$ was added in 0.5 eq increments with an addition funnel over a period of 6h.

| Factors | Symbol | Level 1 | Level 2 | Level 3 |
|---|---|---|---|---|
| BA* | $X_1$ | 1 (-) | 2 (0) | gradual (+) |
| Temp. (°C) | $X_2$ | 25 (-) | 60 (0) | 80 (+) |
| Exp | | Run order | $X_1$ | $X_2$ |
| 33 | | 4 | - | - |
| 34 | | 5 | - | 0 |
| 35 | | 1 | - | + |
| 36 | | 10 | 0 | - |
| 37 | | 2 | 0 | 0 |
| 38 | | 11 | 0 | + |
| 39 | | 12 | + | - |
| 40 | | 3 | + | 0 |
| 41 | | 6 | + | + |
| 42 | | 8 | 0 | 0 |
| 43 | | 9 | 0 | 0 |
| 44 | | 7 | 0 | 0 |

For the analysis of the full FD (Design 7), partial least square regression (PLS) was used to fit the following equation.

$Y=\beta_0 +\beta_1X_1 +\beta_2X_2 +\beta_{12}X_1X_2 +\beta_{11}(X_1)^2 +\beta_{22}(X_2)^2$

Y represents the response variable. $X_1$ and $X_2$ are the two factors ($NaHCO_3$ BA and temperature, respectively), each at three levels (-1, 0, and 1). $\beta_0$ represents the intercept or the constant term in the model. $\beta_1$ and $\beta_2$ are the main effects of factors $X_1$ and $X_2$, respectively. $\beta_{12}$ represents the interaction effect between factors $X_1$ and $X_2$. $\beta_{11}$ and $\beta_{22}$ are the quadratic effects for $X_1$ and $X_2$, respectively.

### *3.4.3.2 Full Factorial Design – TMC (Design 8, exp 73-84)*

Following a series of batch experiments (exp 45-72) investigating new potential bases and solvents as well as dilutions of the reaction medium, a full FD (Design 8) was performed in Response Surface Methodology (RSM) optimization mode to investigate the main effects of two factors, the BA of DIPEA and the molar ratio of MeI/chitosan on three levels (-1, 0 and 1) on the DTM (%) response. The experimental design was generated using MODDE 12.1 software (Sartorius GmbH), with the goal of maximizing the DTM response.

The independent variables and the factor levels of Design 8 are displayed in Table 3.

Table 3. Full FD (Design 8) for the synthesis of TMC with two factors (the molar ratio of MeI/chitosan and the DIPEA base addition (BA)) on three levels ($3^2$). *The BA refers to the amount of increments the 4 eq DIPEA was divided into.

| Factors | Symbol | Level 1 | Level 2 | Level 3 |
|---|---|---|---|---|
| MeI (eq) | $X_1$ | 6 (-) | 9 (0) | 12 (+) |
| BA* | $X_2$ | 4 (-) | 6 (0) | 8 (+) |

| Exp | Run order | $X_1$ | $X_2$ |
|---|---|---|---|
| 73 | 7 | - | - |
| 74 | 10 | 0 | - |
| 75 | 1 | + | - |
| 76 | 6 | - | 0 |
| 77 | 9 | 0 | 0 |
| 78 | 4 | + | 0 |
| 79 | 3 | - | + |
| 80 | 12 | 0 | + |
| 81 | 2 | + | + |
| 82 | 8 | 0 | 0 |
| 83 | 11 | 0 | 0 |
| 84 | 5 | 0 | 0 |

For the analysis of Design 8, partial least square regression (PLS) was applied to fit the equation used for Design 7. In this case, $X_1$, and $X_2$ refer to the factors the molar ratio of MeI/chitosan and the DIPEA base addition (BA).

### *3.4.3.3 Full Factorial Design – Chitosan-cinnamic acid conjugate (Design 9, exp 85-95)*

The synthesis of chitosan-cinnamic acid conjugate was optimized with a full FD. The effects of three factors (molar ratio of cinnamoyl chloride/chitosan, molar ratio of TEA/chitosan, and reaction time) were investigated on two levels (-1 and 1) on the DS (%) response. An orthogonal (balanced) design was carried out with all combinations of the factor levels (8 runs). The independent variables and the factor levels of Design 9 are displayed in Table 4 (next page).

The experiments (exp 85-95) were initially conducted as part of the MS thesis project [220]. At that time, the decision to investigate only three factors on two levels was made to allow for manual analysis without the use of MODDE software. As a result, a simplified design was employed, with no specific run order. During the PhD project, these results

were re-analyzed using MODDE software to gain deeper insights into the experimental outcomes.

Table 4. Full FD (Design 9) for the synthesis of chitosan-cinnamic acid with three factors (the molar ratio of cinnamoyl chloride/chitosan, molar ratio of TEA/chitosan, and reaction time) on two levels ($2^3$).

| Factors | Symbol | Level 1 | Level 2 |
|---|---|---|---|
| Cinnamoyl Cl (eq) | $X_1$ | 0.25 (-) | 1 (+) |
| TEA (eq) | $X_2$ | 2 (-) | 7.6 (+) |
| Time (h) | $X_3$ | 24 (-) | 48 (+) |
| Exp | $X_1$ | $X_2$ | $X_3$ |
| 85 | - | - | - |
| 86 | + | - | - |
| 87 | - | + | - |
| 88 | + | + | - |
| 89 | - | - | + |
| 90 | + | - | + |
| 91 | - | + | + |
| 92 | + | + | + |
| 93 | - | - | - |
| 94 | - | + | - |
| 95 | - | + | + |

For the analysis of the full FD (Design 9), multiple linear regression (MLR) was used to fit the following equation.

$$Y=\beta_0 +\beta_1X_1 +\beta_2X_2 +\beta_3X_3 + \beta_{123}X_1X_2X_3$$

Y represents the response variable. $X_1$, $X_2$ and $X_3$ are the three factors (molar ratio of cinnamoyl Cl/chitosan, molar ratio of TEA/chitosan, and time, respectively), each at two levels (-1 and 1). $\beta_0$ represents the intercept or the constant term in the model. $\beta_1$, $\beta_2$ and $\beta_3$ are the main effects of factors $X_1$, $X_2$ and $X_3$, respectively. $\beta_{123}$ represents the interaction effect between factors $X_1$, $X_2$ and $X_3$.

#### *3.4.3.4 Full Factorial Design – N-betaine chitosan (Design 10, exp 112-123)*

After a series of preliminary experiments (exp 107-111) and some additional experiments carried out by Luca Protti (investigating the use of TEA instead of DIPEA as well as various solvent systems), a full FD (Design 10) in system characterization mode was conducted to examine the main effects of two factors in the *N*-betaine chitosan synthesis: the molar ratios of HATU and TEA were varied, each tested at three levels (-1, 0, and 1) on the DS

(%) response. The experimental design was generated using MODDE 12.1 software (Sartorius GmbH), with the goal of maximizing the DS response. A full FD was selected, resulting in a total of 12 experiments (exp 112-123) (Quadratic mode). The independent variables and factor levels of the screening design are shown in Table 5.

Table 5. Full FD (Design 10) for the synthesis of *N*-betaine chitosan with two factors (the molar ratios of HATU and TEA) on three levels ($3^2$).

| Factors | Symbol | Level 1 | Level 2 | Level 3 |
|---|---|---|---|---|
| HATU (eq) | $X_1$ | 0.75 (-) | 1.5 (0) | 3 (+) |
| TEA (eq) | $X_2$ | 5.5 (-) | 11.5 (0) | 16 (+) |
| Exp | | Run order | $X_1$ | $X_2$ |
| 112 | | 9 | - | - |
| 113 | | 4 | 0 | - |
| 114 | | 12 | + | - |
| 115 | | 6 | - | 0 |
| 116 | | 10 | 0 | 0 |
| 117 | | 8 | + | 0 |
| 118 | | 2 | - | + |
| 119 | | 3 | 0 | + |
| 120 | | 1 | + | + |
| 121 | | 7 | 0 | 0 |
| 122 | | 15 | 0 | 0 |
| 123 | | 5 | 0 | 0 |

For the analysis of Design 10, partial least square regression (PLS) was applied to fit the equation used for Design 7. In this case, $X_1$, and $X_2$ refer to the factors the molar ratios of HATU and TEA, respectively.

### *3.4.3.5 Analysis of results*

Designs 1-5 were planned and analyzed manually. Design 9 was planned manually and analyzed by MODDE software. The experiments of Designs 6-8, and 10 were conducted in the sequence specified by the MODDE software. The data was checked for normal distribution to identify potential outliers. A replicate plot was then created to assess the variation in replicate experiments compared to the overall variation across the entire design. Overall variability includes both systematic and random variations from all experimental runs, while replicate variability focuses on variations within repeated experiments (pure error), which should ideally be much lower than the overall variability. After reviewing the raw data, adjusting the responses as needed, and eliminating any outliers, a regression analysis was performed. The model was fitted using the respective

equation for each design, and its statistical significance was evaluated by calculating the proportion of response variation explained by the model (R2) and the proportion of variation predicted by the model (Q2). These values, ranging from 0 to 1, indicate model fit, with 1 representing a perfect fit. For a model to be statistically significant, R2 should be greater than 0.5, and Q2 should exceed 0.1 (ideally 0.5 for a strong model). The model determines the regression coefficients, and the significance of experimental factors is assessed by their confidence intervals. Removing non-significant factors should improve both R2 and Q2 values. The software provides a square test for the coefficients plot when significant square terms are detected, and an interaction test helps identify significant interaction terms. Lastly, summary statistics for four parameters (R2, Q2, Model Validity, and Reproducibility) are provided, where a value of 1 (or 100%) indicates a perfect model. A Model Validity below 0.25 suggests issues such as outliers, an incorrect model, or a problem with data transformation, or it may indicate missing terms like interactions or square terms. For a reliable model, reproducibility should be higher than 0.5 [221].

# 4 Results and Discussion

The results and discussion section is divided into two parts. The first part includes the synthesis, synthesis optimization, and characterization of *N*-alkyl and *N*-acyl chitosan derivatives. The second part includes the cytotoxicity and NP forming capability of TMC, and the antibacterial and antioxidant activities of the chitosan-hydroxycinnamic acid conjugates.

## 4.1 Synthesis of chitosan *N*-derivatives

The first part of the research aimed to optimize procedures for *N*-alkylation of the primary amino group at the C-2 position on the glucosamine monomer and, thus, provide water-soluble *N*-derivatives with improved biological properties. More specifically, this work focused on optimizing TMC synthesis by utilizing several methods to find an efficient, single-step procedure that would give TMC with high DTM and no *O*-methylation while minimizing reaction time and reagent use.

The second part of the research work aimed to explore and optimize the synthesis of *N*-acyl chitosan, namely chitosan-hydroxycinnamic acid conjugates and *N*-betaine derivatives. The chitosan-hydroxycinnamic acid conjugates were prepared by TBDMS protection strategy, where TBDMS was used to protect the secondary hydroxyl group of chitosan at the C-3 position, and the primary hydroxyl group at the C-6 position, and the hydroxyl groups of the hydroxycinnamic acids. This was done to allow controllable and selective modification and to give derivatives with high DS. *N*-betaine chitosan derivatives were also prepared using the HATU coupling strategy, with the aim of developing an efficient, single-step method for the *N*-acylation of chitosan.

The synthesis methods for the *N*-alkyl and *N*-acyl derivatives were optimized with DoE approach.

### 4.1.1 TMC synthesis

TMC was synthesized using various methods, guided by a series of eight DoE designs. In each design, the optimal result served as the foundation for the subsequent design, allowing for iterative refinement and enhancement of the synthesis process to meet evolving objectives.

#### *4.1.1.1 Sequential designs – Designs 1-5*

In the initial sequential designs (Designs 1-5), the goal was to dissolve the starting material in a solvent, add reagents, and isolate the product in a single step without the

need for additional reagent rounds. Based on preliminary experiments, it was determined that the starting material must fully dissolve before adding the alkylating agent, and the reaction mixture should maintain low viscosity for efficient stirring. HCl was used to aid in dissolving the chitosan, with 1 gram of starting material and 40 mL of solvent used in all experiments, followed by BA after introducing the alkylating reagent. The methodology was refined iteratively by adjusting experimental conditions based on feedback from previous runs. The goal was to identify the optimal solvent system, alkylating agent, base, reaction time, and temperature (Scheme 3). These designs and their analyses were conducted without the use of MODDE software.

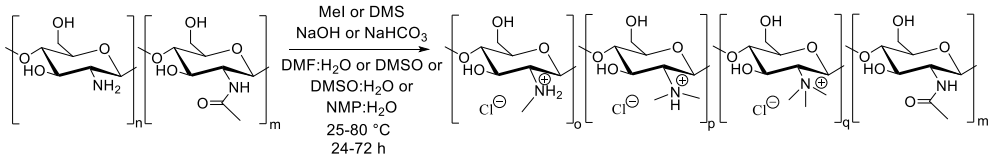


Scheme 3. Synthesis methods for the production of TMC throughout Designs 1-5.

As shown in Figure 4 (next page), in Design 1, the effects of using a strong or mild base (1 M NaOH or $NaHCO_3$) and varying the BA (one or two additions) were investigated. With one addition, all of the base (4 eq) was added 30 min after the alkylating agent (MeI). For two additions, the first base (2 eq) was added after 30 min, followed by the second (2 eq) 24h later. Using 1 M $NaHCO_3$ with two additions resulted in the highest DTM (21%) for this design. In Design 2, $NaHCO_3$ was tested both as a 1 M solution and as a solid powder, along with varying the DMF:$H_2O$ solvent ratio (1:1, 1:3, 3:1). The highest DTM (24%) was achieved with a 1:1 DMF:$H_2O$ ratio and $NaHCO_3$ in solution form. In Design 3, the effects of different alkylating agents (MeI/DMS) and solvent systems (DMF:$H_2O$/DMSO:$H_2O$/NMP:$H_2O$) were investigated. MeI in DMF:$H_2O$ produced the most favorable result, though other solvent systems also showed efficacy. In Design 4, the effects of temperature (25°C/80°C) and reaction time (24/48/72h) were tested. The optimal conditions were 48h with 9h of reflux at 80°C, yielding a DTM of 50%. In Design 5, chitosan and its mesylate salt were tested as starting materials with MeI and DMS alkylating agents. DMS proved unsuitable for the synthesis (DTM 0–2%). Comparing the DTM results of experiments 13 (50%) and 18 (27%) highlights the advantage of using DMF:$H_2O$ solvent system. In Design 5, the highest DTM (46%) was achieved with mesylate salt and MeI in DMSO solvent (17), demonstrating the potential of chitosan mesylate salt for efficient trimethylation. However, for simplicity and to avoid multistep reactions, chitosan as a starting material remains preferable for this study's objectives. No *O*-methylation was detected in the experiments.

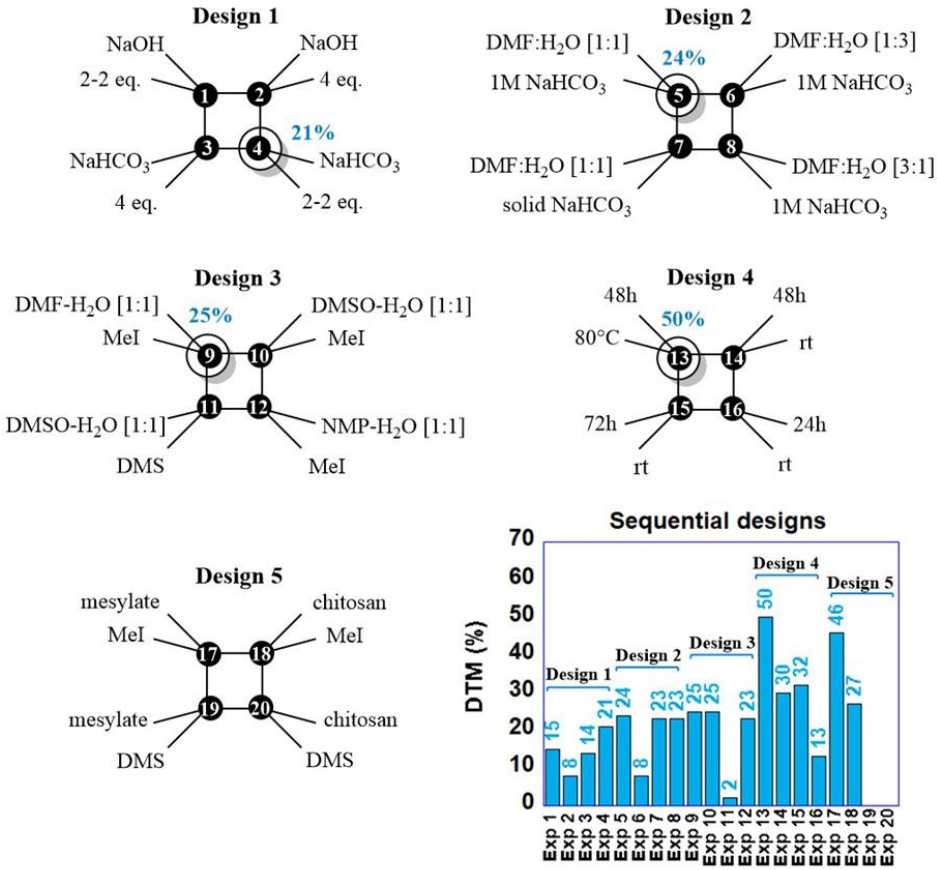


Figure 4. The schematic representation of the sequential designs (Designs 1-5), where two factors were varied at two or three levels in each design. The circled numbers identify the experiments that yielded the optimal result (i.e., the highest DTM in each respective design). These optimal conditions were then fixed for the subsequent designs, allowing other factors to be explored. The column chart provides a summary of all the experimental outcomes.

### *4.1.1.2 Fractional FD – TMC (Design 6)*

After completing the five sequential designs, a screening phase was conducted using a fractional FD (Design 6). The previous findings established the foundation for setting up the design in MODDE. As a starting point, chitosan was used as the base material, MeI as the alkylating agent, $NaHCO_3$ as the base, and DMF:$H_2O$ with 1.5 eq HCl as the solvent system. In this screening design, the impact of the molar ratios of MeI/chitosan and $NaHCO_3$/chitosan, temperature, and reaction time at three levels ($3^4$) was evaluated, with the DTM (%) selected as the response variable (Scheme 4, next page).

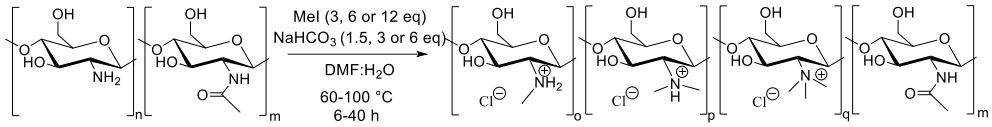


Scheme 4. Synthesis methods for the production of TMC in Design 6.

The design included 12 experiments, with three replicates. Table 6 outlines the reaction conditions and results. The screening utilized an L9 design (3 levels), incorporating both linear and quadratic terms in the model to capture potential linear and non-linear effects on the DTM, allowing for the estimation of square terms but not factor interactions.

Table 6. The reaction conditions for the synthesis of TMC were investigated using a fractional FD, with four factors varied across three levels (Design 6). The DTM (%) was used as the response variable. The highest DTM achieved in this design was 59%.

| Exp | MeI (eq) | $NaHCO_3$ (eq) | Temp. (°C) | Time (h) | DTM (%) |
|---|---|---|---|---|---|
| 21 | 3 | 1.5 | 60 | 6 | 10 |
| 22 | 3 | 3 | 80 | 20 | 20 |
| 23 | 3 | 6 | 100 | 40 | 14 |
| 24 | 6 | 1.5 | 80 | 40 | 7 |
| 25 | 6 | 3 | 100 | 6 | 14 |
| 26 | 6 | 6 | 60 | 20 | 34 |
| 27 | 12 | 1.5 | 100 | 20 | 8 |
| 28 | 12 | 3 | 60 | 40 | 59 |
| 29 | 12 | 6 | 80 | 6 | 53 |
| 30 | 6 | 3 | 80 | 20 | 57 |
| 31 | 6 | 3 | 80 | 20 | 42 |
| 32 | 6 | 3 | 80 | 20 | 50 |

Figure 5A (next page) presents the summary of fit, showing that the fractional FD demonstrates high significance (R2 = 0.86), good model validity (0.72) without the need for transformation, accurate future prediction precision (Q2 = 0.60), and strong reproducibility (0.87). Among the four factors tested, the molar ratio of MeI/chitosan (p=0.02), the molar ratio of $NaHCO_3$/chitosan (p=0.02), and reaction temperature (p=0.04) were significant, while reaction time (p=0.93) was not (Figure 5B). A term is considered significant in the software if it is far from the y=0 line and its uncertainty does not cross the line. Conversely, a non-significant term is close to the y=0 line, with its uncertainty crossing it. Statistical significance is indicated by the P-value, which ranges from 0 to 1, with lower values showing that observed differences are unlikely to be due to chance [222]. Non-significant factors, like time ($X_4$), were removed from the equation used to enhance the model fit (see 3.4.2., page 34). The absence of a square term for the molar ratio of MeI/chitosan led to the exclusion of $\beta_{11}$ from the equation as well. Therefore, reducing reaction time should not negatively impact the response. The molar

ratio of MeI/chitosan exhibited a linear relationship with increasing DTM, while temperature and base acted as square terms. Results showed that increasing temperature reduced DTM within the tested range of 60–100°C, suggesting an optimal temperature for the reaction. The residuals normal probability plot (Figure 5C) confirmed that residuals are normally distributed with no outliers. The replicate plot (Figure 5D) displayed tight clustering of the three replicates, confirming high repeatability. DTMs of the replicates were obtained with 6% relative standard deviation (RSD).

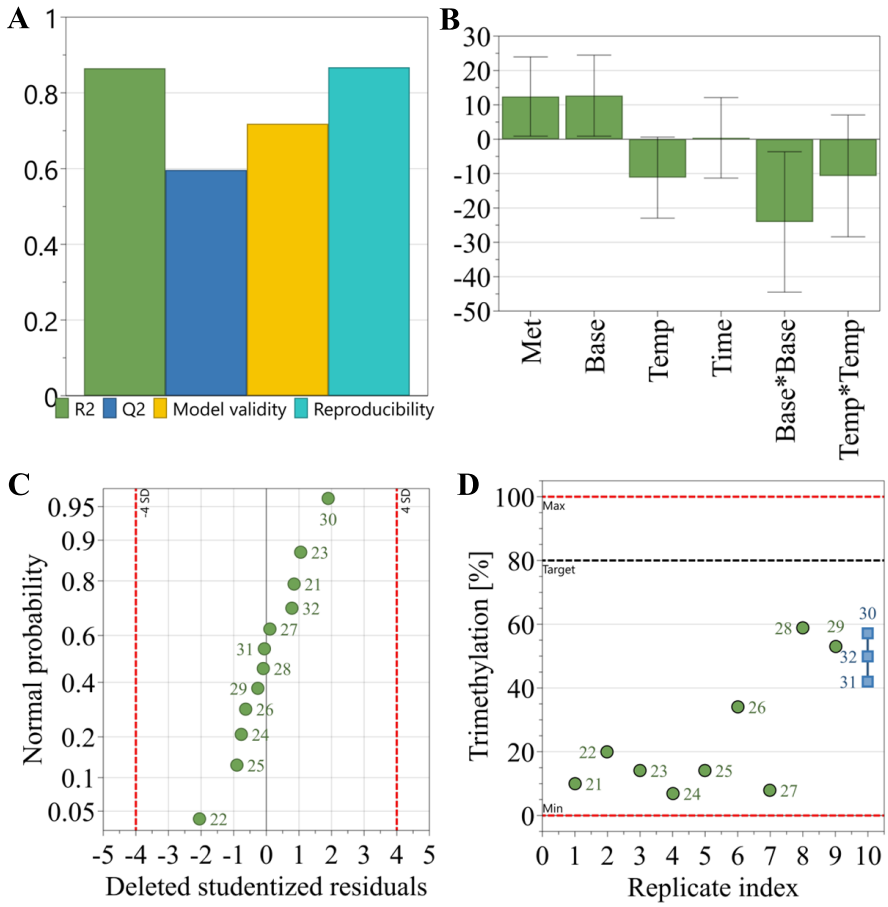


Figure 5. Results of the fractional FD (Design 6). A: Summary of fit plot for the fractional FD from MODDE, after excluding non-significant model terms. The R2 (green) value represents the fit of the experimental model, while Q2 (blue) estimates the accuracy of future predictions. B: Coefficient plot displays the factors (from left to right): molar ratio of MeI/chitosan (Met), molar ratio of $NaHCO_3$/chitosan (base), temperature (temp), time, base*base (square term of the molar ratio of $NaHCO_3$/chitosan), and temp*temp (square term of the temperature). C: Residuals Normal Probability Plot, illustrating that the residuals follow a normal distribution. D: Replicate plot, showing the replicates (exp 30, 31, and 32) in light blue.

The contour plot analysis (Figure 6) provides valuable insights into the relationship between experimental factors and the response variable. It illustrates the effect of the

base/chitosan molar ratio on the DTM, showing that initially increasing the molar ratio enhances trimethylation. However, the plot reveals a critical threshold where further increases in the base begin to reduce trimethylation efficiency. This detailed analysis identifies the optimal conditions for maximizing the response and clarifies the subtle interactions between the factors and their impact on the chemical process.

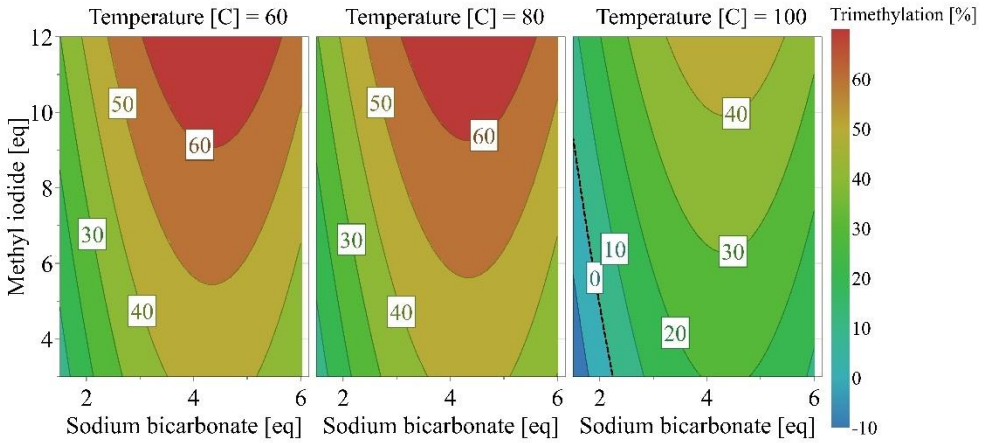


Figure 6. Response Contour Plot of Design 6. The X-axis represents the molar ratio of $NaHCO_3$/chitosan, and the Y-axis represents the molar ratio of MeI/chitosan. The plot is divided into three panels, showing temperature levels from left to right: 60°C, 80°C, and 100°C. The color gradient indicates different trimethylation degrees, with blue representing the lowest values and red the highest. The plot reveals that increasing the base/chitosan molar ratio enhances DTM until a critical point, after which further base addition reduces trimethylation efficiency.

Fractional FDs are primarily designed to identify main effects and highlight the individual impact of factors, but they provide limited insights into complex factor interactions. Additionally, quadratic terms are often used as approximations, and in this case, the precision of the temperature's square term is reduced, as indicated by a significant uncertainty range that crosses the y=0 line. As a result, further investigation of temperature was considered necessary using a more detailed design. Moreover, the study of BA was extended due to issues related to viscosity. No *O*-methylation was detected in the experiments.

### *4.1.1.3 Full FDs – TMC (Designs 7-8)*

A full FD (Design 7) was conducted with two factors—temperature and BA—each at three levels ($3^2$) (Scheme 5, next page), with DTM (%) as the response variable.

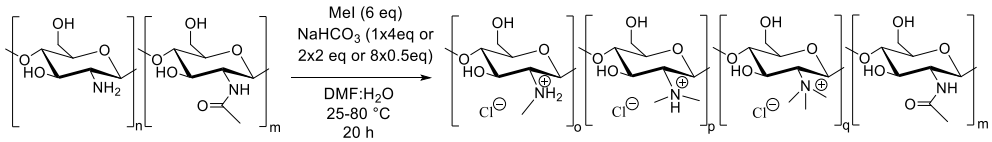

Scheme 5. Synthesis methods for the production of TMC in Design 7.

The earlier fractional FD (Design 6) established a linear relationship between the molar ratio of MeI/chitosan and DTM, with sufficient trimethylation observed at the midpoint (6 eq). In the screening design, the highest DTM (59%) was achieved using 12 eq MeI, while 6 eq MeI yielded up to 57% trimethylation. Since the study also aimed to minimize reagent use, the molar ratio of MeI was fixed at 6 eq for Design 7. The molar ratio of $NaHCO_3$/chitosan, previously identified as a square term, was estimated to have an optimum at 4 eq. However, BA increased viscosity, making it difficult to stir the reaction mixture. To address this, the possibility of divided BA was explored as the second factor in the full FD. The molar ratio of $NaHCO_3$/chitosan was fixed at 4 eq, and three levels were chosen for the BA: a single addition (1x4 eq), two additions (2x2 eq) 6h apart, and gradual addition (8x0.5 eq) over 6h using an addition funnel. Since time was found to be non-significant in earlier experiments, 20h was selected as the reaction time for practical work-up purposes, although 6h would have been sufficient. The full FD included 12 experiments, with four replicates. The temperature was varied at 25°C, 60°C, and 80°C. The reaction conditions and corresponding results are shown in Table 7.

Table 7. Reaction conditions and results for the synthesis of TMC, a full FD with two factors varied on three levels ($3^2$) with DTM (%) as the response (Design 7). BA=base addition. The highest DTM obtained was 72%. *For the gradual addition, the base was introduced in small, 0.5 eq increments using an addition funnel over a 6h period.

| Exp | BA | Temp. (°C) | DTM (%) |
|---|---|---|---|
| 33 | 1 | 25 | 18 |
| 34 | 1 | 60 | 41 |
| 35 | 1 | 80 | 54 |
| 36 | 2 | 25 | 8 |
| 37 | 2 | 60 | 72 |
| 38 | 2 | 80 | 41 |
| 39 | Gradual* | 25 | 14 |
| 40 | Gradual* | 60 | 42 |
| 41 | Gradual* | 80 | 15 |
| 42 | 2 | 60 | 70 |
| 43 | 2 | 60 | 66 |
| 44 | 2 | 60 | 51 |

In Design 7, the highest DTM achieved was 72%, recorded in experiment 37 (60°C with two BA). Figure 7A (next page) presents a summary of fit, showing that the model has high significance (R2=0.68), good model validity (0.61), no need for transformation, and sufficient predictive precision (Q2=0.58). The model also demonstrates good reproducibility (0.83). No interaction was found between BA and temperature, and the BA was determined to be a non-significant factor (p=0.16, Figure 7B). This indicates

that the base can be added incrementally without affecting the DTM, which is important for addressing viscosity issues. Adding the base in two or more portions reduces the reaction mixture's viscosity, facilitating stirring. While gradual BA is not necessary for optimal DTM, it plays a crucial role in preventing viscosity problems. Temperature was confirmed as a square term (Figure 7B), consistent with the previous fractional FD results. The temperature's effect was non-linear, with the highest DTM achieved at 60°C. Performing the reaction at rt (25°C) resulted in insufficient trimethylation and increased viscosity, which should be avoided. Higher temperatures (60°C and 80°C) prevented viscosity issues when paired with incremental BA. However, 60°C yielded better DTM results compared to 80°C due to the non-linear nature of the temperature factor. The residuals normal probability plot (Figure 7C) shows normally distributed residuals with no outliers. Figure 7D displays the four replicates, confirming high repeatability. DTMs of the replicates were obtained with 13% RSD.

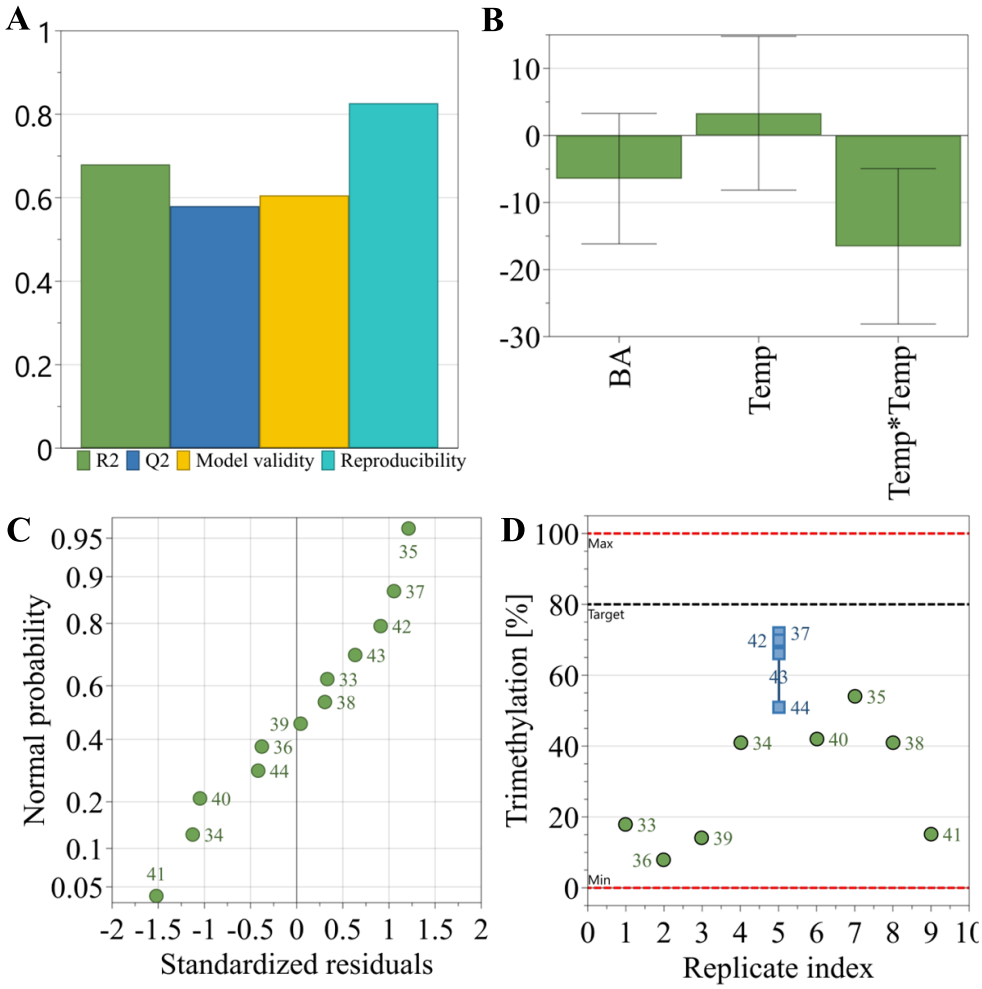

Figure 7. Results of the full FD (Design 7). A: Summary of fit plot for the full FD, after removing non-significant model terms. The R2 (green) indicates the model's fit, while Q2 (blue) estimates the precision of future predictions. B: Coefficient plot, showing (from left to right) the factors: BA = base addition, temperature, and temp*temp (square term of temperature). C: Residuals Normal Probability Plot, demonstrating that the residuals follow a normal distribution. D: Replicate plot, with the replicates (exp 37, 42, 43, and 44) displayed in light blue and connected by a straight line.

The reaction conditions for achieving the highest DTM (72%) in Design 7 were as follows: 1 eq chitosan, 40 mL DMF:$H_2O$ (1:1) with 1.5 eq HCl, 6 eq MeI, 4 eq $NaHCO_3$ added in two portions (2x2 eq, 6h apart), with a reaction time of 20h at 60°C. No *O*-methylation was detected in the experiments.

When comparing these results with previously reported methods for TMC synthesis, the benefits of the newly developed process become clear. The Muzzarelli method [44], though achieving up to 35% DTM, is time-consuming, requiring multiple steps. Other reductive methylation techniques [177,223,224] reach high DQ but also involve long reaction times and excessive reagent use. Methods using DMS offer a cost-effective alternative but result in significant *O*-methylation [182]. Additionally, in our experiments, using DMS resulted in only 0-2% DTM. In contrast, while TBDMS-based approaches achieve up to 100% DTM, they involve complicated multi-step procedures that are not cost-effective or scalable [181]. A study by Senra *et al*. using DoE for TMC synthesis optimization identified that the primary factors influencing DTM were the interaction between NaOH concentration and MeI molar ratio, along with the linear effects of NaOH concentration, reaction time, and MeI molar ratio, all of which increased DTM [207]. However, interaction terms such as reaction time with NaOH concentration and MeI ratio negatively impacted DTM. Our findings also showed a linear correlation between MeI molar ratio and increasing DTM, but reaction time was non-significant, and the base effect followed a square term pattern, possibly due to using $NaHCO_3$ instead of NaOH. Furthermore, their method resulted in 67% DTM with significant *O*-methylation using 36 eq MeI, while ours achieved 72% DTM with only 6 eq MeI and no *O*-methylation, demonstrating a more efficient and economical approach.

#### *4.1.1.4 Assessment of different bases and solvent systems (exp 45-72)*

Notably, Design 7 achieved a significant reduction in reagent use, and a shorter reaction time of 20h, thereby lowering costs. Despite these reductions, a highly *N*-substituted product (up to 72% DTM) was obtained in a single step, without any detectable *O*-methylation. The use of $NaHCO_3$ proved beneficial for achieving high DTM. However, as $NaHCO_3$ reacts with HCl, it releases $CO_2$, leading to gas evolution. The incremental addition of $NaHCO_3$ addressed these concerns to some extent, though this approach poses scalability challenges in closed systems due to the risk of pressure buildup.

Thus, NaOH, $NaHCO_3$, and seven non-nucleophilic bases (TEA, DBU, DBN, KOtBu, DtBP, DEA, and DIPEA) were used in the synthesis of TMC (exp 45-62, Scheme 6). For each base, two experiments were performed: in the first, the base (4 eq) was added in a single portion, while in the second, it was added in two equal portions (2 eq each)

with a 6h interval. Additional experiments (exp 63-72) were carried out using DIPEA, testing increased solvent volumes and different solvent systems. Furthermore, the viscosity of the reaction mixtures was monitored. The reaction conditions and the results are summarized in Table 8 (next page).

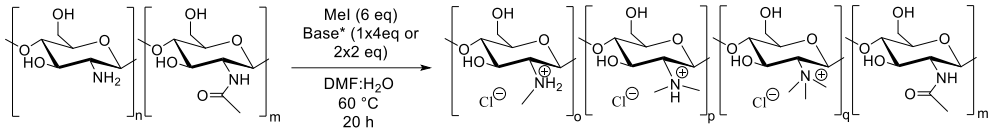


*NaOH, $NaHCO_3$, TEA, DBU, DBN, KOtBu, DtBP, DEA, and DIPEA

Scheme 6. Synthesis methods for the production of TMC in the base experiments (exp 45-62).

Table 8. Base evaluation experiments for TMC synthesis. The experiments were conducted using NaOH, $NaHCO_3$, and seven non-nucleophilic bases. In each experiment, 6 eq MeI and a DMF:$H_2O$ solvent system with 1.5 eq HCl were used. Each base underwent two trials (see base addition in the table): in the first, 4 eq of base was added all at once, while in the second, the base was added in two equal portions (2 eq-2 eq) with a 6h interval. The concentration of chitosan in the solvent was maintained at 25 mg/mL across all experiments, and viscosity measurements were taken at 60°C, 30 min after the full base addition.*Exp 62B is the result of a repeated trimethylation.

| Exp | Base | Base addition | DTM (%) | DDM (%) | DMM (%) | Viscosity at 60°C (cP) |
|---|---|---|---|---|---|---|
| 45 | NaOH | 1 | 7 | 57 | 36 | >300 |
| 46 | NaOH | 2 | 15 | 77 | 8 | >300 |
| 47 | $NaHCO_3$ | 1 | 41 | 58 | 1 | 97.3 |
| 48 | $NaHCO_3$ | 2 | 72 | 28 | 0 | 58.7 |
| 49 | TEA | 1 | 10 | 49 | 41 | 11.7 |
| 50 | TEA | 2 | 3 | 57 | 40 | 7.1 |
| 51 | DBU | 1 | 0 | 0 | 0 | 106 |
| 52 | DBU | 2 | 0 | 0 | 0 | 90.3 |
| 53 | KOtBu | 1 | 5 | 50 | 45 | >300 |
| 54 | KOtBu | 2 | 10 | 66 | 24 | 242 |
| 55 | DEA | 1 | 5 | 54 | 41 | 7.9 |
| 56 | DEA | 2 | 6 | 54 | 40 | 6 |
| 57 | DBN | 1 | 3 | 40 | 57 | 67.2 |
| 58 | DBN | 2 | 10 | 74 | 16 | 45.7 |
| 59 | DtBP | 1 | 0 | 15 | 85 | >300 |
| 60 | DtBP | 2 | 0 | 27 | 73 | >300 |
| 61 | DIPEA | 1 | 27 | 71 | 2 | 31.9 |
| 62 | DIPEA | 2 | 58 | 41 | 1 | 19.1 |
| 62B | DIPEA | 2 | 93* | 7 | 0 | 22.3 |

While certain bases (TEA, DEA, DBU, DBN) resulted in low viscosity, they also contributed to low DTM (0-10%). On the other hand, bases like NaOH, KOtBu, and DtBP caused increased viscosity upon addition, along with limited DTM (0-15%). $NaHCO_3$ proved to be the most effective, yielding the highest DTM (72%) with lower viscosity compared to NaOH, a commonly used base for TMC synthesis. Thus, $NaHCO_3$ stands out as a favorable alternative, offering improvements in both viscosity and trimethylation efficiency. However, for upscaling the reaction, further viscosity reduction is crucial to ensure proper stirring. DIPEA (exp 61, 62) showed promising results, with lower viscosity (31.9 and 19.1 cP) compared to $NaHCO_3$ (97.3 and 58.7 cP), while still achieving good trimethylation (27% and 58%). When the product of exp 62 underwent repeated trimethylation, nearly full trimethylation was achieved (exp 62B, 93%).

Additionally, the BA method proved to be significant; adding the base in two equal portions, 6h apart, consistently reduced viscosity compared to single-step addition in all experiments. Notably, adding all 4 eq of NaOH at once (exp 45) resulted in a gel-like mixture that hindered stirring, leading to low DTM (7%). In most experiments, the two-step addition method improved DTM, highlighting the importance of maintaining low viscosity and effective stirring for optimal trimethylation.

The subsequent experiments (exp 63-72) focused on using DIPEA as the base while diluting the reaction medium with various solvents and examining the effects of gradual BA. The reaction conditions and the results are summarized in Table 9.

Table 9. TMC synthesis using DIPEA base in various solvent systems, including DMF:$H_2O$ (1:1), DMF, and DMSO, with different chitosan/solvent concentrations (25, 12.5, and 8.3 mg/mL). All experiments were carried out at 60°C for 20h, with 6 eq MeI and 4 eq DIPEA. The base addition refers to the amount of increments the 4 eq base was divided into. *In case of gradual addition, 0.095 eq (approximately 1 drop) of DIPEA was added every 8.5 min, for a total of 42 additions.

| Exp | Solvent | Chitosan conc. (mg/mL) | MeI conc. (mg/mL) | Base (DIPEA) addition | DTM (%) | DDM (%) | DMM (%) | Viscosity at 60°C (cP) |
|---|---|---|---|---|---|---|---|---|
| 62 | DMF:$H_2O$ | 25 | 130 | 2 | 58 | 41 | 1 | 19.1 |
| 63 | DMF | 25 | 130 | 2 | 68 | 30 | 2 | 23.4 |
| 64 | DMSO | 25 | 130 | 2 | 56 | 31 | 13 | 28 |
| 65 | DMF:$H_2O$ | 12.5 | 65 | 2 | 23 | 71 | 6 | 17.1 |
| 66 | DMF | 12.5 | 65 | 2 | 10 | 79 | 11 | 17.5 |
| 67 | DMSO | 12.5 | 65 | 2 | 67 | 30 | 3 | 19.3 |
| 68 | DMF | 12.5 | 65 | gradual* | 65 | 30 | 5 | 9.9 |
| 69 | DMF:$H_2O$ | 8.3 | 43.3 | 2 | 20 | 75 | 5 | 7.7 |
| 70 | DMF | 8.3 | 43.3 | 2 | 8 | 75 | 17 | 8.4 |
| 71 | DMSO | 8.3 | 43.3 | 2 | 53 | 39 | 8 | 8.6 |
| 72 | DMF | 8.3 | 43.3 | gradual* | 47 | 49 | 4 | 5.9 |

Using DMF:$H_2O$ solvent (exp 62, 65, 69) resulted in high DTM only at a chitosan/solvent concentration of 25 mg/mL. Increasing the solvent volume negatively impacted DTM, showing that dilution does not support effective trimethylation. A similar trend was observed with pure DMF solvent (exp 63, 66, and 70). In contrast, when DMSO was used (exp 64, 67, 71), it consistently produced satisfactory trimethylation across all tested concentrations. However, the increased solvent volume with DMSO posed challenges during work-up, as DMSO crystals formed during cold EtOH precipitation, complicating product isolation. Therefore, DMSO was deemed unsuitable

for TMC synthesis in a diluted medium. Pure DMF, while not yielding high DTM at larger solvent volumes (exp 67, 71), maintained low reaction mixture viscosity, simplifying the work-up and improving yield. This led to further evaluation of DMF in combination with gradual DIPEA BA (exp 68, 72). Incremental BA (0.095 eq DIPEA every 8.5 min) resulted in better DTM compared to the two-step method. Exp 68, with a chitosan/solvent concentration of 12.5 mg/mL, yielded a DTM of 65%. Exp 72 with a concentration of 8.3 mg/mL, resulted in 47% DTM. Recognizing the difficulty of manually adding DIPEA in precise intervals (0.095 eq every 8.5 min), a full FD was implemented to optimize the process of incremental BA. These findings prompted further exploration of using DMF solvent with incremental DIPEA addition in a full FD (Design 8), aiming to optimize the incremental BA process for practical large-scale application.

The findings from the base experiments (exp 45-62) and the evaluation of various solvent systems and chitosan concentrations (exp 63-72) provided the foundation for the next full FD (Design 8) which examined two factors across three levels. Variations in the molar ratio of the MeI/chitosan (6, 9, and 12 eq) and BA addition (4, 6, or 8 equal increments, added dropwise at regular intervals using an addition funnel) were studied (Scheme 7).

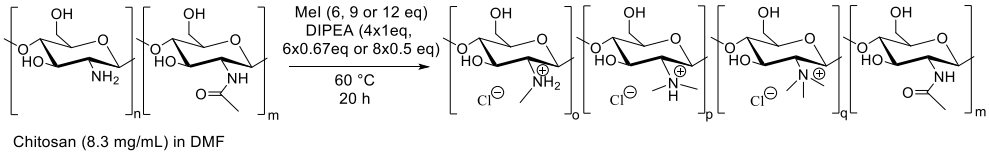


Scheme 7. Synthesis methods for the production of TMC in Design 8.

The aim was to achieve high DTM in a diluted medium. As a result, the chitosan concentration was maintained at 8.3 mg/mL in all experiments, with MeI concentrations of 43, 65, and 87 mg/mL corresponding to the 6, 9, and 12 eq molar ratios, respectively. The results are summarized in Table 10 (next page).

Table 10. Reaction conditions and results for the synthesis of TMC, a full FD with two factors varied on three levels ($3^2$) with DTM (%) as the response. BA = Base addition. All experiments were carried out at 60°C for 20h with 4 eq DIPEA. The highest DTM obtained was 68%. The base addition refers to the number of increments into which the 4 eq DIPEA was divided.

| Exp | MeI (eq) | BA | DTM (%) |
|---|---|---|---|
| 73 | 6 | 4 | 18 |
| 74 | 9 | 4 | 27 |
| 75 | 12 | 4 | 48 |
| 76 | 6 | 6 | 24 |
| 77 | 9 | 6 | 32 |
| 78 | 12 | 6 | 50 |
| 79 | 6 | 8 | 47 |
| 80 | 9 | 8 | 56 |
| 81 | 12 | 8 | 68 |
| 82 | 9 | 6 | 28 |
| 83 | 9 | 6 | 27 |
| 84 | 9 | 6 | 33 |

In the full FD (Design 8), the highest DTM achieved was 68% (exp 81), using 12 eq MeI and 8 increments of DIPEA (0.5 eq added every 2.5h). This result is comparable to the 68% trimethylation observed in exp 63, where a higher chitosan concentration of 25 mg/mL in DMF was used. It demonstrates that the same DTM can be attained in a more diluted medium (8.3 mg/mL chitosan concentration) by increasing the molar ratio of the alkylating agent. Although more MeI was needed, its concentration in the reaction medium was lower (87 mg/mL) compared to exp 63 (130 mg/mL). This result is also similar to exp 48 (72% DTM), where $NaHCO_3$ was used as the base, but with the advantage of avoiding increased viscosity in the reaction mixture, confirming the effectiveness of this new method. Figure 8A (next page) presents the summary of fit, highlighting the model's high significance (R2=0.97), strong predictive precision (Q2=0.87), model validity (0.84), and excellent reproducibility (0.96). Figure 8B shows the coefficient plot, indicating that both the molar ratio of MeI/chitosan and BA were significant model terms, with regression coefficients of 9.50 and 9.62, respectively. Both factors also showed non-linear effects, as reflected by their square terms, with regression coefficients of 3.12 and 5.17, respectively. The interaction term MeI*BA was non-significant (-1.23).

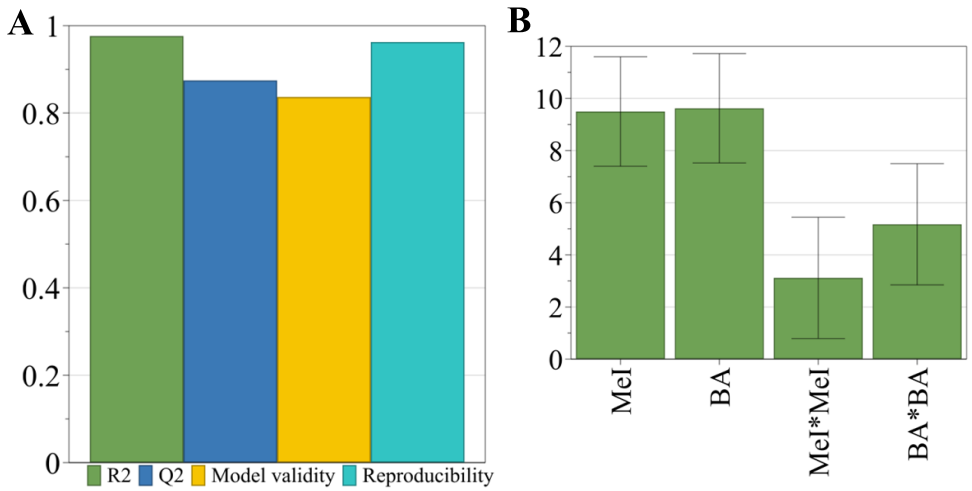


Figure 8. Results of the full FD (Design 8). A: Summary of fit plot for the full FD, after removing non-significant model terms. The R2 (green) indicates the model's fit, while Q2 (blue) estimates the precision of future predictions. B: Coefficient plot, showing (from left to right) the factors: MeI = MeI/chitosan molar ratio, BA = base addition, MeI*MeI (square term of MeI/chitosan molar ratio, and BA*BA (square term of BA).

The residuals normal probability plot (Figure 9A) indicates that there are no outliers, with the residuals displaying a normal distribution, shown as a straight line along the diagonal. The replicate plot (Figure 9B) illustrates the variation across all experiments, with replicated experiments (exp 77, 82 ,83, 84) appearing in blue and connected by a line. The small variability observed among the replicates suggests the model's robustness, with replicate variability being significantly lower than the overall variability.

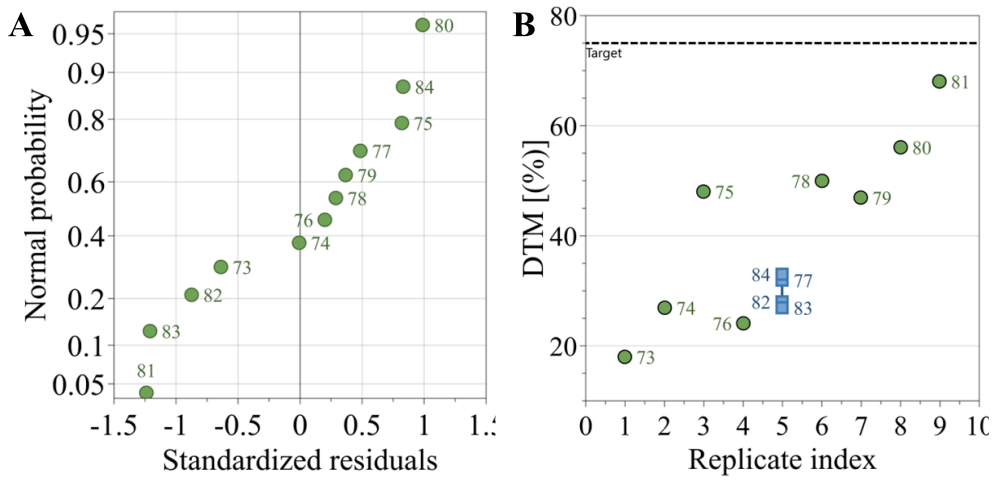


Figure 9. Results of the full FD (Design 8). A: Residuals Normal Probability Plot, demonstrating that the residuals follow a normal distribution. B: Replicate plot, with the replicates (exp 77, 82, 83, and 84) displayed in light blue and connected by a straight line.

The response contour plot (Figure 10) provides detailed insights into the interaction between experimental factors and the response variable. It shows that incremental additions of the base positively influence DTM, with more increments leading to enhanced trimethylation. Additionally, the plot highlights that higher molar ratios of MeI/chitosan result in increased trimethylation. Both factors demonstrate non-linear behavior, suggesting optimal conditions for maximizing the desired response.

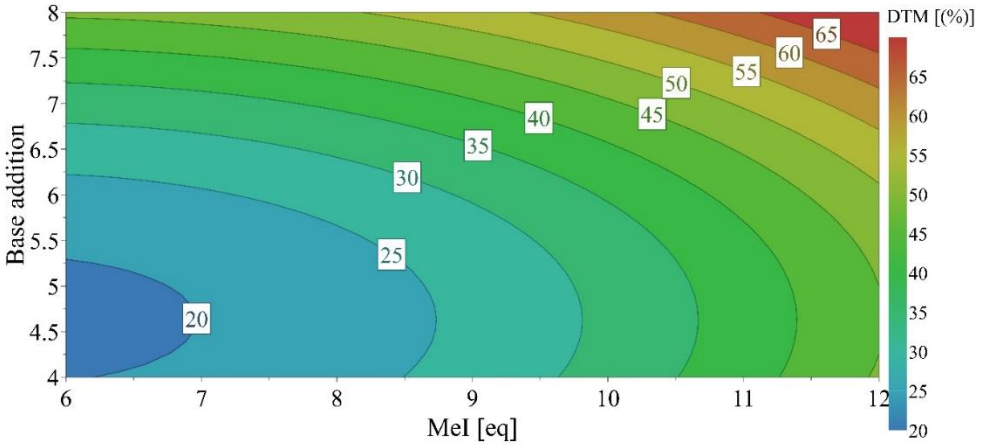


Figure 10. Response Contour Plot of Design 8. The X-axis represents the molar ratio of MeI/chitosan, and the Y-axis represents the base addition (BA). The color gradient indicates different trimethylation degrees, with blue representing the lowest values and red the highest.

With the optimized method, high trimethylation can be achieved in a diluted medium, within a low-viscosity solution, and without gas production, making it adaptable for large-scale synthesis in a closed reactor. This study marks the first successful use of DIPEA as a base in TMC synthesis, proving to be a superior alternative to NaOH and $NaHCO_3$. DIPEA effectively maintains a stable pH throughout the reaction, crucial for controlling reaction kinetics and minimizing side reactions and by-products. Additionally, no *O*-methylation was observed in the TMC products.

### 4.1.2 *N*-acylation of chitosan

This part of the work sought to optimize the *N*-acylation procedures focusing on two types of *N*-acyl chitosan, namely chitosan-hydroxycinnamic acid conjugates and *N*-betaine chitosan. The chitosan-hydroxycinnamic conjugates were synthesized using the TBDMS protection strategy, masking the hydroxyl groups of the polymer, as well as the hydroxyl groups of the antioxidants, to result in amide linkages. Next, *N*-betaine chitosan products were synthesized with HATU coupling strategy. Both methods were investigated by a full FD DoE design.

### *4.1.2.1 Full FD– Chitosan-cinnamic acid conjugate (Design 9)*

The synthesis optimization of chitosan-hydroxycinnamic acid conjugates initially began as part of my MSc project at the University of Iceland, under the supervision of Prof. Már Másson, entitled "*Chitosan-natural antioxidant conjugates: Synthesis, antimicrobial and antioxidant properties*". During the PhD studies, some data of the MSc research were re-analyzed. The manual DoE design used for synthesis optimization was input into MODDE software to gain a deeper understanding of the effects of different factors. A full FD (Design 9) which examined three factors across two levels was manually designed and conducted. The molar ratio of the cinnamoyl Cl/chitosan (0.25 and 1 eq), the molar ratio of the TEA/chitosan (2 and 7.6 eq) and the reaction time (24h and 48h) were studied (Scheme 8).

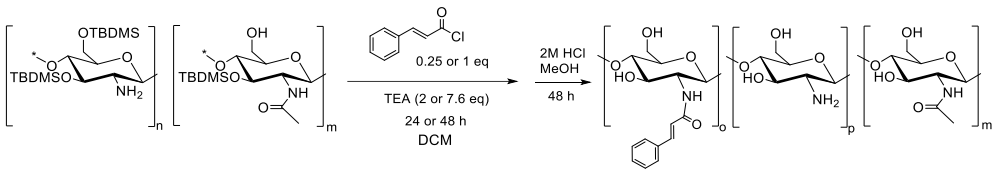


Scheme 8. Synthesis processes for the production of chitosan-cinnamic acid conjugates (Design 9).

The aim was to achieve high DS. Working with three factors at only two levels made the design and the analysis feasible without using specialized software. Three experiments (exp 85, 87, 91) were manually chosen for replication. The results are summarized in Table 11. Later, these results were analyzed using MODDE to understand the effect of the factors better.

Table 11. Reaction conditions and results for the synthesis of chitosan-cinnamic acid conjugates (Design 9), a full FD with three factors varied on two levels ($2^3$) with DS (%) as the response. The highest DS obtained was 15%.

| Exp | Cinnamoyl Cl (eq) | TEA (eq) | Time (h) | DS (%) |
|---|---|---|---|---|
| 85 | 0.25 | 2 | 24 | 9 |
| 86 | 1 | 2 | 24 | 15 |
| 87 | 0.25 | 7.6 | 24 | 9 |
| 88 | 1 | 7.6 | 24 | 13 |
| 89 | 0.25 | 2 | 48 | 9 |
| 90 | 1 | 2 | 48 | 15 |
| 91 | 0.25 | 7.6 | 48 | 8 |
| 92 | 1 | 7.6 | 48 | 15 |
| 93 | 0.25 | 2 | 24 | 10 |
| 94 | 0.25 | 7.6 | 24 | 10 |
| 95 | 0.25 | 7.6 | 48 | 7 |

In the full FD (Design 9), the highest DS achieved was 15% (exp 86, 90, 92). In all these experiments, 1 eq cinnamoyl Cl was used, highlighting the need for an excess of acyl chloride in the synthesis. Figure 11A (next page) presents the summary of fit, highlighting the model's high significance (R2=0.96), strong predictive precision (Q2=0.86), good model validity (0.78), and excellent reproducibility (0.95). Figure 11B shows the coefficient plot, indicating that the molar ratio of cinnamoyl Cl/chitosan was a significant model term, with a regression coefficient of 2.84. While the molar ratio of TEA/chitosan and the reaction time were non-significant model terms, with regression coefficients of -0.38 and -0.09, respectively, an interaction term was established between the time and molar ratio of cinnamoyl Cl/chitosan (0.60). The interaction between cinnamoyl Cl/chitosan molar ratio and reaction time suggests a synergistic effect, meaning that the combined influence of these factors enhances the DS more than each factor individually. However, the reaction time alone was a non-significant factor, implying that varying the time independently has little to no effect on the DS. The residuals normal probability plot (Figure 11C) indicates that there are no outliers, with the residuals displaying a normal distribution. The replicate plot (Figure 11D) illustrates the variation across all experiments, with replicated experiments (exp 85 and 93, 87 and 94, 91 and 95) appearing in blue and connected by a line. This experimental design was created manually, without the use of MODDE software and prior to formal training in DoE. As a result, the replicates were handled differently than ideal. Ideally, the same conditions would have been repeated 3-4 times for a more precise repeatability assessment. Nevertheless, the repeated experiments consistently produced strong results, highlighting the robustness of the design.

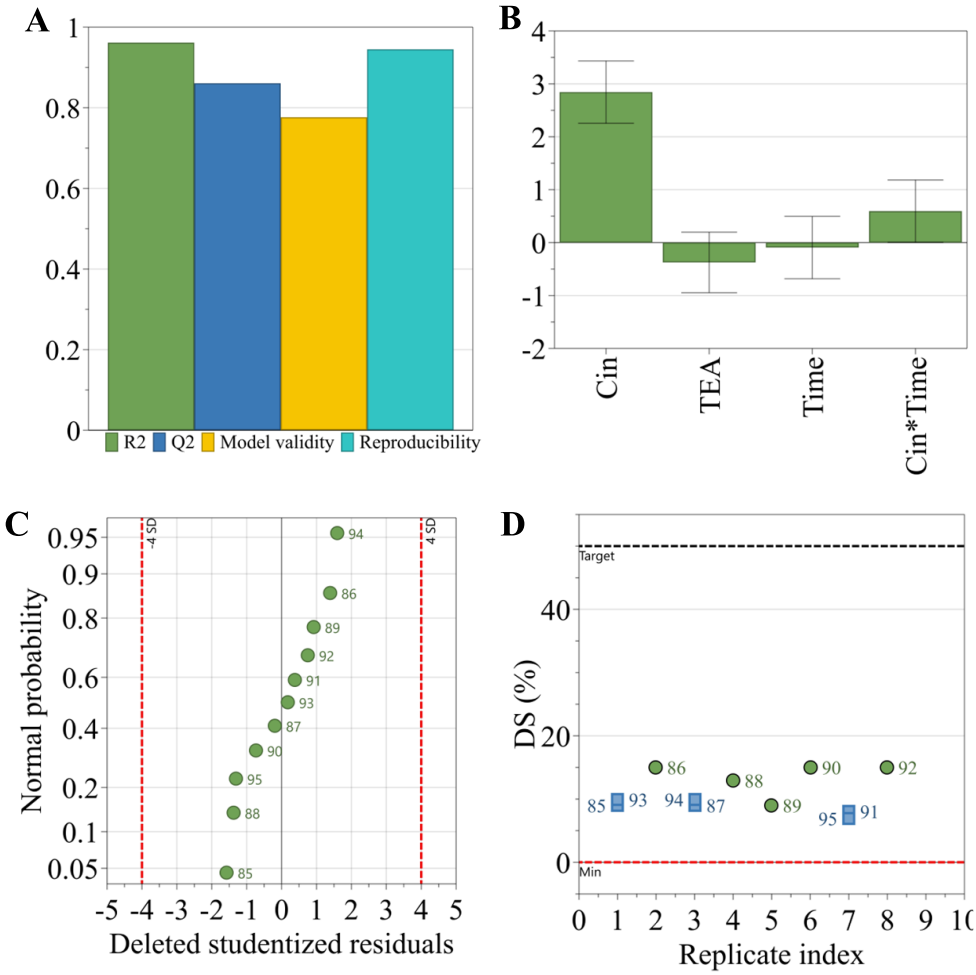


Figure 11. Results of the full FD (Design 9). A: Summary of fit plot for the full FD, after removing non-significant model terms. The R2 (green) indicates the model's fit, while Q2 (blue) estimates the precision of future predictions. B: Coefficient plot, showing (from left to right) the factors: Cin = cinnamoyl Cl/chitosan molar ratio, TEA = TEA/chitosan molar ratio, Time, Cin*Time = interaction term of cinnamoyl Cl/chitosan molar ratio and time. C: Residuals Normal Probability Plot, demonstrating that the residuals follow a normal distribution. D: Replicate plot, with the replicates (exp 85, 93, 87, 94, 91 and 95) displayed in light blue and connected by a straight line.

While the results did not fully achieve the goal of a high DS, the evident relationship between the molar ratio of cinnamoyl Cl to chitosan and the model's strong predictive accuracy suggests that increasing the equivalents of cinnamoyl Cl should lead to higher DS. However, since quadratic terms were excluded from the design, it remains uncertain whether this effect is purely linear or potentially non-linear.

Next, cinnamoyl Cl was applied in excess, with ratios of 2:1 (exp 96) and 3:1 (exp 97) of cinnamoyl Cl/chitosan, using 2 eq TEA and 24h reaction time. DS of 36% and 60% were obtained, respectively (Table 12).

Table 12. Synthesis of chitosan-cinnamic acid conjugate using excess cinnamoyl chloride.

| Exp | Cinnamoyl Cl (eq) | TEA (eq) | Time (h) | DS (%) |
|---|---|---|---|---|
| **86** | 1 | 2 | 24 | 15 |
| **96** | 2 | 2 | 24 | 36 |
| **97** | 3 | 2 | 24 | 60 |

Next, the remaining conjugates were synthesized (exp 98-106), with the following reaction conditions (based on the outcome of the optimization): The corresponding acyl chlorides were applied in 1:1, 2:1 and 3:1 molar ratio to chitosan. The reaction time was set to 24h with 2 eq TEA, in DCM solvent at 30-40°C (Scheme 9). The results are shown in Table 13.

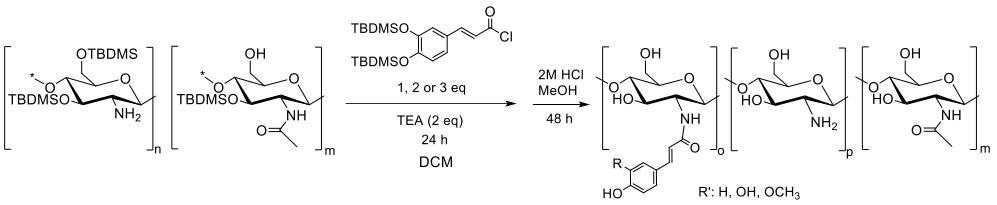


Scheme 9. Synthesis processes for the production of chitosan-hydroxycinnamic acid conjugates (exp 98-106).

Table 13. Synthesis of chitosan-antioxidant conjugates with ferulic, *p*-coumaric and caffeic acid.

| Exp | Reagent | Acyl chloride (eq) | DS (%) |
|---|---|---|---|
| 98 | TBDMS-Coumaroyl chloride | 1 | 9 |
| 99 | TBDMS-Coumaroyl chloride | 2 | 35 |
| 100 | TBDMS-Coumaroyl chloride | 3 | 40 |
| 101 | TBDMS-Feruloyl chloride | 1 | 3 |
| 102 | TBDMS-Feruloyl chloride | 2 | 17 |
| 103 | TBDMS-Feruloyl chloride | 3 | 27 |
| 104 | di-TBDMS-Caffeoyl chloride | 1 | 5 |
| 105 | di-TBDMS-Caffeoyl chloride | 2 | 13 |
| 106 | di-TBDMS-Caffeoyl chloride | 3 | 21 |

Chitosan-coumaric acid conjugates (exp 98-100) were obtained with 9%, 35% and 40% DS. Chitosan-ferulic acid conjugates (exp 101-103) were obtained with 3%, 17% and 25% DS. Lastly, chitosan-caffeic acid conjugates (exp 104-106) were obtained with 5%, 13% and 21% DS. The conversion was similar to cinnamoyl chloride for the TBDMS-coumaroyl chloride. In contrast, it was 50% less for the TBDMS-feruloyl- and di-TBDMS-caffeoyl chlorides. This variation may be due to the unstable nature of acyl chlorides, which tend to degrade or react prematurely, reducing their effectiveness in achieving higher DS. Acyl chlorides are highly reactive and susceptible to hydrolysis, particularly in the presence of moisture, which can lead to side reactions and decreased efficiency in the desired modification process.

### *4.1.2.2 Full FD– N-betaine chitosan (Design 10)*

*N*-betaine chitosan derivatives were prepared with HATU coupling strategy (exp 107-123), based on a previously published method [219], with the aim of developing an efficient, single-step method for *N*-acyl derivatives. Initially, preliminary experiments (exp 107-111, Scheme 10) were carried out using COS and chitosan (II). The details of the preliminary experiments are listed in Table 14. All experiments were carried out in DMSO solvent, with the addition of MSA in the case of using chitosan as the starting material.

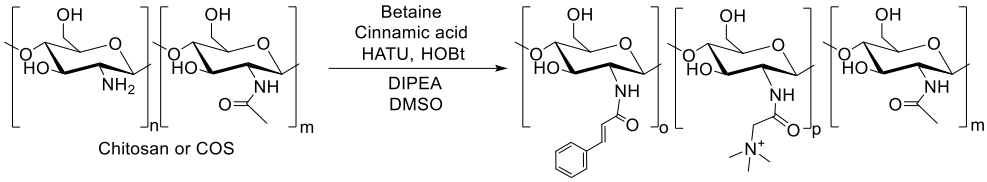


Scheme 10. Preliminary synthesis processes for the production of *N*-betaine chitosan (exp 107-111).

Table 14. Preliminary experiments for the synthesis of *N*-acyl chitosan. In all experiments, 15 ml DMSO solvent was used. In experiments 110-111, MSA was also added (3 eq).

| Exp | Starting material | Starting material (eq) | Cinnamic acid (eq) | Betaine (eq) | HATU (eq) | HOBt (eq) | DIPEA (eq) | Betaine DS (%) | Cinnamoyl DS (%) |
|---|---|---|---|---|---|---|---|---|---|
| 107 | COS | 5 | 0 | 1 | 1.1 | 1.1 | 1 | 20 | N/A |
| 108 | COS | 5 | 0 | 3 | 3.3 | 3.3 | 3 | 27 | N/A |
| 109 | COS | 5 | 1.5 | 1.5 | 3.3 | 3.3 | 3 | 30 | 9 |
| 110 | Chitosan II | 5 | 0 | 1 | 1.1 | 1.1 | 1 | 9 | N/A |
| 111 | Chitosan II | 5 | 0 | 3 | 3.3 | 3.3 | 3 | 11 | N/A |

Based on the preliminary experiments, it was concluded that the reaction works well when COS starting material is used, resulting in a full conversion (exp 107) for the betainoyl

DS (20%) (Figure 12A). In an attempt to increase the DS, the equivalents of the betaine, the coupling reagents as well as the DIPEA base were increased (exp 108). However, the conversion was not quantitative in this case. Instead of the expected 60% betainoyl DS, only 27% was observed (Figure 12B). Next, the addition of cinnamic acid was tested, to investigate the possibility of using HATU coupling for the synthesis of a chitosan-cinnamic acid conjugate (exp 109). Cinnamic acid and betaine were used in equal portions. While the betainoyl DS resulted in a quantitative conversion (30%), the cinnamoyl DS was found to be low (9%) (Figure 12C). Next, the reactions (exp 107-108) were repeated using chitosan as the starting material (exp 110-111). The betanoyl DS was found to be lower compared to the results with COS, indicating that the conversion is not quantitative. Hence, it was decided that the method for using polymeric chitosan would be optimized via DoE (Design 10).

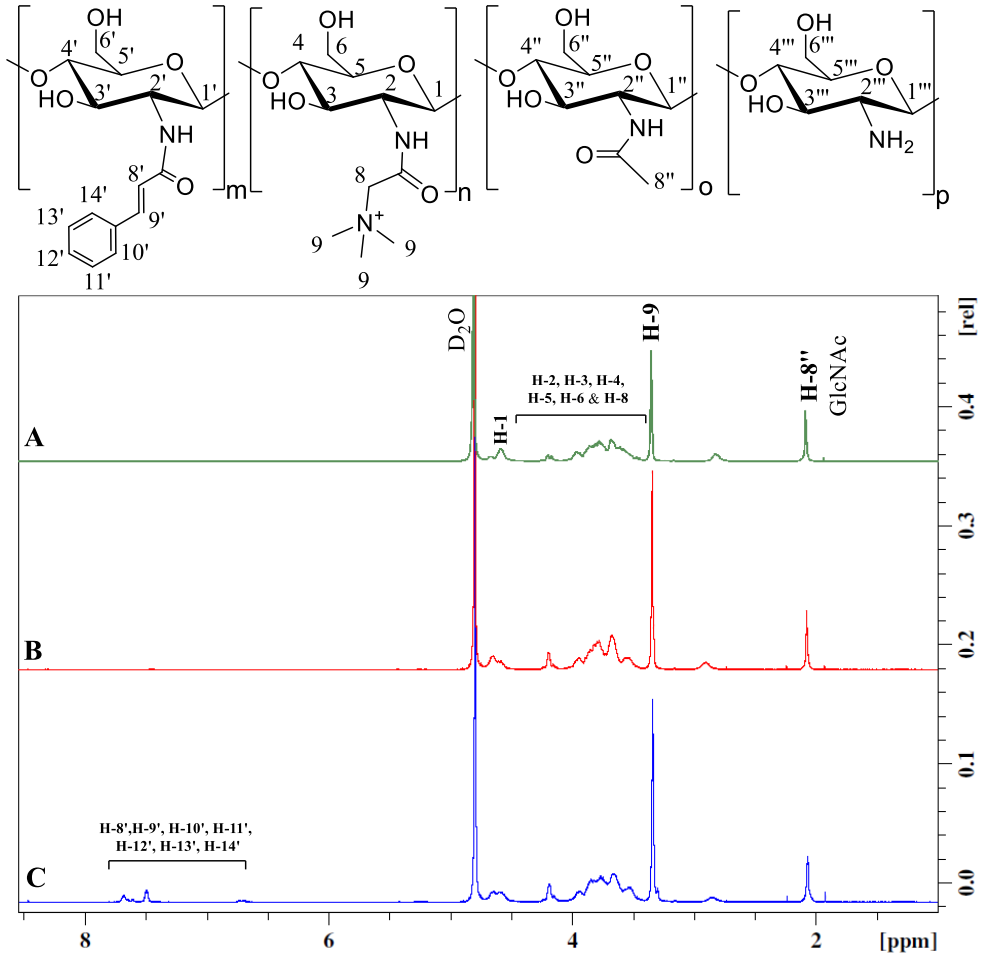


Figure 12. H NMR spectra of *N*-betaine COS. A: exp 107. B: exp 108. C: exp 109.

Before planning and performing the experiments of Design 10, further preliminary experiments were carried out by Luca Protti, testing various solvent systems and comparing TEA and DIPEA bases for the synthesis. His findings showed that TEA was a

better base for the reactions and that DMSO provided the best results as the solvent. I planned the experimental design, while the experiments of Design 10 and their H NMR analysis were carried out by Luca Protti. I analyzed the data using MODDE software in collaboration with Luca Protti. The aim was to achieve quantitative conversion of the betaine reagent into an *N*-acyl derivative, to facilitate the synthesis of chitosan derivatives with high DS and also to allow full control of the DS.

A full FD (Design 10) was performed to examine two factors that were varied across three levels. The factors were molar ratios of the HATU (0.75, 1.5 and 3 eq) and the TEA (5.5, 11.5 and 16 eq) relative to the betaine reagent (Scheme 11). All experiments were carried out at 60°C for 2h in DMSO solvent. HOBt and HATU were applied in equal portions.

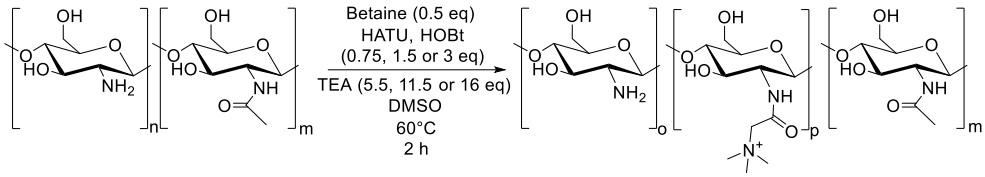


Scheme 11. Synthesis processes for the production of *N*-betaine chitosan (Design 10).

The results are summarized in Table 15.

Table 15. Reaction conditions and results for the synthesis of *N*-betaine chitosan (Design 10), a full FD with two factors varied on three levels ($3^2$) with DS (%) as the response. The highest DS obtained was 100%.

| Exp | HATU (eq) | TEA (eq) | DS (%) |
|---|---|---|---|
| 112 | 0.75 | 5.5 | 73 |
| 113 | 1.5 | 5.5 | 90 |
| 114 | 3 | 5.5 | 69 |
| 115 | 0.75 | 11.5 | 100 |
| 116 | 1.5 | 11.5 | 88 |
| 117 | 3 | 11.5 | 89 |
| 118 | 0.75 | 16 | 89 |
| 119 | 1.5 | 16 | 92 |
| 120 | 3 | 16 | 100 |
| 121 | 1.5 | 11.5 | 88 |
| 122 | 1.5 | 11.5 | 83 |
| 123 | 1.5 | 11.5 | 88 |

In the full FD (Design 10), the highest DS achieved was 100% (exp 115 and 120). Additionally, most experiments resulted in a DS of >83%. Figure 13A presents the summary of fit, highlighting the model's high significance (R2=0.87), good model validity (0.62), and good reproducibility (0.79). Based on the summary of fit, the

predictive precision of the model is low (Q2=0.33). However, this might be due to the fact that all experiments resulted in a high DS and that neither experimental factor was found significant as individual model terms. The interaction between non-significant factors may introduce noise, reducing predictive accuracy for future experiments. Figure 13B shows the coefficient plot, indicating that the molar ratio of TEA and HATU were non-significant model terms independently, with regression coefficients of -2.01 and 0.54, respectively. However, TEA was a square term, with a coefficient of 2.79, and an interaction term was established between TEA and HATU (4.22). The interaction suggests a synergistic effect, meaning that while varying these factors individually makes no difference, the combined influence of TEA and HATU enhances the DS.

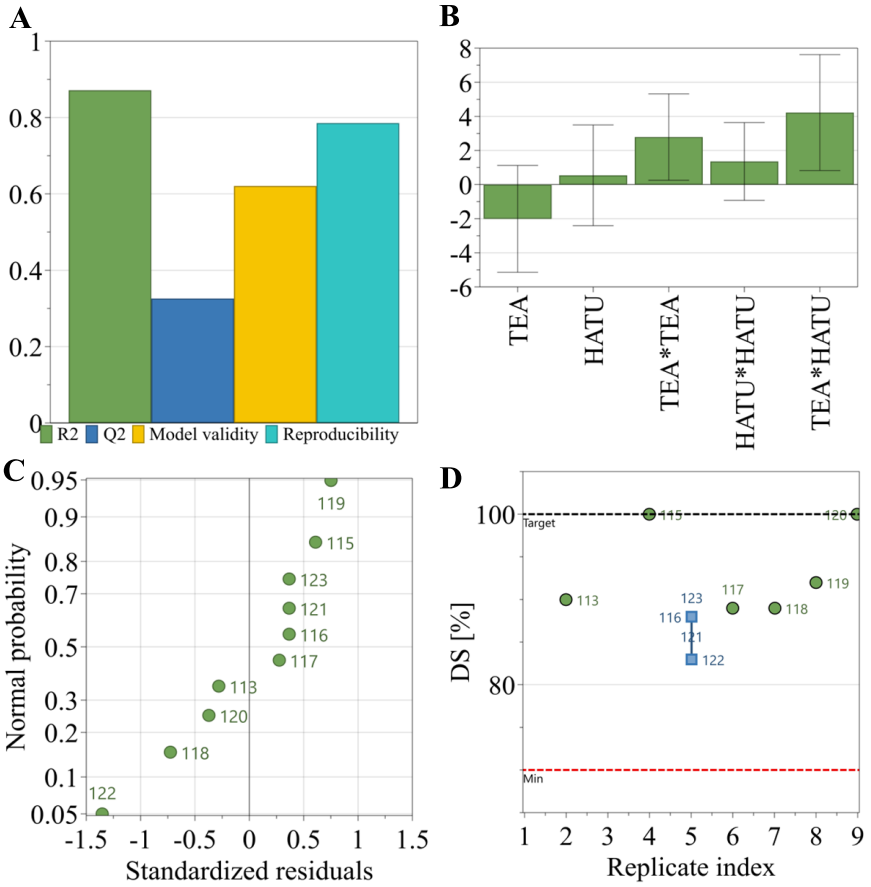


Figure 13. Results of the full FD (Design 10). A: Summary of fit plot for the full FD. The R2 (green) indicates the model's fit, while Q2 (blue) estimates the precision of future predictions. B: Coefficient plot, showing (from left to right) the factors: TEA = molar ratio of TEA, HATU = molar ratio of HATU, TEA*TEA and HATU*HATU = square terms of TEA and HATU, TEA*HATU = interaction term of TEA and HATU. C: Residuals Normal Probability Plot, demonstrating that the residuals follow a normal distribution (after the removal of outliers). D: Replicate plot, with the replicates (exp 116, 121, 122, and 123) displayed in light blue and connected by a straight line.

The residuals normal probability plot (Figure 13C) indicated outliers (exp 112 and 114), thus these were removed to provide a normal distribution. The replicate plot (Figure 13D) illustrates the variation across all experiments, with replicated experiments (exp 116, 121, 122 and 123) appearing in blue and connected by a line.

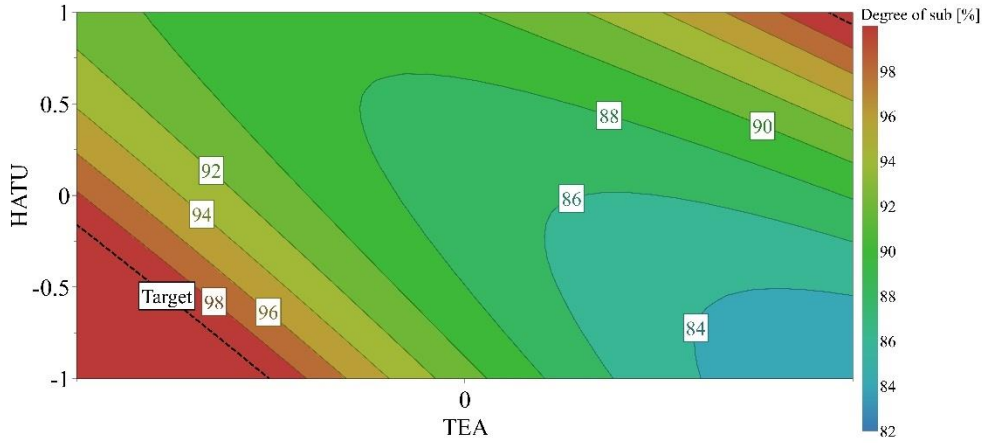


Figure 14. Response Contour Plot of Design 10. The X-axis represents the molar ratio of TEA (-1, 0 and -1 corresponding to 5.5, 11.5 and 16 eq TEA, respectively) and the Y-axis represents the molar ratio of HATU (-1, 0 and 1 corresponding to 0.75, 1.5 and 3 eq of HATU, respectively). The color gradient indicates different DS levels, with blue representing the lowest values and red the highest.

The response contour plot (Figure 14) provides detailed insights into the interaction between the molar ratios of TEA and HATU. It indicates that the molar ratios of HATU and the TEA should both be at either the lowest (-1) or highest (1) factor level in order to provide high DS.

To gain a more detailed understanding of significant experimental factors and to refine reagent amounts for developing a cost-effective process, further research is necessary. However, the preliminary results are promising, with the current method yielding high DS (>80%) even without extensive optimization. The HATU coupling method used in accordance to Viktorsson *et al.* [219] was successfully applied for *N*-betaine chitosan synthesis, achieving DS >80% in one step without the need for protection group strategies, using HATU, HOBt, and TEA in DMSO with MSA, at 60°C in 2h. Moreover, HATU coupling was effective for synthesizing a chitosan-cinnamic acid conjugate (DS = 9%, exp 106), suggesting its potential for efficiently producing chitosan-hydroxycinnamic acid derivatives with further refinements.

## 4.2 Biological properties and applications

The biological properties of the chitosan-hydroxycinnamic acid conjugates were investigated. The antibacterial activity against Gram-negative *E. coli* and Gram-positive *S. aureus* was assessed. The antioxidant activity was measured using the DPPH assay. The *in vitro* cytotoxicity of five TMC samples with varying DTM and TMC-ChS NPs was assessed with HUVECs, as well as two human ovarian cancer cell lines (SKOV-3, OVISE).

### 4.2.1 Antibacterial activity of the chitosan-hydroxycinnamic acid conjugates

The antibacterial activity of the chitosan starting material (Chitosan I), the hydroxycinnamic acids, and the synthesized conjugates were investigated against *E. coli* and *S. aureus*. using 5% (v/v) DMSO in water as the solvent. The MIC and MLC were measured at pH 5.5, and the results are displayed in Table 16 (next page). The MLC and MIC values were equal in all cases, indicating that all tested materials were bactericidal. All control experiments produced expected results, confirming the validity of the testing procedure and outcomes.

Table 16. Antibacterial activity of chitosan, hydroxycinnamic acids and chitosan-hydroxycinnamic acids against *E. coli* (ATCC 25922) and *S. aureus* (ATCC 29213).

| Compound (exp) | DS (%) | MIC/MLC values (μg/mL)* | |
|---|---|---|---|
| | | *S.aureus* | *E.coli* |
| Chitosan I | | 256 | 256 |
| Cinnamic acid | | 512 | 1024 |
| p-Coumaric acid | | 512 | 512 |
| Ferulic acid | | 512 | 1024 |
| Caffeic acid | | 1024 | 1024 |
| Cinnamic conjugate (95) | 7 | 256 | 128 |
| Cinnamic conjugate (85) | 9 | 128 | 64 |
| Cinnamic conjugate (86) | 15 | 128 | 128 |
| Cinnamic conjugate (96) | 36 | ≥2048 | 512 |
| Cinnamic conjugate (97) | 60 | ≥2048 | ≥2048 |
| p-Coumaric conjugate (98) | 9 | 256 | 128 |
| p-Coumaric conjugate (99) | 35 | 1024 | 512 |
| p-Coumaric conjugate (100) | 40 | 1024 | 256 |
| Ferulic conjugate (101) | 3 | 256 | 256 |
| Ferulic conjugate (102) | 17 | 1024 | 256 |
| Ferulic conjugate (103) | 27 | 1024 | 1024 |
| Caffeic conjugate (104) | 5 | 1024 | 64 |
| Caffeic conjugate (105) | 13 | 512 | 1024 |
| Caffeic conjugate (106) | 21 | ≥2048 | ≥2048 |

*the MLC and MIC values were equal in all experiments.

The antibacterial activity of the starting chitosan material (Chitosan I) was confirmed with MIC and MLC values of 256 μg/mL against both *E. coli* and *S. aureus*. The hydroxycinnamic acids showed MIC and MLC values between 512 and 1024 μg/mL. Some conjugates with a DS below 20% demonstrated greater activity than unmodified chitosan, with MIC/MLC values of 128 μg/mL. However, this difference was not considered major. In two cases (exp 85 and 104) the MIC/MLC value was 64 μg/mL against *E. coli*, a two-dilution difference compared to unmodified chitosan, which is considered significant. However, higher DS values (>20%) correlated with decreased antibacterial activity, and the highest DS conjugates were inactive at the tested concentrations.

These findings suggest that conjugating hydroxycinnamic acids to chitosan does not enhance antibacterial activity. On the contrary, conjugation reduces the activity by diminishing the number of quaternized amino groups, similar to the effect of increased DA [59]. Lipophilic substituents like cinnamic acid may reduce activity by causing self-association on the polymer chains [225]. Additionally, hydroxypropyl substituents, despite their hydrophilicity and hydrogen-bonding potential, also negatively impacted antibacterial activity [55].

### 4.2.2 Antioxidant activity of the chitosan-hydroxycinnamic acid conjugates

Finding a suitable solvent for the DPPH assay posed challenges. Chitosan and its conjugates dissolved in 1% (v/v) acetic acid, but the hydroxycinnamic acids were insoluble. Adding MeOH fully dissolved all but one *p*-coumaric acid conjugate (exp 99). Table 17 shows the results of the DPPH assay (page 70). Cinnamic acid lacked DPPH scavenging activity, as it lacks an -OH group. The chitosan-cinnamic acid conjugates (exp 86, 96-97) also lacked antioxidant activity. Similarly, *p*-coumaric acid and its conjugates (exp 98, 100) showed limited scavenging activity in the tested concentrations (Figure 15).

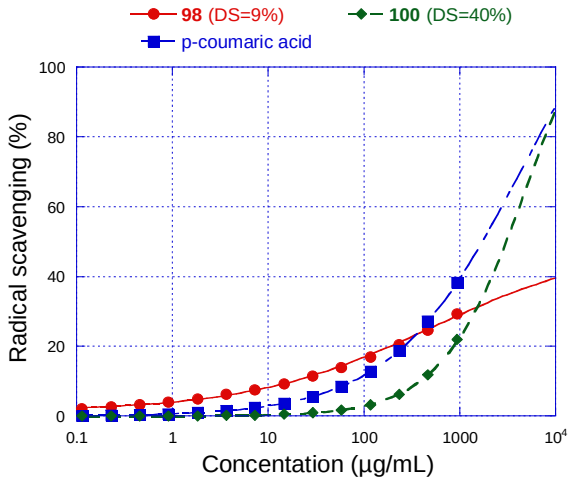


Figure 15. DPPH scavenging activity of *p*-coumaric acid and two chitosan-*p*-coumaric acid conjugates with varying DS (9% and 40%).

Ferulic acid exhibited significant antioxidant activity ($EC_{50}$=5 µg/mL), and its conjugates (exp 101-103) also showed good activity ($EC_{50}$=107-982 µg/mL), though lower than the free acid, likely due to structural changes in the conversion to amide form. Their antioxidant activity increased with the increase in DS (Figure 16, next page).

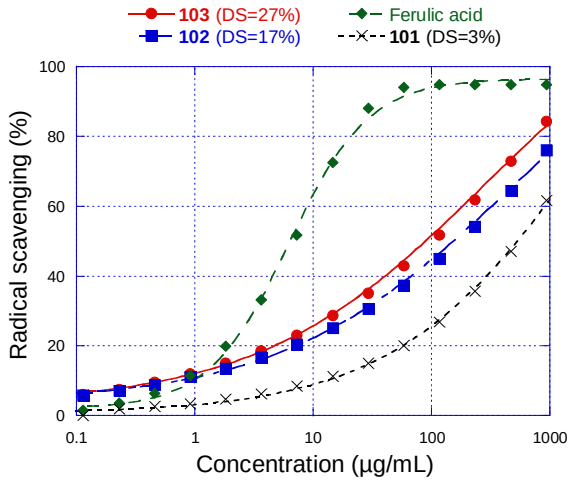


Figure 16. DPPH scavenging activity of ferulic acid and three chitosan-ferulic acid conjugates with varying DS (3%, 17% and 27%).

Caffeic acid ($EC_{50}$=2 µg/mL), and the chitosan-caffeic acid conjugates (exp 104-106) exhibited high DPPH scavenging activities ($EC_{50}$ values between 0.7-406 µg/mL), and the activity correlated with the DS. The conjugation of caffeic acid to chitosan enhanced its antioxidant activity compared to the free caffeic acid, resulting in significant DPPH scavenging activity ($EC_{50}$=0.7 µg/mL), an unexpected finding (Figure 17). This suggests that intramolecular hydrogen bonding between the di-hydroxylated aromatic groups could help to increase the antioxidant capacity.

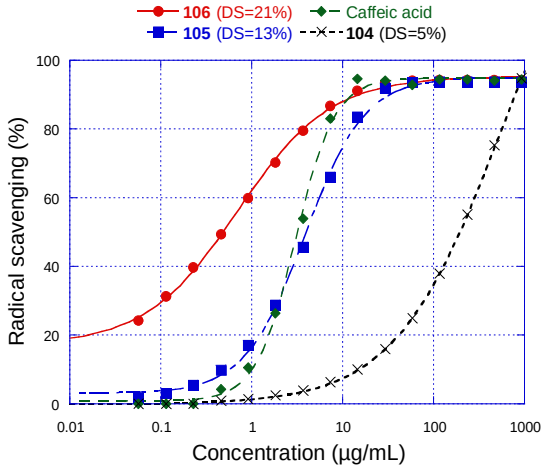


Figure 17. DPPH scavenging activity of caffeic acid and three chitosan-caffeic acid conjugates with varying DS (5%, 13% and 21%).

Our results align with previous studies, which also report that unmodified chitosan exhibits minimal antioxidant activity and that conjugating hydroxycinnamic acids greatly improves the polymer's antioxidant properties [48].

Table 17. DPPH scavenging activity of the hydroxycinnamic acids and the chitosan-hydroxycinnamic acid conjugates. L-ascorbic acid was used as positive control.

| Name (exp) | DS (%) | $EC_{50}$ (µg/mL) |
|---|---|---|
| Chitosan I | | 2777±0.1 |
| L-Ascorbic acid | | 7±0.8 |
| Cinnamic acid | | ≥10000* |
| *p*-Coumaric acid | | 1503±107* |
| Ferulic acid | | 5±0.3 |
| Caffeic acid | | 2±0.08 |
| Chitosan-cinnamic acid conjugate (86) | 15 | ≥10000* |
| Chitosan-cinnamic acid conjugate (96) | 36 | ≥10000* |
| Chitosan-cinnamic acid conjugate (97) | 60 | ≥10000* |
| Chitosan-*p*-coumaric acid conjugate (98) | 9 | 2989±112* |
| Chitosan-*p*-coumaric acid conjugate (100) | 40 | 1735±62* |
| Chitosan-ferulic acid conjugate (101) | 3 | 982±59 |
| Chitosan-ferulic acid conjugate (102) | 17 | 470±17 |
| Chitosan-ferulic acid conjugate (103) | 27 | 107±8.1 |
| Chitosan-caffeic acid conjugate (104) | 5 | 406±24 |
| Chitosan-caffeic acid conjugate (105) | 13 | 4±0.2 |
| Chitosan-caffeic acid conjugate (106) | 21 | 0.70±0.05 |

*DPPH scavenging at 5616 µg/mL: cinnamic acid=6%; *p*-coumaric acid: 38%; conjugates 86, 96 and 97=0%; conjugate 98=22%; conjugate 100=30%.

### 4.2.3 TMC-ChS NP preparation

TMC-ChS NPs were prepared by dissolving TMC (50% DTM and $M_w$=66 kDa) and ChS at 1.5 mg/mL. Neither TMC nor ChS formed NPs on their own based on DLS measurements. A range of TMC/ChS weight ratios was evaluated to optimize particle size, with a 1:1 ratio yielding the smallest particles (188 nm ± 3) and optimal PDI (0.155 ± 0.011). The NPs were found to be stable even after dilution, as particle size remained unaffected (Figure 18, next page).

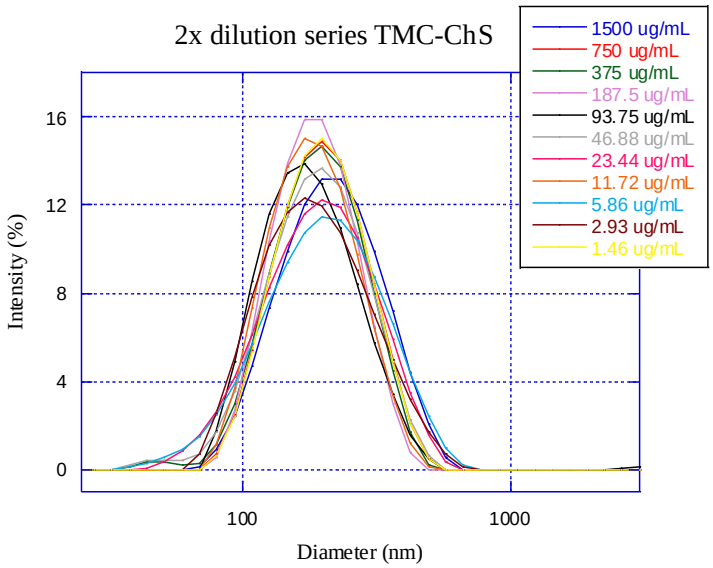


Figure 18. Testing the stability of the TMC-ChS NPs by measuring the particle size of a dilution series.

### 4.2.4 *In vitro* cytotoxicity of the TMC-ChS NPs

The *in vitro* cytotoxicity of unmodified chitosan, five well characterized TMC samples (Table 18), and TMC-ChS NPs were investigated.

Table 18. $^{1}$H NMR spectroscopy and GPC measurements of five TMC samples with varying levels of DTM.

| Sample (exp) | $^{1}$H NMR | | | GPC | |
|---|---|---|---|---|---|
| | DTM (%) | DDM (%) | DMM (%) | $M_w$ (kDa) | Average PDI |
| TMC-1 (7) | 23 | 68 | 8 | 161 | 1.1 |
| TMC-2 (15) | 32 | 63 | 5 | 232 | 4.3 |
| TMC-3 (17) | 46 | 54 | 0 | 96 | 3.3 |
| TMC-4 (78) | 50 | 38 | 12 | 66 | 3.6 |
| TMC-5 (*) | 99 | 1 | 0 | 290 | 4.4 |

*TMC-5 (99% DTM) is the result of a repeated trimethylation reaction.

#### *4.2.4.1 HUVECs*

The *in vitro* cell viability of five TMC samples and the TMC-ChS NPs was assessed using HUVEC cells (Figure 19, next page).

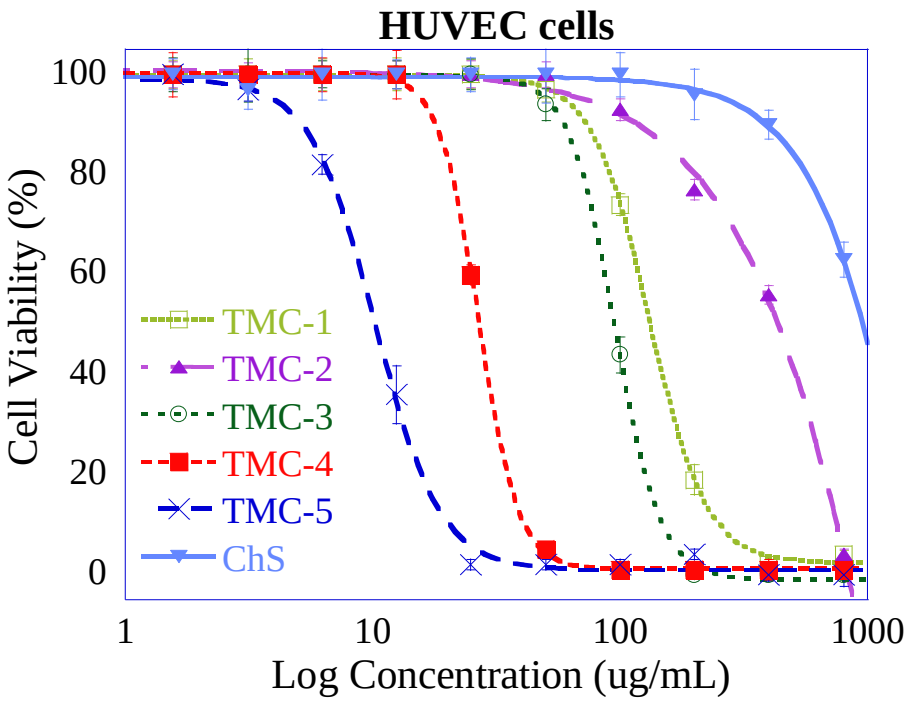


Figure 19. The effects of five TMC samples on the cell viability of HUVECs (after 24h). ChS was used as a non-toxic control. The error bars depict the standard deviation (%) observed across eight measurements. TMC-1 (□, 23% DTM, 161 kDa), TMC-2 (▲, 32% DTM, 232 kDa), TMC-3 (○, 46% DTM, 96 kDa), TMC-4 (■, 50% DTM, 66 kDa), TMC-5 (×, 99% DTM, 290 kDa), ChS (▼).

As shown in Figure 19, both DTM and Mw had a notable influence on the cell viability of HUVECs. Notably, TMC-5 with the highest DTM (99%) showed the most toxicity, followed by TMC-4 (DTM 50%) and TMC-3 (DTM 46%). Additionally, an inverse relationship between Mw and toxicity was observed, with lower Mw corresponding to higher toxicity, except for TMC-5, where high DTM overruled the protective effect of Mw. For samples with lower DTM, higher Mw reduced toxicity, as seen with TMC-2 (DTM 32%, 232 kDa), which showed the lowest toxicity, while the lowest DTM sample (TMC-1, DTM 23%) demonstrated slightly higher cytotoxicity. The varying toxicity profiles of TMC-3 and TMC-4 (similar DTM but different Mw) highlight that Mw plays a significant role in determining cytotoxicity. This finding contrasts with the work of Mao and colleagues [95], who reported a different relationship between Mw and toxicity. Moreover, the balance between DTM and Mw suggests that higher Mw can mitigate toxicity in lower DTM samples, though this is not the case when DTM reaches extremely high levels, such as in TMC-5. Thanou *et al.* found no toxicity in TMC samples with 20-60% DTM on Caco-2 cells at 1.0% concentration, though their results were based on a short incubation period (4h) [91]. Verheul *et al.*, however, reported an increase in cytotoxicity with increasing DTM (33-76%) in Caco-2 cells [93]. Our results are consistent with the latter, supporting the hypothesis that higher DTM contributes to increased cytotoxicity, specifically in HUVECs.

Kean *et al*. also reported a similar trend in COS-7 and MCF-7 cells, though they found that TMC with 93% DTM exhibited lower toxicity than that with 76% DTM, which they attributed to hydrolysis-induced Mw reduction [92]. Our results, however, reveal a different Mw-cytotoxicity correlation in HUVECs.

The TMC-ChS NPs (TMC-4 with 50% DTM, ChS, weight ratio of 1:1, tested across a concentration range of 250-0.49 µg/mL) were evaluated for cytotoxicity on HUVECs. The absorbance data (Figure 20) showed that the NPs exhibited significantly lower toxicity in comparison to the starting TMC-4 material, highlighting a reduction in cytotoxicity when formulated as NPs.

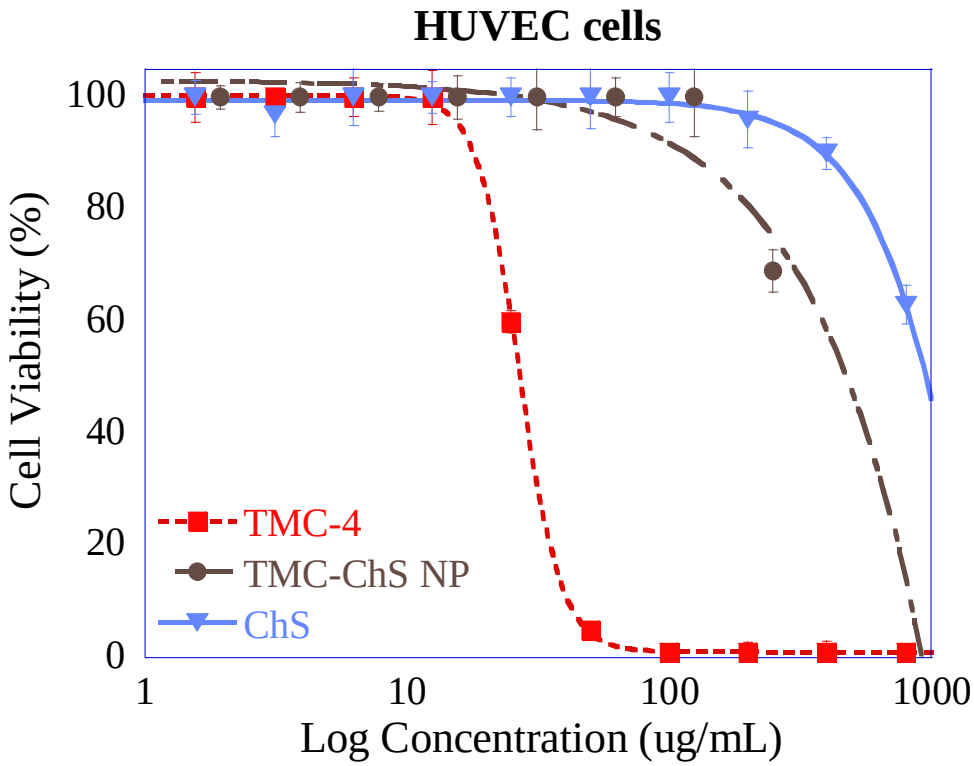


Figure 20. Cytotoxicity comparison of TMC (DTM 50%), ChS, and TMC-ChS NPs with HUVEC cells. The error bars show the standard deviation (%) observed across eight measurements. TMC-4 (■, 50% DTM, 66 kDa), TMC-ChS NP (●), ChS (▼).

Based on results displayed in Figure 20, the TMC-ChS NPs exhibited significantly lower toxicity compared to the TMC starting material and behaved similarly to the non-toxic control, ChS. While the TMC sample showed cytotoxicity at concentrations as low as 31 µg/mL (11% cell viability), the TMC-ChS NPs remained non-toxic up to 250 µg/mL, with 71% cell viability. These findings align with previous studies [155]. Additionally, the current study demonstrated non-toxicity up to 250 µg/mL, as it was previously only measured up to 56 µg/mL. The reduction in toxicity could be due to the neutralized

charge in the NP structure, reducing electrostatic interactions with cell membranes. Additionally, the inclusion of ChS, known for its biocompatibility, likely further mitigated cytotoxic effects. This modification highlights the potential of using NP formulations to improve the safety and efficacy of TMC in pharmaceutical and medical applications.

#### *4.2.4.2 In vitro cytotoxicity against human ovarian cancer cells*

Five TMC samples with varying DTM, ChS and the TMC-ChS NPs underwent *in vitro* cytotoxicity testing against SKOV-3 cancer cells (Figure 21). Among the tested samples, TMC-3, -4, and -5, with DTM values of 46%, 50%, and 99%, respectively, showed toxicity against SKOV-3 cells in the tested concentration range.

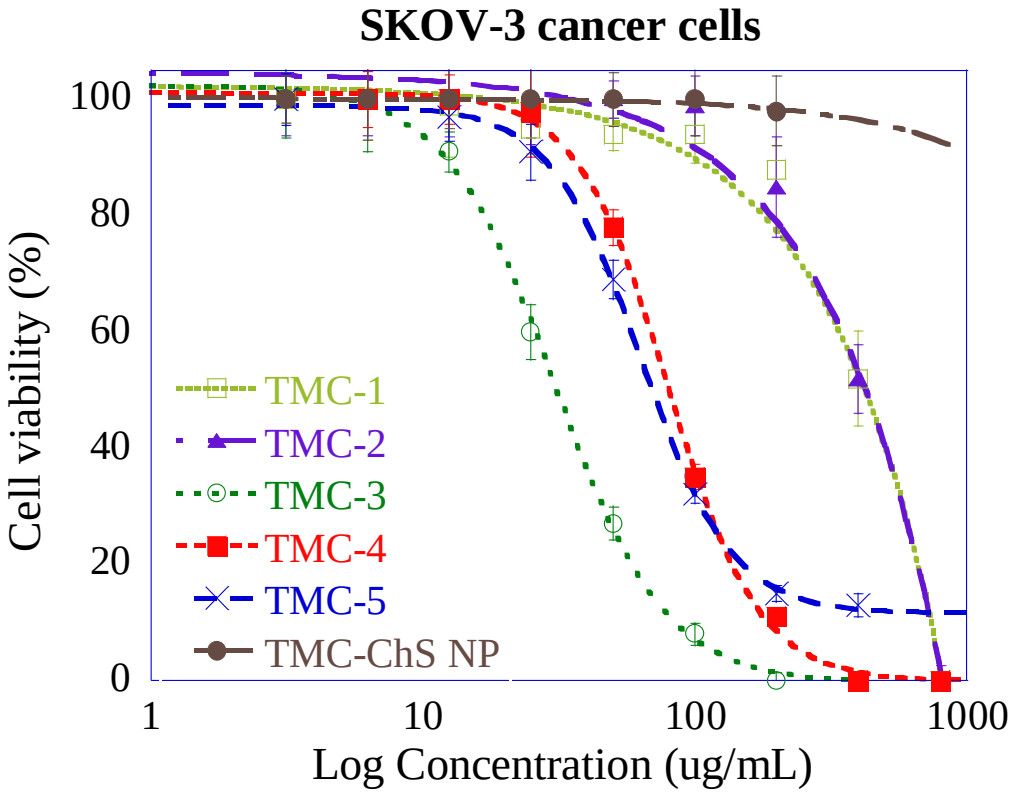


Figure 21. The effects of five TMC samples with varying DTM and TMC-ChS NPs against SKOV-3 cancer cells. The error bars depict the standard deviation (%) observed across eight measurements. TMC-1 (□, 23% DTM, 161 kDa), TMC-2 (▲, 32% DTM, 232 kDa), TMC-3 (○, 46% DTM, 96 kDa), TMC-4 (■, 50% DTM, 66 kDa), TMC-5 (×, 99% DTM, 290 kDa), TMC-ChS NP (●).

Table 19. *In vitro* cytotoxicity of ChS, five TMC samples and TMC-ChS NPs on HUVEC primary cells, SKOV-3 and OVISE cancer cell lines.

| Sample | DTM (%) | $M_w$ (kDa) | $IC_{50}$ in HUVEC cells | | $IC_{50}$ in SKOV-3 cancer cells | | $IC_{50}$ in OVISE cancer cells | |
|---|---|---|---|---|---|---|---|---|
| | | | µg/mL | µM | µg/mL | µM | µg/mL | µM |
| ChS | N/A | N/A | >800 | N/A | >800 | N/A | >800 | N/A |
| TMC-1 | 23 | 161 | 130.89 | 0.63 | >800 | >3.86 | N/A | N/A |
| TMC-2 | 32 | 232 | 412.24 | 1.94 | >800 | >3.77 | 0.12 | $5.66 \times 10^{-4}$ |
| TMC-3 | 46 | 96 | 95.16 | 0.43 | 30.51 | 0.14 | 10.21 | $4.64 \times 10^{-2}$ |
| TMC-4 | 50 | 66 | 26.84 | 0.12 | 79.72 | 0.36 | 5.79 | $2.64 \times 10^{-2}$ |
| TMC-5 | 99 | 290 | 10.25 | 0.04 | 63.59 | 0.26 | 15.73 | $6.38 \times 10^{-2}$ |
| NP | 50 | N/A | 674.88 | N/A | >800 | N/A | >800 | N/A |

TMC-3 (DTM 46%) exhibited the highest toxicity with an $IC_{50}$ of 0.14 µM (Table 19), followed by TMC-5 and TMC-4 with $IC_{50}$ values of 0.26 µM and 0.36 µM, respectively, suggesting a non-linear pattern where an optimal DTM influences TMC's cytotoxicity in SKOV-3 cells. Mw also played a role, with higher Mw generally mitigating toxicity. However, this mitigating effect disappears at very high DTM levels. TMC-ChS NPs, in contrast, showed no toxicity, reinforcing the notion that NP formation can reduce TMC's cytotoxic effects.

To further explore the effects of TMC on ovarian cancer cells, OVISE cell lines were tested with TMC samples, ChS, and TMC-ChS NPs. The results, shown in Figure 22 (next page), indicate that most TMC samples exhibit anticancer activity within the tested concentrations. The dose-response toxicity profiles of TMC 2-5 did not show significant differences, while TMC-1 (DTM=23%) demonstrated notably lower anticancer activity, suggesting that a lower DTM correlates with reduced anticancer efficacy in OVISE cells.

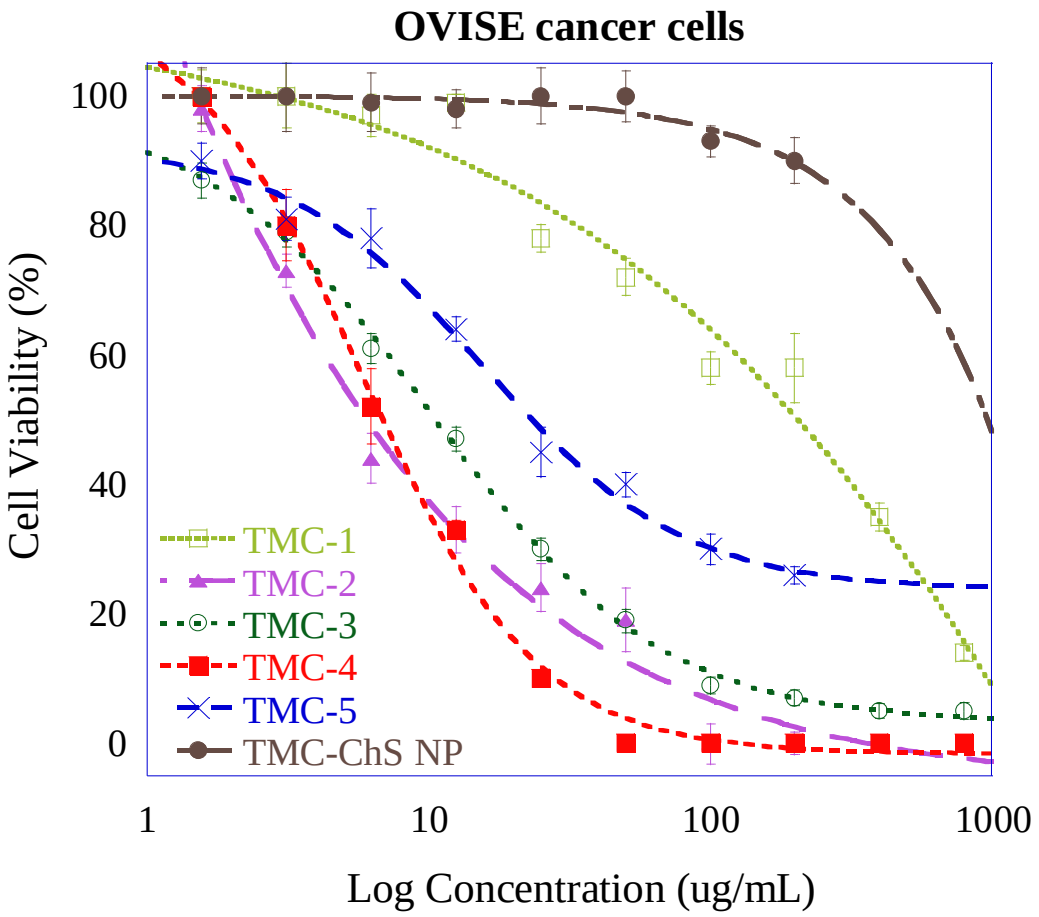


Figure 22. The effects of five TMC samples with varying DTM and TMC-ChS NPs against OVISE cancer cells. The error bars depict the standard deviation (%) observed across four measurements. TMC-1 (□, 23% DTM, 161 kDa), TMC-2 (▲, 32% DTM, 232 kDa), TMC-3 (○, 46% DTM, 96 kDa), TMC-4 (■, 50% DTM, 66 kDa), TMC-5 (×, 99% DTM, 290 kDa), TMC-ChS NP (●).

Remarkably, the cytotoxicity of TMC samples was more pronounced against OVISE cancer cells compared to SKOV-3 cells. TMC-3 and TMC-5 exhibited 3- and 4-fold lower $IC_{50}$ values against OVISE, while TMC-4 (DTM=50%) showed a 14-fold lower $IC_{50}$ ($2.64 \times 10^{-2}$ **μ**M) compared to SKOV-3. TMC-2, inactive against SKOV-3, displayed outstanding activity against OVISE with an $IC_{50}$ of $5.66 \times 10^{-4}$ **μ**M, indicating that optimal DTM, rather than a linear relationship, plays a key role. The impact of Mw was less evident with OVISE cells, where TMC-2 (Mw 232 kDa) demonstrated the highest activity. These findings suggest that both DTM and Mw must be fine-tuned depending on the cell type. Moreover, TMC-ChS NPs consistently exhibited non-toxicity within the tested concentrations.

# 5 Summary, Conclusions & Future Perspectives

This research focused on developing scalable and efficient methods for synthesizing *N*-alkyl and *N*-acyl chitosan derivatives and conjugates with enhanced biological properties suitable for pharmaceutical and medical applications. The study employed a Design of Experiments (DoE) approach to optimize the reaction conditions, synthesize high-substitution derivatives, and evaluate their biocompatibility, cytotoxicity, and biological activities.

The synthesis of *N,N,N*-trimethyl chitosan (TMC) was optimized. Through a series of sequential and factorial DoE designs, the reaction parameters were optimized, achieving a fivefold increase in trimethylation (up to 72% DTM) without *O*-methylation using $NaHCO_3$ base, MeI alkylating agent in DMF:$H_2O$ (and HCl) solvent system. However, viscosity and gas production concerns prompted the exploration of other, non-nucleophilic bases. The use of DIPEA as an alternative base was successfully implemented, offering scalability, reduced viscosity, and improved efficiency. The final method yielded high DTM in a single step with no *O*-methylation, minimal reagent usage and short reaction times, showcasing its potential for industrial applications and production in closed reactors.

In parallel, a new synthetic method for chitosan-hydroxycinnamic acid conjugates was developed using a TBDMS protection strategy. The approach yielded conjugates with degrees of substitution (DS) between 5% and 60%. The conjugates exhibited enhanced antioxidant activities compared to unmodified chitosan, particularly with caffeic acid conjugates showing the strongest DPPH scavenging activity. Antibacterial assays confirmed the antimicrobial activity of these conjugates against *E. coli* and *S. aureus*, with lower DS values maintaining antibacterial efficacy, although higher DS resulted in reduced activity. The results suggest that conjugation with antioxidant hydroxycinnamic acids can significantly enhance the antioxidant properties of chitosan, although antibacterial activity is affected by DS.

Finally, a new one-step method for synthesizing *N*-betaine chitosan using HATU coupling was implemented, achieving high DS in a shorter, more efficient process compared the previously published methods. Additionally, the HATU coupling strategy provides a promising avenue for conjugating hydroxycinnamic acids to chitosan.

The application of DoE was central to the successful optimization of the various synthesis methods explored in this thesis. This structured approach not only improved efficiency but also provided deeper insights into the relationship between key parameters and the desired outcomes of maximizing the DS, leading to scalable, reproducible methods with

broad pharmaceutical potential. The successful use of DoE for the syntheses highlights how this approach could be used for the development and optimization of other chitosan derivatives and conjugates.

The biocompatibility and cytotoxicity of TMC were also investigated in human endothelial (HUVECs) and ovarian cancer cells (OVISE, SKOV-3). The findings revealed a nuanced relationship between the DTM and molecular weight (Mw), with higher DTM generally contributing to increased toxicity. In HUVECs and SKOV-3 cells, the increasing Mw had a toxicity mitigating effect, however, at very high DTM (99%) this trend did not persist. The relationship between DTM and anticancer activity showed a non-linear pattern, indicating that there is an optimal DTM level that maximizes anticancer efficacy. The formation of TMC-chondroitin sulfate (ChS) polyelectrolyte complex nanoparticles (NPs) significantly reduced toxicity, highlighting the potential of NP formulation to mitigate TMC's cytotoxicity and enhance its biocompatibility for drug delivery systems. These results demonstrate the versatility of TMC for both non-toxic pharmaceutical applications and targeted anticancer therapies, depending on the cell type and formulation.

Future perspectives of the work include exploring the scale-up of the TMC synthesis, conducting further DoE optimization of the *N*-betaine chitosan synthesis investigating more experimental factors, exploring the HATU coupling strategy for the synthesis of chitosan-hydroxycinnamic conjugates and optimizing the method with DoE. Biological studies could include testing the *in vitro* and *in vivo* cytotoxicity of TMC materials and TMC-based NPs with more DTM and Mw data points, exploring more cells, higher concentrations, and establishing structure-activity relationships for other biological properties.

# References


[1] R.N. Tharanathan, F.S. Kittur, Chitin — The Undisputed Biomolecule of Great Potential, Crit Rev Food Sci Nutr 43 (2003) 61–87. https://doi.org/10.1080/10408690390826455.

[2] C. Hatchett, XVIII. Experiments and observations on shell and bone, Philos Trans R Soc Lond (1799) 315–334. https://doi.org/10.1098/rstl.1799.0019.

[3] H. Braconnot, Sur la nature des champibnons, Ann Chi 79 (1881) 265–304.

[4] A. Odier, Mémoire sur la composition chimique des parties cornées des insectes, Mem. Soc. Hist. Paris 1 (1823) 29–42.

[5] M. Bo, G. Bavestrello, D. Kurek, S. Paasch, E. Brunner, R. Born, R. Galli, A.L. Stelling, V.N. Sivkov, O. V Petrova, D. Vyalikh, K. Kummer, S.L. Molodtsov, D. Nowak, J. Nowak, H. Ehrlich, Isolation and identification of chitin in the black coral Parantipathes larix (Anthozoa: Cnidaria), Int J Biol Macromol 51 (2012) 129–137. https://doi.org/10.1016/j.ijbiomac.2012.04.016.

[6] M. Rinaudo, Chitin and chitosan: Properties and applications, Prog Polym Sci 31 (2006) 603–632. https://doi.org/10.1016/j.progpolymsci.2006.06.001.

[7] R.A.A. Muzzarelli, Chitin Nanostructures in Living Organisms, in: N.S. Gupta (Ed.), Chitin: Formation and Diagenesis, Springer Netherlands, Dordrecht, 2011: pp. 1–34. https://doi.org/10.1007/978-90-481-9684-5_1.

[8] C.K.S. Pillai, W. Paul, C.P. Sharma, Chitin and chitosan polymers: Chemistry, solubility and fiber formation, Prog Polym Sci 34 (2009) 641–678. https://doi.org/10.1016/j.progpolymsci.2009.04.001.

[9] G.A.F. Roberts, G.A.F. Roberts, Chitin chemistry, Springer, 1992. https://doi.org/10.1007/978-1-349-11545-7_1.

[10] K. Kurita, Controlled functionalization of the polysaccharide chitin, Prog Polym Sci 26 (2001) 1921–1971. https://doi.org/10.1016/S0079-6700(01)00007-7.

[11] M. Lavertu, Z. Xia, A.N. Serreqi, M. Berrada, A. Rodrigues, D. Wang, M.D. Buschmann, A. Gupta, A validated 1H NMR method for the determination of the degree of deacetylation of chitosan, J Pharm Biomed Anal 32 (2003) 1149–1158. https://doi.org/10.1016/s0731-7085(03)00155-9.

[12] A. Standard, F2260-03 (2008), Standard test method for determining degree of deacetylation in chitosan salts by proton nuclear magnetic resonance (1H NMR) spectroscopy, ASTM International, West Conshohocken, PA, (n.d.).

[13] S.H. Pangburn, P. V Trescony, J. Heller, Lysozyme degradation of partially deacetylated chitin, its films and hydrogels, Biomaterials 3 (1982) 105–108. https://doi.org/10.1016/0142-9612(82)90043-6.

[14] S. Rodrigues, M. Dionísio, C. Remunan Lopez, A. Grenha, Biocompatibility of chitosan carriers with application in drug delivery, J Funct Biomater 3 (2012) 615–641. https://doi.org/10.3390/jfb3030615.

[15] J. Frigaard, J.L. Jensen, H.K. Galtung, M. Hiorth, The potential of chitosan in nanomedicine: An overview of the cytotoxicity of chitosan based nanoparticles, Front Pharmacol 13 (2022) 880377. https://doi.org/10.3389/fphar.2022.880377.

[16] A. Chaudhury, S. Das, Recent advancement of chitosan-based nanoparticles for oral controlled delivery of insulin and other therapeutic agents, AAPS PharmSciTech 12 (2011) 10–20. https://doi.org/10.1208/s12249-010-9561-2.

[17] J. Li, S. Zhuang, Antibacterial activity of chitosan and its derivatives and their interaction mechanism with bacteria: Current state and perspectives, Eur Polym J 138 (2020) 109984. https://doi.org/10.1016/j.eurpolymj.2020.109984.

[18] A. Verlee, S. Mincke, C. V Stevens, Recent developments in antibacterial and antifungal chitosan and its derivatives, Carbohydr Polym 164 (2017) 268–283. https://doi.org/10.1016/j.carbpol.2017.02.001.

[19] N. Moramkar, P. Bhatt, Insight into chitosan derived nanotherapeutics for anticancer drug delivery and imaging, Eur Polym J 154 (2021) 110540. https://doi.org/10.1016/j.eurpolymj.2021.110540.

[20] P. He, S.S. Davis, L. Illum, In vitro evaluation of the mucoadhesive properties of chitosan microspheres, Int J Pharm 166 (1998) 75–88. https://doi.org/10.1016/S0378-5173(98)00027-1.

[21] J.H. Hamman, C.M. Schultz, A.F. Kotzé, N-trimethyl chitosan chloride: optimum degree of quaternization for drug absorption enhancement across epithelial cells, Drug Dev Ind Pharm 29 (2003) 161–172. https://doi.org/10.1081/DDC-120016724.

[22] P. Baharlouei, A. Rahman, Chitin and chitosan: prospective biomedical applications in drug delivery, cancer treatment, and wound healing, Mar Drugs 20 (2022) 460. https://doi.org/10.3390/md20070460.

[23] A. Moeini, P. Pedram, P. Makvandi, M. Malinconico, G.G. d'Ayala, Wound healing and antimicrobial effect of active secondary metabolites in chitosan-based wound dressings: A review, Carbohydr Polym 233 (2020) 115839. https://doi.org/10.1016/j.carbpol.2020.115839.

[24] P. Fan, Y. Zeng, D. Zaldivar-Silva, L. Agüero, S. Wang, Chitosan-based hemostatic hydrogels: The concept, mechanism, application, and prospects, Molecules 28 (2023) 1473. https://doi.org/10.3390/molecules28031473.

[25] Y. Okamoto, K. Kawakami, K. Miyatake, M. Morimoto, Y. Shigemasa, S. Minami, Analgesic effects of chitin and chitosan, 2002. https://doi.org/10.1016/S0144-8617(01)00316-2.

[26] R. Ylitalo, S. Lehtinen, E. Wuolijoki, P. Ylitalo, T. Lehtimäki, Cholesterol-lowering properties and safety of chitosan, Arzneimittelforschung 52 (2002) 1–7. https://doi.org/10.1055/s-0031-1299848.

[27] M.R. Kasaai, Various Methods for Determination of the Degree of N-Acetylation of Chitin and Chitosan: A Review, J Agric Food Chem 57 (2009) 1667–1676. https://doi.org/10.1021/jf803001m.

[28] J. Kumirska, M.X. Weinhold, J. Thöming, P. Stepnowski, Biomedical Activity of Chitin/Chitosan Based Materials—Influence of Physicochemical Properties Apart from Molecular Weight and Degree of N-Acetylation, Polymers (Basel) 3 (2011) 1875–1901. https://doi.org/10.3390/polym3041875.

[29] R.C. Goy, D. de Britto, O.B.G. Assis, A review of the antimicrobial activity of chitosan, Polímeros 19 (2009) 241–247. https://doi.org/10.1590/S0104-14282009000300013.

[30] N. Kubota, Y. Eguchi, Facile preparation of water-soluble N-acetylated chitosan and molecular weight dependence of its water-solubility, Polym J 29 (1997) 123. https://doi.org/10.1295/polymj.29.123.

[31] P.J. Flory, Principles of Polymer Chemistry, Cornell University Press, 1953. https://doi.org/10.1126/science.119.3095.555.b.

[32] B. Moussian, Chitin: Structure, Chemistry and Biology, in: Q. Yang, T. Fukamizo (Eds.), Targeting Chitin-Containing Organisms, Springer Singapore, Singapore, 2019: pp. 5–18. https://doi.org/10.1007/978-981-13-7318-3_2.

[33] A. Tolaimate, J. Desbrieres, M. Rhazi, A. Alagui, Contribution to the preparation of chitins and chitosans with controlled physico-chemical properties, Polymer (Guildf) 44 (2003) 7939–7952. https://doi.org/10.1016/j.polymer.2003.10.025.

[34] V. Ghormade, E.K. Pathan, M. V Deshpande, Can fungi compete with marine sources for chitosan production?, Int J Biol Macromol 104 (2017) 1415–1421. https://doi.org/10.1016/j.ijbiomac.2017.01.112.

[35] K. Mohan, A.R. Ganesan, T. Muralisankar, R. Jayakumar, P. Sathishkumar, V. Uthayakumar, R. Chandirasekar, N. Revathi, Recent insights into the extraction, characterization, and bioactivities of chitin and chitosan from insects, Trends Food Sci Technol 105 (2020) 17–42. https://doi.org/10.1016/j.tifs.2020.08.016.

[36] T. Huq, A. Khan, D. Brown, N. Dhayagude, Z. He, Y. Ni, Sources, production and commercial applications of fungal chitosan: A review, Journal of Bioresources and Bioproducts 7 (2022) 85–98. https://doi.org/10.1016/j.jobab.2022.01.002.

[37] S. Crognale, C. Russo, M. Petruccioli, A. D'Annibale, Chitosan Production by Fungi: Current State of Knowledge, Future Opportunities and Constraints, Fermentation 8 (2022). https://doi.org/10.3390/fermentation8020076.

[38] M. Jang, B. Kong, Y. Jeong, C.H. Lee, J. Nah, Physicochemical characterization of α-chitin, β-chitin, and γ-chitin separated from natural resources, J Polym Sci A Polym Chem 42 (2004) 3423–3432. https://doi.org/10.1002/pola.20176.

[39] J.-Y. Je, S.-K. Kim, Antimicrobial action of novel chitin derivative, Biochimica et Biophysica Acta (BBA)-General Subjects 1760 (2006) 104–109. https://doi.org/10.1016/j.bbagen.2005.09.012.

[40] Z. Chen, X. Yao, L. Liu, J. Guan, M. Liu, Z. Li, J. Yang, S. Huang, J. Wu, F. Tian, Blood coagulation evaluation of N-alkylated chitosan, Carbohydr Polym 173 (2017) 259–268. https://doi.org/10.1016/j.carbpol.2017.05.085.

[41] W. Xie, P. Xu, W. Wang, Q. Liu, Preparation and antibacterial activity of a water-soluble chitosan derivative, Carbohydr Polym 50 (2002) 35–40. https://doi.org/10.1016/S0144-8617(01)00370-8.

[42] Y. Peng, B. Han, W. Liu, X. Xu, Preparation and antimicrobial activity of hydroxypropyl chitosan, Carbohydr Res 340 (2005) 1846–1851. https://doi.org/10.1016/j.carres.2005.05.009.

[43] S.-H. Lim, S.M. Hudson, Synthesis and antimicrobial activity of a water-soluble chitosan derivative with a fiber-reactive group, Carbohydr Res 339 (2004) 313–319. https://doi.org/10.1016/j.carres.2003.10.024.

[44] R.A.A. Muzzarelli, F. %J C.P. Tanfani, The N-permethylation of chitosan and the preparation of N-trimethyl chitosan iodide, 5 (1985) 297–307. https://doi.org/10.1016/0144-8617(85)90037-2.

[45] J. Holappa, M. Hjálmarsdóttir, M. Másson, Ö. Rúnarsson, T. Asplund, P. Soininen, T. Nevalainen, T. Järvinen, Antimicrobial activity of chitosan N-betainates, Carbohydr Polym 65 (2006) 114–118. https://doi.org/10.1016/j.carbpol.2005.11.041.

[46] C. Le Tien, M. Lacroix, P. Ispas-Szabo, M.-A. Mateescu, N-acylated chitosan: hydrophobic matrices for controlled drug release, Journal of Controlled Release 93 (2003) 1–13. https://doi.org/10.1016/S0168-3659(03)00327-4.

[47] Y. Hu, Y. Du, J. Yang, Y. Tang, J. Li, X. Wang, Self-aggregation and antibacterial activity of N-acylated chitosan, Polymer (Guildf) 48 (2007) 3098–3106. https://doi.org/10.1016/j.polymer.2007.03.063.

[48] W. Pasanphan, S. Chirachanchai, Conjugation of gallic acid onto chitosan: An approach for green and water-based antioxidant, Carbohydr Polym 72 (2008) 169–177. https://doi.org/10.1016/j.carbpol.2007.08.002.

[49] S.B. Schreiber, J.J. Bozell, D.G. Hayes, S. Zivanovic, Introduction of primary antioxidant activity to chitosan for application as a multifunctional food packaging material, Food Hydrocoll 33 (2013) 207–214. https://doi.org/10.1016/j.foodhyd.2013.03.006.

[50] D. Raafat, K. Von Bargen, A. Haas, H.-G. Sahl, Insights into the mode of action of chitosan as an antibacterial compound, Appl Environ Microbiol 74 (2008) 3764–3773. https://doi.org/10.1128/AEM.00453-08.

[51] R.G. Cuero, G. Osuji, A. Washington, N-carboxymethylchitosan inhibition of aflatoxin production: Role of zinc, Biotechnol Lett 13 (1991) 441–444. https://doi.org/10.1007/BF01030998.

[52] K. Divya, S. Vijayan, T.K. George, M.S. Jisha, Antimicrobial properties of chitosan nanoparticles: Mode of action and factors affecting activity, Fibers and Polymers 18 (2017) 221–230. https://doi.org/10.1007/s12221-017-6690-1.

[53] K.F. El-Tahlawy, M.A. El-Bendary, A.G. Elhendawy, S.M. Hudson, The antimicrobial activity of cotton fabrics treated with different crosslinking agents and chitosan, Carbohydr Polym 60 (2005) 421–430. https://doi.org/10.1016/j.carbpol.2005.02.019.

[54] F. Devlieghere, A. Vermeulen, J. Debevere, Chitosan: antimicrobial activity, interactions with food components and applicability as a coating on fruit and vegetables, Food Microbiol 21 (2004) 703–714. https://doi.org/10.1016/j.fm.2004.02.008.

[55] M. Másson, Antimicrobial properties of chitosan and its derivatives, in: Chitosan for Biomaterials III: Structure-Property Relationships, Springer, 2021: pp. 131–168. https://doi.org/10.1007/12_2021_104.

[56] Y. Andres, L. Giraud, C. Gerente, P. Le Cloirec, Antibacterial effects of chitosan powder: mechanisms of action, Environ Technol 28 (2007) 1357–1363. https://doi.org/10.1080/09593332808618893.

[57] T. Hongpattarakere, O. Riyaphan, Effect of deacetylation conditions on antimicrobial activity of chitosans prepared from carapace of black tiger shrimp., Songklanakarin Journal of Science & Technology 30 (2008).

[58] G.U.O. Tsai, W.-H. Su, H.-C. Chen, C.-L. Pan, Antimicrobial activity of shrimp chitin and chitosan from different treatments, Fisheries Science 68 (2002) 170–177. https://doi.org/10.1046/j.1444-2906.2002.00404.x.

[59] I. Younes, S. Sellimi, M. Rinaudo, K. Jellouli, M. Nasri, Influence of acetylation degree and molecular weight of homogeneous chitosans on antibacterial and antifungal activities, 185 (2014) 57–63. https://doi.org/10.1016/j.ijfoodmicro.2014.04.029.

[60] S. Aiba, Studies on chitosan: 4. Lysozymic hydrolysis of partially N-acetylated chitosans, Int J Biol Macromol 14 (1992) 225–228. https://doi.org/10.1016/S0141-8130(05)80032-7.

[61] C. Chatelet, O. Damour, A. Domard, Influence of the degree of acetylation on some biological properties of chitosan films, Biomaterials 22 (2001) 261–268. https://doi.org/10.1016/S0142-9612(00)00183-6.

[62] J. Yang, F. Tian, Z. Wang, Q. Wang, Y. Zeng, S. Chen, Effect of chitosan molecular weight and deacetylation degree on hemostasis, J Biomed Mater Res B Appl Biomater 84 (2008) 131–137. https://doi.org/10.1002/jbm.b.30853.

[63] S. Sreekumar, J. Wattjes, A. Niehues, T. Mengoni, A.C. Mendes, E.R. Morris, F.M. Goycoolea, B.M. Moerschbacher, Biotechnologically produced chitosans with nonrandom acetylation patterns differ from conventional chitosans in properties and activities, Nat Commun 13 (2022) 7125. https://doi.org/10.1038/s41467-022-34483-3.

[64] N. Liu, X.-G. Chen, H.-J. Park, C.-G. Liu, C.-S. Liu, X.-H. Meng, L.-J. Yu, Effect of MW and concentration of chitosan on antibacterial activity of Escherichia coli, Carbohydr Polym 64 (2006) 60–65. https://doi.org/10.1016/j.carbpol.2005.10.028.

[65] H.K. No, N. Young Park, S. Ho Lee, S.P. Meyers, Antibacterial activity of chitosans and chitosan oligomers with different molecular weights, Int J Food

Microbiol 74 (2002) 65–72. https://doi.org/10.1016/S0168-1605(01)00717-6.

[66] S.N. Kulikov, S.A. Lisovskaya, P. V Zelenikhin, E.A. Bezrodnykh, D.R. Shakirova, I. V Blagodatskikh, V.E. Tikhonov, Antifungal activity of oligochitosans (short chain chitosans) against some Candida species and clinical isolates of Candida albicans: Molecular weight–activity relationship, Eur J Med Chem 74 (2014) 169–178. https://doi.org/10.1016/j.ejmech.2013.12.017.

[67] M.S. Benhabiles, R. Salah, H. Lounici, N. Drouiche, M.F.A. Goosen, N. Mameri, Antibacterial activity of chitin, chitosan and its oligomers prepared from shrimp shell waste, Food Hydrocoll 29 (2012) 48–56. https://doi.org/10.1016/j.foodhyd.2012.02.013.

[68] P. Sahariah, D. Cibor, D. Zielińska, M.Á. Hjálmarsdóttir, D. Stawski, M. Másson, The Effect of Molecular Weight on the Antibacterial Activity of N,N,N-Trimethyl Chitosan (TMC), Int J Mol Sci 20 (2019) 1743. https://doi.org/10.3390/ijms20071743.

[69] Y. Omura, M. Shigemoto, T. Akiyama, H. Saimoto, Y. Shigemasa, I. Nakamura, T. Tsuchido, Antimicrobial activity of chitosan with different degrees of acetylation and molecular weights, Biocontrol Sci 8 (2003) 25–30. https://doi.org/10.4265/bio.8.25.

[70] L.-Y. Zheng, J.-F. Zhu, Study on antimicrobial activity of chitosan with different molecular weights, Carbohydr Polym 54 (2003) 527–530. https://doi.org/10.1016/j.carbpol.2003.07.009.

[71] M. Másson, The quantitative molecular weight-antimicrobial activity relationship for chitosan polymers, oligomers, and derivatives, Carbohydr Polym 337 (2024) 122159. https://doi.org/10.1016/j.carbpol.2024.122159.

[72] C. Alburquenque, S.A. Bucarey, A. Neira-Carrillo, B. Urzúa, G. Hermosilla, C. V Tapia, Antifungal activity of low molecular weight chitosan against clinical isolates of Candida spp., Med Mycol 48 (2010) 1018–1023. https://doi.org/10.3109/13693786.2010.486412.

[73] Y. Mei, X. Dai, W. Yang, X. Xu, Y. Liang, Antifungal activity of chitooligosaccharides against the dermatophyte Trichophyton rubrum, Int J Biol Macromol 77 (2015) 330–335. https://doi.org/10.1016/j.ijbiomac.2015.03.042.

[74] S.N. Chirkov, The Antiviral Activity of Chitosan (Review), Appl Biochem Microbiol 38 (2002) 1–8. https://doi.org/10.1023/A:1013206517442.

[75] H. Van der Weken, E. Cox, B. Devriendt, Advances in oral subunit vaccine design, Vaccines (Basel) 9 (2020) 1. https://doi.org/10.3390/vaccines9010001.

[76] Ö.V. Rúnarsson, J. Holappa, T. Nevalainen, M. Hjálmarsdóttir, T. Järvinen, T. Loftsson, J.M. Einarsson, S. Jónsdóttir, M. Valdimarsdóttir, M. Másson, Antibacterial activity of methylated chitosan and chitooligomer derivatives: Synthesis and structure activity relationships, Eur Polym J 43 (2007) 2660–2671. https://doi.org/10.1016/j.eurpolymj.2007.03.046.

[77] A.F. Martins, S.P. Facchi, H.D.M. Follmann, A.G.B. Pereira, A.F. Rubira, E.C. Muniz, Antimicrobial activity of chitosan derivatives containing N-quaternized moieties in its backbone: a review, Int J Mol Sci 15 (2014) 20800–20832. https://doi.org/10.3390/ijms151120800.

[78] Z. Jia, W. Xu, Synthesis and antibacterial activities of quaternary ammonium salt of chitosan, Carbohydr Res 333 (2001) 1–6. https://doi.org/10.1016/S0008-6215(01)00112-4.

[79] S. Rathinam, S. Ólafsdóttir, S. Jónsdóttir, M.Á. Hjálmarsdóttir, M. Másson, Selective synthesis of N,N,N-trimethylated chitosan derivatives at different degree of substitution and investigation of structure-activity relationship for activity against P. aeruginosa and MRSA, Int J Biol Macromol 160 (2020) 548–557. https://doi.org/10.1016/j.ijbiomac.2020.05.109.

[80] Rathinam, Solodova, Kristjánsdóttir, Hjálmarsdóttir, Másson, The antibacterial structure-activity relationship for common chitosan derivatives, Int J Biol Macromol 165 (2020) 1686–1693. https://doi.org/10.1016/j.ijbiomac.2020.09.200.

[81] D.-S. Lee, J.-Y. Je, Gallic acid-grafted-chitosan inhibits foodborne pathogens by a membrane damage mechanism, J Agric Food Chem 61 (2013) 6574–6579. https://doi.org/10.1021/jf401254g.

[82] Y.S. Cho, D.S. Lee, Y.M. Kim, C.B. Ahn, D.H. Kim, W.K. Jung, J.Y. Je, Protection of Hepatic Cell Damage and Antimicrobial Evaluation of Chitosan-Catechin Conjugate, J Korean Soc Appl Biol Chem 56 (2013) 701–707. https://doi.org/10.1007/s13765-013-3168-8.

[83] D.S. Lee, J.Y. Woo, C.B. Ahn, J.Y. Je, Chitosan-hydroxycinnamic acid conjugates: preparation, antioxidant and antimicrobial activity, Food Chem 148 (2014) 97–104. https://doi.org/10.1016/j.foodchem.2013.10.019.

[84] K. Li, G. Guan, J. Zhu, H. Wu, Q. Sun, Antibacterial activity and mechanism of a laccase-catalyzed chitosan–gallic acid derivative against Escherichia coli and

Staphylococcus aureus, Food Control 96 (2019) 234–243. https://doi.org/10.1016/j.foodcont.2018.09.021.

[85] N.G.M. Schipper, K.M. Vårum, P. Artursson, Chitosans as absorption enhancers for poorly absorbable drugs. 1: Influence of molecular weight and degree of acetylation on drug transport across human intestinal epithelial (Caco-2) cells, Pharm Res 13 (1996) 1686–1692. https://doi.org/10.1023/A:1016444808000.

[86] T. Wijesekara, B. Xu, New Insights into Sources, Bioavailability, Health-Promoting Effects, and Applications of Chitin and Chitosan, J Agric Food Chem 72 (2024) 17138–17152. https://doi.org/10.1021/acs.jafc.4c02162.

[87] M. Huang, E. Khor, L.-Y. Lim, Uptake and Cytotoxicity of Chitosan Molecules and Nanoparticles: Effects of Molecular Weight and Degree of Deacetylation, Pharm Res 21 (2004) 344–353. https://doi.org/10.1023/B:PHAM.0000016249.52831.a5.

[88] A. Denuziere, D. Ferrier, O. Damour, A. Domard, Chitosan–chondroitin sulfate and chitosan–hyaluronate polyelectrolyte complexes: biological properties, Biomaterials 19 (1998) 1275–1285. https://doi.org/10.1016/S0142-9612(98)00036-2.

[89] Y.S. Wimardhani, D.F. Suniarti, H.J. Freisleben, S.I. Wanandi, N.C. Siregar, M.-A. Ikeda, Chitosan exerts anticancer activity through induction of apoptosis and cell cycle arrest in oral cancer cells, J Oral Sci 56 (2014) 119–126. https://doi.org/10.2334/josnusd.56.119.

[90] A.-M. Olaru, L. Marin, S. Morariu, G. Pricope, M. Pinteala, L. Tartau-Mititelu, Biocompatible chitosan based hydrogels for potential application in local tumour therapy, Carbohydr Polym 179 (2018) 59–70. https://doi.org/10.1016/j.carbpol.2017.09.066.

[91] M.M. Thanou, J.C. Verhoef, S.G. Romeijn, J.F. Nagelkerke, F.W.H.M. Merkus, H.E. Junginger, Effects of N-trimethyl chitosan chloride, a novel absorption enhancer, on Caco-2 intestinal epithelia and the ciliary beat frequency of chicken embryo trachea, Int J Pharm 185 (1999) 73–82. https://doi.org/10.1016/S0378-5173(99)00126-X.

[92] T. Kean, S. Roth, M. Thanou, Trimethylated chitosans as non-viral gene delivery vectors: cytotoxicity and transfection efficiency, Journal of Controlled Release 103 (2005) 643–653. https://doi.org/10.1016/j.jconrel.2005.01.001.

[93] R.J. Verheul, M. Amidi, S. van der Wal, E. van Riet, W. Jiskoot, W.E. Hennink, Synthesis, characterization and in vitro biological properties of O-methyl free

N,N,N-trimethylated chitosan, Biomaterials 29 (2008) 3642–3649. https://doi.org/10.1016/j.biomaterials.2008.05.026.

[94] A. Jintapattanakit, S. Mao, T. Kissel, V.B. Junyaprasert, Physicochemical properties and biocompatibility of N-trimethyl chitosan: Effect of quaternization and dimethylation, European Journal of Pharmaceutics and Biopharmaceutics 70 (2008) 563–571. https://doi.org/10.1016/j.ejpb.2008.06.002.

[95] S. Mao, X. Shuai, F. Unger, M. Wittmar, X. Xie, T. Kissel, Synthesis, characterization and cytotoxicity of poly(ethylene glycol)-graft-trimethyl chitosan block copolymers, Biomaterials 26 (2005) 6343–6356. https://doi.org/10.1016/j.biomaterials.2005.03.036.

[96] S. Borandeh, I. Laurén, A. Teotia, J. Niskanen, J. Seppälä, Dual functional quaternary chitosans with thermoresponsive behavior: structure–activity relationships in antibacterial activity and biocompatibility, J Mater Chem B 11 (2023) 11300–11309. https://doi.org/10.1039/D3TB02066E.

[97] T. Feng, Y. Du, J. Li, Y. Hu, J.F. Kennedy, Enhancement of antioxidant activity of chitosan by irradiation, Carbohydr Polym 73 (2008) 126–132. https://doi.org/10.1016/j.carbpol.2007.11.003.

[98] T. Sun, D. Zhou, J. Xie, F. Mao, Preparation of chitosan oligomers and their antioxidant activity, European Food Research and Technology 225 (2007) 451–456. https://doi.org/10.1007/s00217-006-0439-1.

[99] M.J. Moreno-Vasquez, E.L. Valenzuela-Buitimea, M. Plascencia-Jatomea, J.C. Encinas-Encinas, F. Rodriguez-Felix, S. Sanchez-Valdes, E.C. Rosas-Burgos, V.M. Ocano-Higuera, A.Z. Graciano-Verdugo, Functionalization of chitosan by a free radical reaction: Characterization, antioxidant and antibacterial potential, Carbohydr Polym 155 (2017) 117–127. https://doi.org/10.1016/j.carbpol.2016.08.056.

[100] S. Woranuch, R. Yoksan, Preparation, characterization and antioxidant property of water-soluble ferulic acid grafted chitosan, Carbohydr Polym 96 (2013) 495–502. https://doi.org/10.1016/j.carbpol.2013.04.006.

[101] T.-K. Eom, M. Senevirathne, S.-K. Kim, Synthesis of phenolic acid conjugated chitooligosaccharides and evaluation of their antioxidant activity, Environ Toxicol Pharmacol 34 (2012) 519–527. https://doi.org/10.1016/j.etap.2012.05.004.

[102] N.S. Chatterjee, S.K. Panda, M. Navitha, K.K. Asha, R. Anandan, S. Mathew, Vanillic acid and coumaric acid grafted chitosan derivatives: improved grafting ratio and potential application in functional food, J Food Sci Technol 52 (2015) 7153–7162. https://doi.org/10.1007/s13197-015-1874-4.

[103] H. İlyasoğlu, M. Nadzieja, Z. Guo, Caffeic acid grafted chitosan as a novel dual-functional stabilizer for food-grade emulsions and additive antioxidant property, Food Hydrocoll 95 (2019) 168–176. https://doi.org/10.1016/j.foodhyd.2019.04.043.

[104] A.K. Singla, M. Chawla, Chitosan: Some pharmaceutical and biological aspects-an update, Journal of Pharmacy and Pharmacology 53 (2001) 1047–1067. https://doi.org/10.1211/0022357011776441.

[105] M. Matthee, The codex alimentarius commission and its standards, (2007). https://doi.org/10.1007/978-90-6704-515-5.

[106] E. EFSA, European food safety authority, (2010).

[107] I. Wedmore, J.G. McManus, A.E. Pusateri, J.B. Holcomb, A special report on the chitosan-based hemostatic dressing: experience in current combat operations, Journal of Trauma and Acute Care Surgery 60 (2006) 655–658. https://doi.org/10.1097/01.ta.0000199392.91772.44.

[108] K. Food, D. Adminstration, Food additives code, (1995).

[109] M.N.V.R. Kumar, A review of chitin and chitosan applications, React Funct Polym 46 (2000) 1–27. https://doi.org/10.1016/S1381-5148(00)00038-9.

[110] Grand View Research, Chitosan market site, share & trends analysis report by application, (2022).

[111] W. Paul, C.P. Sharma, Chitosan and alginate wound dressings: a short review, Trends Biomater Artif Organs 18 (2004) 18–23.

[112] T. Dai, M. Tanaka, Y.-Y. Huang, M.R. Hamblin, Chitosan preparations for wounds and burns: antimicrobial and wound-healing effects, Expert Rev Anti Infect Ther 9 (2011) 857–879. https://doi.org/10.1586/eri.11.59.

[113] Y. Zhou, H. Yang, X. Liu, J. Mao, S. Gu, W. Xu, Potential of quaternization-functionalized chitosan fiber for wound dressing, Int J Biol Macromol 52 (2013) 327–332. https://doi.org/10.1016/j.ijbiomac.2012.10.012.

[114] R. Jayakumar, M. Prabaharan, S. V Nair, H. Tamura, Novel chitin and chitosan nanofibers in biomedical applications, Biotechnol Adv 28 (2010) 142–150. https://doi.org/10.1016/j.biotechadv.2009.11.001.

[115] L. Marin, B.-I. Andreica, A. Anisiei, S. Cibotaru, M. Bardosova, E.M. Materon, O.N. Oliveira, Quaternized chitosan (nano)fibers: A journey from preparation to high performance applications, Int J Biol Macromol 242 (2023) 125136. https://doi.org/10.1016/j.ijbiomac.2023.125136.

[116] H. Tamura, T. Furuike, S. V Nair, R. Jayakumar, Biomedical applications of chitin hydrogel membranes and scaffolds, Carbohydr Polym 84 (2011) 820–824. https://doi.org/10.1016/j.carbpol.2010.06.001.

[117] Y. Luo, L. Cui, L. Zou, Y. Zhao, L. Chen, Y. Guan, Y. Zhang, Mechanically strong and on-demand dissoluble chitosan hydrogels for wound dressing applications, Carbohydr Polym 294 (2022) 119774. https://doi.org/10.1016/j.carbpol.2022.119774.

[118] M.-M. Iftime, S. Morariu, L. Marin, Salicyl-imine-chitosan hydrogels: Supramolecular architecturing as a crosslinking method toward multifunctional hydrogels, Carbohydr Polym 165 (2017) 39–50. https://doi.org/10.1016/j.carbpol.2017.02.027.

[119] R. Lungu, M.-A. Paun, D. Peptanariu, D. Ailincai, L. Marin, M.-V. Nichita, V.-A. Paun, V.-P. Paun, Biocompatible Chitosan-Based Hydrogels for Bioabsorbable Wound Dressings, Gels 8 (2022). https://doi.org/10.3390/gels8020107.

[120] R. Augustine, S.R.U. Rehman, R. Ahmed, A.A. Zahid, M. Sharifi, M. Falahati, A. Hasan, Electrospun chitosan membranes containing bioactive and therapeutic agents for enhanced wound healing, Int J Biol Macromol 156 (2020) 153–170. https://doi.org/10.1016/j.ijbiomac.2020.03.207.

[121] M.N. Kantak, S.S. Bharate, Analysis of clinical trials on biomaterial and therapeutic applications of chitosan: A review, Carbohydr Polym 278 (2022) 118999. https://doi.org/10.1016/j.carbpol.2021.118999.

[122] R. Jayakumar, M. Prabaharan, P.T. Sudheesh Kumar, S. V Nair, H. Tamura, Biomaterials based on chitin and chitosan in wound dressing applications, Biotechnol Adv 29 (2011) 322–337. https://doi.org/10.1016/j.biotechadv.2011.01.005.

[123] S.-I. Ahn, S. Cho, N.-J. Choi, Effectiveness of Chitosan as a Dietary Supplement in Lowering Cholesterol in Murine Models: A Meta-Analysis, Mar Drugs 19 (2021). https://doi.org/10.3390/md19010026.

[124] O. Kanauchi, K. Deuchi, Y. Imasato, M. Shizukuishi, E. Kobayashi, Mechanism for the inhibition of fat digestion by chitosan and for the synergistic effect of ascorbate, Biosci Biotechnol Biochem 59 (1995) 786–790. https://doi.org/10.1271/bbb.59.786.

[125] Q. Jin, H. Yu, P. Li, The evaluation and utilization of marine-derived bioactive compounds with anti-obesity effect, Curr Med Chem 25 (2018) 861–878. https://doi.org/10.2174/0929867324666170602082620.

[126] H.L. Lauzon, G.H. Kristjánsdóttir, V. Árnadóttir, Fat-binding affinity of LipoSan Ultra® a chitosan fibre to promote health, (n.d.).

[127] F. Allaert, C. Melero, CO-42: Observational study of the effect of substituting NaCl with NaCl+ chitosan 3% (Symbiosal®) in the diet of elderly subjects on their blood pressure values, Ann Cardiol Angeiol (Paris) 64 (2015) S19. https://doi.org/10.1016/S0003-3928(16)30042-7.

[128] S. Navarro, US Environmental Health Effects and Treatment of Mercury Exposure, (2006).

[129] I. Aranaz, M. Mengíbar, R. Harris, I. Paños, B. Miralles, N. Acosta, G. Galed, Á. Heras, Functional characterization of chitin and chitosan, Curr Chem Biol 3 (2009) 203–230. https://doi.org/10.2174/187231309788166415.

[130] A.K. Singh, Engineered nanoparticles: structure, properties and mechanisms of toxicity, Academic Press, 2015. https://doi.org/10.1016/C2013-0-18974-X.

[131] M. Nurunnabi, V. Revuri, K.M. Huh, Y. Lee, Polysaccharide based nano/microformulation: An effective and versatile oral drug delivery system, in: Nanostructures for Oral Medicine, Elsevier, 2017: pp. 409–433. https://doi.org/10.1016/B978-0-323-47720-8.00015-8.

[132] Z. Liu, Y. Jiao, Y. Wang, C. Zhou, Z. Zhang, Polysaccharides-based nanoparticles as drug delivery systems, Adv Drug Deliv Rev 60 (2008) 1650–1662. https://doi.org/10.1016/j.addr.2008.09.001.

[133] A.D. Kulkarni, H.M. Patel, S.J. Surana, Y.H. Vanjari, V.S. Belgamwar, C. V Pardeshi, N,N,N-Trimethyl chitosan: An advanced polymer with myriad of opportunities in nanomedicine, Carbohydr Polym 157 (2017) 875–902. https://doi.org/10.1016/j.carbpol.2016.10.041.

[134] M. Amidi, E. Mastrobattista, W. Jiskoot, W.E. Hennink, Chitosan-based delivery systems for protein therapeutics and antigens, Adv Drug Deliv Rev 62 (2010) 59–82. https://doi.org/10.1016/j.addr.2009.11.009.

[135] A.M. de Campos, Y. Diebold, E.L.S. Carvalho, A. Sánchez, M. José Alonso, Chitosan nanoparticles as new ocular drug delivery systems: in vitro stability, in vivo fate, and cellular toxicity, Pharm Res 21 (2004) 803–810. https://doi.org/10.1023/B:PHAM.0000026432.75781.cb.

[136] B. Shah, D. Khunt, M. Misra, H. Padh, "Application of Box-Behnken design for optimization and development of quetiapine fumarate loaded chitosan nanoparticles for brain delivery via intranasal route* ," Int J Biol Macromol 89 (2016) 206–218. https://doi.org/10.1016/j.ijbiomac.2016.04.076.

[137] K. Zhao, Y. Zhang, X. Zhang, W. Li, C. Shi, C. Guo, C. Dai, Q. Chen, Z. Jin, Y. Zhao, Preparation and efficacy of Newcastle disease virus DNA vaccine encapsulated in chitosan nanoparticles, Int J Nanomedicine (2014) 389–402. https://doi.org/10.2147/IJN.S54226.

[138] E. Rostami, Progresses in targeted drug delivery systems using chitosan nanoparticles in cancer therapy: A mini-review, J Drug Deliv Sci Technol 58 (2020) 101813. https://doi.org/10.1016/j.jddst.2020.101813.

[139] J.-J. Cheng, J. Zhu, X.-S. Liu, D.-N. He, J.-R. Xu, L.-M. Wu, J. Zhou, Q. Feng, Gadolinium-chitosan nanoparticles as a novel contrast agent for potential use in clinical bowel-targeted MRI: a feasibility study in healthy rats, Acta Radiol 53 (2012) 900–907. https://doi.org/10.1258/ar.2012.110017.

[140] M. Thanou, J.C. Verhoef, H.E. Junginger, Oral drug absorption enhancement by chitosan and its derivatives, Adv Drug Deliv Rev 52 (2001) 117–126. https://doi.org/10.1016/S0169-409X(01)00231-9.

[141] A.M.M. Sadeghi, F.A. Dorkoosh, M.R. Avadi, P. Saadat, M. Rafiee-Tehrani, H.E. Junginger, Preparation, characterization and antibacterial activities of chitosan, N-trimethyl chitosan (TMC) and N-diethylmethyl chitosan (DEMC) nanoparticles loaded with insulin using both the ionotropic gelation and polyelectrolyte complexation methods, Int J Pharm 355 (2008) 299–306. https://doi.org/10.1016/j.ijpharm.2007.11.052.

[142] S. Cafaggi, E. Russo, R. Stefani, B. Parodi, G. Caviglioli, G. Sillo, A. Bisio, C. Aiello, M. Viale, Preparation, characterisation and preliminary antitumour activity evaluation of a novel nanoparticulate system based on a cisplatin-hyaluronate complex and N-trimethyl chitosan, Invest New Drugs 29 (2011) 443–455. https://doi.org/10.1007/s10637-009-9373-y.

[143] S.P. Facchi, D.B. Scariot, P.V.A. Bueno, P.R. Souza, L.C. Figueiredo, H.D.M. Follmann, C.S. Nunes, J.P. Monteiro, E.G. Bonafé, C. V Nakamura, Preparation and cytotoxicity of N-modified chitosan nanoparticles applied in curcumin delivery, Int J Biol Macromol 87 (2016) 237–245. https://doi.org/10.1016/j.ijbiomac.2016.02.063.

[144] R.-F. Song, X.-J. Li, X.-L. Cheng, A.-R. Fu, Y.-H. Wang, Y.-J. Feng, Y. Xiong, Paclitaxel-loaded trimethyl chitosan-based polymeric nanoparticle for the effective treatment of gastroenteric tumors, Oncol Rep 32 (2014) 1481–1488. https://doi.org/10.3892/or.2014.3344.

[145] M. Guan, Y. Zhou, Q.-L. Zhu, Y. Liu, Y.-Y. Bei, X.-N. Zhang, Q. Zhang, N-trimethyl chitosan nanoparticle-encapsulated lactosyl-norcantharidin for liver

cancer therapy with high targeting efficacy, Nanomedicine 8 (2012) 1172–1181. https://doi.org/10.1016/j.nano.2012.01.009.

[146] Z.-J. Huang, N. Yang, T.-W. Xu, J.-Q. Lin, Antitumor efficacy of docetaxel-loaded nanocarrier against esophageal cancer cell bearing mice model, Drug Res (2014) 403–409. https://doi.org/10.1055/s-0034-1385907.

[147] M. Amidi, S.G. Romeijn, G. Borchard, H.E. Junginger, W.E. Hennink, W. Jiskoot, Preparation and characterization of protein-loaded N-trimethyl chitosan nanoparticles as nasal delivery system, Journal of Controlled Release 111 (2006) 107–116. https://doi.org/10.1016/j.jconrel.2005.11.014.

[148] I.E. Elkholi, N.M. Hazem, W.F. ElKashef, M.A. Sobh, D. Shaalan, M. Sobh, I.M. El-Sherbiny, Evaluation of anti-cancer potential of capsaicin-loaded trimethyl chitosan-based nanoparticles in HepG2 hepatocarcinoma cells, J. Nanomed. Nanotechnol 5 (2014) 10.4172. https://doi.org/10.4172/2157-7439.1000240.

[149] Y. Yan, Y. Sun, P. Wang, R. Zhang, C. Huo, T. Gao, C. Song, J. Xing, Y. Dong, Mucoadhesive nanoparticles-based oral drug delivery systems enhance ameliorative effects of low molecular weight heparin on experimental colitis, Carbohydr Polym 246 (2020) 116660. https://doi.org/10.1016/j.carbpol.2020.116660.

[150] R. Sharma, K. Kuche, P. Thakor, V. Bhavana, S. Srivastava, N.K. Mehra, S. Jain, Chondroitin Sulfate: Emerging biomaterial for biopharmaceutical purpose and tissue engineering, Carbohydr Polym 286 (2022) 119305. https://doi.org/10.1016/j.carbpol.2022.119305.

[151] J. Egea, A.G. García, J. Verges, E. Montell, M.G. López, Antioxidant, antiinflammatory and neuroprotective actions of chondroitin sulfate and proteoglycans, Osteoarthritis Cartilage 18 (2010) S24–S27. https://doi.org/10.1016/j.joca.2010.01.016.

[152] M.A.S. Abourehab, S. Baisakhiya, A. Aggarwal, A. Singh, M.A. Abdelgawad, A. Deepak, M.J. Ansari, S. Pramanik, Chondroitin sulfate-based composites: a tour d'horizon of their biomedical applications, J Mater Chem B 10 (2022) 9125–9178. https://doi.org/10.1039/D2TB01514E.

[153] P.-X. Gong, Y.-C. Wu, X. Chen, Z.-L. Zhou, X. Chen, S.-Z. Lv, Y. You, H.-J. %J C.P. Li, Immunological effect of fucosylated chondroitin sulfate and its oligomers from Holothuria fuscogilva on RAW 264.7 cells, 287 (2022) 119362. https://doi.org/10.1016/j.carbpol.2022.119362.

[154] A. Rani, R. Baruah, A. Goyal, Prebiotic Chondroitin Sulfate Disaccharide Isolated from Chicken Keel Bone Exhibiting Anticancer Potential Against Human

Colon Cancer Cells, Nutr Cancer 71 (2019) 825–839. https://doi.org/10.1080/01635581.2018.1521446.

[155] J. Young, C. Chen, Y. Chen, K. Cheng, H.-J. Yen, Y. Huang, T.-N. %J C. polymers Tsai, Positively and negatively surface-charged chondroitin sulfate-trimethylchitosan nanoparticles as protein carriers, 137 (2016) 532–540. https://doi.org/10.1016/j.carbpol.2015.10.095.

[156] J.K. Francis Suh, H.W.T. Matthew, Application of chitosan-based polysaccharide biomaterials in cartilage tissue engineering: a review, Biomaterials 21 (2000) 2589–2598. https://doi.org/10.1016/S0142-9612(00)00126-5.

[157] M. Fermani, V. Platania, R.-M. Kavasi, C. Karavasili, P. Zgouro, D. Fatouros, M. Chatzinikolaidou, N. Bouropoulos, 3D-printed scaffolds from alginate/methyl cellulose/trimethyl chitosan/silicate glasses for bone tissue engineering, Applied Sciences 11 (2021) 8677. https://doi.org/10.3390/app11188677.

[158] S. Deepthi, J. Venkatesan, S.K. Kim, J.D. Bumgardner, R. Jayakumar, An overview of chitin or chitosan/nano ceramic composite scaffolds for bone tissue engineering, Int J Biol Macromol 93 (2016) 1338–1353. https://doi.org/10.1016/j.ijbiomac.2016.03.041.

[159] A. Ressler, Chitosan-Based Biomaterials for Bone Tissue Engineering Applications: A Short Review, Polymers (Basel) 14 (2022). https://doi.org/10.3390/polym14163430.

[160] L.R. Yadav, S.V. Chandran, K. Lavanya, N. Selvamurugan, Chitosan-based 3D-printed scaffolds for bone tissue engineering, Int J Biol Macromol 183 (2021) 1925–1938. https://doi.org/10.1016/j.ijbiomac.2021.05.215.

[161] M. Taghizadeh, A. Taghizadeh, M.K. Yazdi, P. Zarrintaj, F.J. Stadler, J.D. Ramsey, S. Habibzadeh, S.H. Rad, G. Naderi, M.R. Saeb, Chitosan-based inks for 3D printing and bioprinting, Green Chemistry 24 (2022) 62–101. https://doi.org/10.1039/D1GC01799C.

[162] I. Aranaz, N. Acosta, C. Civera, B. Elorza, J. Mingo, C. Castro, M.D.L.L. Gandía, A. Heras Caballero, Cosmetics and cosmeceutical applications of chitin, chitosan and their derivatives, Polymers (Basel) 10 (2018) 213. https://doi.org/10.3390/polym10020213.

[163] P.K. Dutta, J. Dutta, V.S. Tripathi, Chitin and chitosan: Chemistry, properties and applications, (2004).

[164] C. Casadidio, D.V. Peregrina, M.R. Gigliobianco, S. Deng, R. Censi, P. Di Martino, Chitin and chitosans: Characteristics, eco-friendly processes, and

applications in cosmetic science, Mar Drugs 17 (2019) 369. https://doi.org/10.3390/md17060369.

[165] P. Pandey, M.K. Verma, N. De, Chitosan in agricultural context-A review, Bull. Environ. Pharmacol. Life Sci 7 (2018) 87–96.

[166] K. Xing, X. Zhu, X. Peng, S. Qin, Chitosan antimicrobial and eliciting properties for pest control in agriculture: a review, Agron Sustain Dev 35 (2015) 569–588. https://doi.org/10.1007/s13593-014-0252-3.

[167] R.S. Riseh, M. Hassanisaadi, M. Vatankhah, S.A. Babaki, E.A. Barka, Chitosan as a potential natural compound to manage plant diseases, Int J Biol Macromol 220 (2022) 998–1009. https://doi.org/10.1016/j.ijbiomac.2022.08.109.

[168] M. Malerba, R. Cerana, Chitin-and chitosan-based derivatives in plant protection against biotic and abiotic stresses and in recovery of contaminated soil and water, Polysaccharides 1 (2020) 21–30. https://doi.org/10.3390/polysaccharides1010003.

[169] M.A. Abd-Elhakeem, T.A. Alkhulaqi, Simple, rapid and efficient water purification by chitosan coated magnetite nanoparticles, J. Environ. Nanotechnol 3 (2014) 17–20. https://doi.org/10.13074/jent.2014.12.143131.

[170] B.S. Butola, Recent advances in chitosan polysaccharide and its derivatives in antimicrobial modification of textile materials, Int J Biol Macromol 121 (2019) 905–912. https://doi.org/10.1016/j.ijbiomac.2018.10.102.

[171] K. Kurita, H. Ikeda, Y. Yoshida, M. Shimojoh, M. Harata, Chemoselective protection of the amino groups of chitosan by controlled phthaloylation: facile preparation of a precursor useful for chemical modifications, Biomacromolecules 3 (2002) 1–4. https://doi.org/10.1021/bm0101163.

[172] S. Nishimura, O. Kohgo, K. Kurita, H. Kuzuhara, Chemospecific manipulations of a rigid polysaccharide: syntheses of novel chitosan derivatives with excellent solubility in common organic solvents by regioselective chemical modifications, Macromolecules 24 (1991) 4745–4748. https://doi.org/10.1021/ma00017a003.

[173] J. Holappa, T. Nevalainen, J. Savolainen, P. Soininen, M. Elomaa, R. Safin, S. Suvanto, T. Pakkanen, M. Masson, T. Loftsson, Synthesis and characterization of chitosan N-betainates having various degrees of substitution, Macromolecules 37 (2004) 2784–2789. https://doi.org/10.1021/ma0358780.

[174] K. Kurita, M. Hirakawa, Y. Nishiyama, Silylated chitin: A new organosoluble precursor for facile modifications and film casting, Chem Lett 28 (1999) 771–772. https://doi.org/10.1246/cl.1999.771.

[175] Ö.V. Rúnarsson, J. Holappa, S. Jónsdóttir, H. Steinsson, M. Másson, N-selective 'one pot' synthesis of highly N-substituted trimethyl chitosan (TMC), Carbohydr Polym 74 (2008) 740–744. https://doi.org/10.1016/j.carbpol.2008.03.008.

[176] Ö.V. Rúnarsson, C. Malainer, J. Holappa, S.T. Sigurdsson, M. Másson, tert-Butyldimethylsilyl O-protected chitosan and chitooligosaccharides: useful precursors for N-modifications in common organic solvents, Carbohydr Res 343 (2008) 2576–2582. https://doi.org/10.1016/j.carres.2008.08.014.

[177] A. Domard, M. Rinaudo, C. Terrassin, New method for the quaternization of chitosan, Int J Biol Macromol 8 (1986) 105–107. https://doi.org/10.1016/0141-8130(86)90007-3.

[178] A.B. Sieval, M. Thanou, A.F. Kotze, J.C. Verhoef, J. Brussee, H.E. Junginger, Preparation and NMR characterization of highly substituted N-trimethyl chitosan chloride, Carbohydr Polym 36 (1998) 157–165. https://doi.org/10.1016/S0144-8617(98)00009-5.

[179] B. Benediktsdóttir Ólafur, M. Másson, Challenges in evaluation of chitosan and trimethylated chitosan (TMC) as mucosal permeation enhancers: From synthesis to in vitro application, Journal of Controlled Release 173 (2014) 18–31. https://doi.org/10.1016/j.jconrel.2013.10.022.

[180] Y. Kang, Z. Liu, Y. Long, B. Wang, X. Yang, D. Sha, K. Shi, X. Ji, B. Li, Y. Liu, Synthesis and structural characterization of N, N, N-trimethyl chitosan, J Appl Polym Sci 138 (2021) 51811. https://doi.org/10.1002/app.51811.

[181] Benediktsdóttir, V.S. Gaware, Ö. V Rúnarsson, S. Jónsdóttir, K.J. Jensen, M. Másson, Synthesis of N,N,N-trimethyl chitosan homopolymer and highly substituted N-alkyl-N,N-dimethyl chitosan derivatives with the aid of di-tert-butyldimethylsilyl chitosan, Carbohydr Polym 86 (2011) 1451–1460. https://doi.org/10.1016/j.carbpol.2011.06.007.

[182] D. de Britto, O.B.G. Assis, A novel method for obtaining a quaternary salt of chitosan, Carbohydr Polym 69 (2007) 305–310. https://doi.org/10.1016/j.carbpol.2006.10.007.

[183] M. Wu, Z. Long, H. Xiao, C. Dong, Preparation of N, N, N-trimethyl chitosan via a novel approach using dimethyl carbonate, Carbohydr Polym 169 (2017) 83–91. https://doi.org/10.1016/j.carbpol.2017.03.043.

[184] J. Cao, J. You, L. Zhang, J. Zhou, Homogeneous synthesis and characterization of chitosan ethers prepared in aqueous alkali/urea solutions, Carbohydr Polym 185 (2018) 138–144. https://doi.org/10.1016/j.carbpol.2018.01.010.

[185] T. Mahajan, P. Bangde, P. Dandekar, R. Jain, Greener approach for synthesis of N, N, N-trimethyl chitosan (TMC) using ternary deep eutectic solvents (TDESs), Carbohydr Res 493 (2020) 108033. https://doi.org/10.1016/j.carres.2020.108033.

[186] Y. Gao, Z. Zhang, L. Chen, W. Gu, Y. Li, Chitosan N-betainates/DNA self-assembly nanoparticles for gene delivery: In vitro uptake and transfection efficiency, Int J Pharm 371 (2009) 156–162. https://doi.org/10.1016/j.ijpharm.2008.12.012.

[187] E.A. Stepnova, V.E. Tikhonov, T.A. Babushkina, T.P. Klimova, E. V Vorontsov, V.G. Babak, S.A. Lopatin, I.A. Yamskov, New approach to the quaternization of chitosan and its amphiphilic derivatives, Eur Polym J 43 (2007) 2414–2421. https://doi.org/10.1016/j.eurpolymj.2007.02.028.

[188] L. Zhang, H. Sheng, R. Liu, M. Yang, Y. Guo, Q. Xu, L. Hu, S. Liang, H. Xie, Engineering chitosan into fully bio-sourced, water-soluble and enhanced antibacterial poly(aprotic/protic ionic liquid)s packaging membrane, Int J Biol Macromol 230 (2023) 123182. https://doi.org/10.1016/j.ijbiomac.2023.123182.

[189] P. Deemak, S. Wanichwecharungruang, R. Nonthabenjawan, C. Jornjangjun, Controlling the morphology of self-assemble chitosan through derivatization, Journal of Polymer Research 18 (2011) 419–424. https://doi.org/10.1007/s10965-010-9432-2.

[190] T.-K. Eom, B. Ryu, J.-K. Lee, H.-G. Byun, S.-J. Park, S.-K. Kim, β-secretase inhibitory activity of phenolic acid conjugated chitooligosaccharides, J Enzyme Inhib Med Chem 28 (2013) 214–217. https://doi.org/10.3109/14756366.2011.629197.

[191] G.-B. Jiang, Z.-T. Lin, X.-J. Xu, Z. Hai, K. Song, Stable nanomicelles based on chitosan derivative: In vitro antiplatelet aggregation and adhesion properties, Carbohydr Polym 88 (2012) 232–238. https://doi.org/10.1016/j.carbpol.2011.11.089.

[192] M. Božič, S. Gorgieva, V. Kokol, Laccase-mediated functionalization of chitosan by caffeic and gallic acids for modulating antioxidant and antimicrobial properties, Carbohydr Polym 87 (2012) 2388–2398. https://doi.org/10.1016/j.carbpol.2011.11.006.

[193] G. Kumar, P.J. Smith, G.F. Payne, Enzymatic grafting of a natural product onto chitosan to confer water solubility under basic conditions, Biotechnol Bioeng 63 (1999) 154–165. https://doi.org/10.1002/(SICI)1097-0290(19990420)63:2<154::AID-BIT4>3.0.CO;2-R.

[194] W. Pasanphan, G.R. Buettner, S. Chirachanchai, Chitosan gallate as a novel potential polysaccharide antioxidant: an EPR study, Carbohydr Res 345 (2010) 132–140. https://doi.org/10.1016/j.carres.2009.09.038.

[195] G.A. Mun, Z.S. Nurkeeva, S.A. Dergunov, I.K. Nam, T.P. Maimakov, E.M. Shaikhutdinov, S.C. Lee, K. Park, Studies on graft copolymerization of 2-hydroxyethyl acrylate onto chitosan, React Funct Polym 68 (2008) 389–395. https://doi.org/10.1016/j.reactfunctpolym.2007.07.012.

[196] M. Curcio, F. Puoci, F. Iemma, O.I. Parisi, G. Cirillo, U.G. Spizzirri, N. Picci, Covalent insertion of antioxidant molecules on chitosan by a free radical grafting procedure, J Agric Food Chem 57 (2009) 5933–5938. https://doi.org/10.1021/jf900778u.

[197] J. Liu, X. Wen, J. Lu, J. Kan, C. Jin, Free radical mediated grafting of chitosan with caffeic and ferulic acids: structures and antioxidant activity, Int J Biol Macromol 65 (2014) 97–106. https://doi.org/10.1016/j.ijbiomac.2014.01.021.

[198] Q. Li, Y. Mi, W. Tan, Z. Guo, Highly efficient free radical-scavenging property of phenolic-functionalized chitosan derivatives: Chemical modification and activity assessment, Int J Biol Macromol 164 (2020) 4279–4288. https://doi.org/10.1016/j.ijbiomac.2020.08.250.

[199] V. Nagy, M. Másson, Chitosan–Antioxidant Conjugates, 2 (2020) 1031–1050. https://doi.org/10.1002/9781119143802.ch40.

[200] A. Aljawish, I. Chevalot, B. Piffaut, C. Rondeau-Mouro, M. Girardin, J. Jasniewski, J. Scher, L. Muniglia, Functionalization of chitosan by laccase-catalyzed oxidation of ferulic acid and ethyl ferulate under heterogeneous reaction conditions, Carbohydr Polym 87 (2012) 537–544. https://doi.org/10.1016/j.carbpol.2011.08.016.

[201] V.L. Anderson, R.A. McLean, Design of experiments: a realistic approach, Routledge, 2018. https://doi.org/10.1201/9781315141039.

[202] A.S. Dhoot, G.J. Fernandes, A. Naha, M. Rathnanand, L. Kumar, Design of Experiments in Pharmaceutical Development, 53 (2019) 730–735. https://doi.org/10.1007/s11094-019-02070-4.

[203] T. Lundstedt, E. Seifert, L. Abramo, B. Thelin, Å. Nyström, J. Pettersen, R. Bergman, Experimental design and optimization, Chemometrics and Intelligent Laboratory Systems 42 (1998) 3–40. https://doi.org/10.1016/S0169-7439(98)00065-3.

[204] U.A. Thorsteinsdóttir, M. Thorsteinsdóttir, Design of experiments for development and optimization of a liquid chromatography coupled to tandem mass spectrometry bioanalytical assay, 56 (2021) e4727. https://doi.org/10.1002/jms.4727.

[205] R. Mukerjee, C.F.J. Wu, A modern theory of factorial design, Springer Science & Business Media, 2007. https://doi.org/10.1007/0-387-37344-6.

[206] R.F. Gunst, R.L. Mason, Fractional factorial design, Wiley Interdiscip Rev Comput Stat 1 (2009) 234–244. https://doi.org/10.1002/wics.27.

[207] T.D.A. Senra, D.M. Santos, J. Desbrières, S.P. Campana-Filho, Extensive N-methylation of chitosan: evaluating the effects of the reaction conditions by using response surface methodology, Polym Int 64 (2015) 1617–1626. https://doi.org/10.1002/pi.4962.

[208] D. De Britto, F.R. Frederico, O.B. Garrido Assis, Optimization of N, N, N-trimethylchitosan synthesis by factorial design, 60 (2011) 910–915. https://doi.org/10.1002/pi.3038.

[209] A.L. Bukzem, R. Signini, D.M. dos Santos, L.M. Lião, D.P.R. Ascheri, Optimization of carboxymethyl chitosan synthesis using response surface methodology and desirability function, Int J Biol Macromol 85 (2016) 615–624. https://doi.org/10.1016/j.ijbiomac.2016.01.017.

[210] M. Kurniasih, P. Purwati, D. Hermawan, M. Zaki, Optimum conditions for the synthesis of high solubility carboxymethyl chitosan, Malaysian Journal of Fundamental and Applied Sciences 10 (2014). https://doi.org/10.11113/mjfas.v10n4.277.

[211] S.-D. Li, P.-W. Li, Z.-M. Yang, Z. Peng, W.-Y. Quan, X.-H. Yang, L. Yang, J.-J. Dong, Synthesis and characterization of chitosan quaternary ammonium salt and its application as drug carrier for ribavirin, Drug Deliv 21 (2014) 548–552. https://doi.org/10.3109/10717544.2013.853708.

[212] A. Bayat, A.M.M. Sadeghi, M.R. Avadi, M. Amini, M. Rafiee-Tehrani, A. Shafiee, R. Majlesi, H.E. Junginger, Synthesis of N, N-dimethyl N-ethyl chitosan as a carrier for oral delivery of peptide drugs, J Bioact Compat Polym 21 (2006) 433–444. https://doi.org/10.1177/088391150606867.

[213] M.R. Avadi, M. Erfan, A.M.M. Sadeghi, L. Moezi, A.R. Dehpour, P. Younessi, M.R. Tehrani, A. Shafiee, N, N-diethyl N-methyl chitosan as an enhancing agent for colon drug delivery, J Bioact Compat Polym 19 (2004) 421–433. https://doi.org/10.1177/0883911504046679.

[214] F. Li, C. Ding, Optimization of ultrasonic synthesis of N-succinyl-chitosan and adsorption of Zn2+ from aqueous solutions, Desalination Water Treat 52 (2014) 7856–7865. https://doi.org/10.1080/19443994.2013.833867.

[215] E. Curti, D. de Britto, S.P. Campana-Filho, Methylation of chitosan with iodomethane: effect of reaction conditions on chemoselectivity and degree of substitution, Macromol Biosci 3 (2003) 571–576. https://doi.org/10.1002/mabi.200300030.

[216] M100: Performance Standards for Antimicrobial Susceptability Testing, Clinical & Laboratory Standards Institute, 2021.

[217] M. Matsuno, A. Nagatsu, Y. Ogihara, H. Mizukami, Synthesis of 2-O-(4-coumaroyl)-3-(4-hydroxyphenyl) lactic acid, an important intermediate of rosmarinic acid biosynthesis, Chem Pharm Bull (Tokyo) 49 (2001) 1644–1646. https://doi.org/10.1248/cpb.49.1644.

[218] K. Okamoto, N. Hamada, T. Okamura, N. Ueyama, H. Yamamoto, B. Chemistry, Color regulation and stabilization of chromophore by Cys69 in photoactive yellow protein active center, 7 (2009) 3782–3791. https://doi.org/10.1039/B905835D.

[219] E.Ö. Viktorsson, M. Gabrielsen, N. Kumarachandran, I. Sylte, P. Rongved, O.A.H. Åstrand, E.T. Kase, Regulation of liver X receptor target genes by 22-functionalized oxysterols. Synthesis, in silico and in vitro evaluations, Steroids 118 (2017) 119–127. https://doi.org/10.1016/j.steroids.2016.12.003.

[220] V. Nagy, Chitosan-natural antioxidant conjugates: Synthesis, antimicrobial and antioxidant properties, University of Iceland, 2018.

[221] Sartorius, MODDE 12 User Guide, (2017).

[222] T. Dahiru, P - value, a true test of statistical significance? A cautionary note, Ann Ib Postgrad Med 6 (2008) 21–26. https://doi.org/10.4314/aipm.v6i1.64038.

[223] P. Le Dung, M. Milas, M. Rinaudo, J. Desbrières, Water soluble derivatives obtained by controlled chemical modifications of chitosan, Carbohydr Polym 24 (1994) 209–214. https://doi.org/10.1016/0144-8617(94)90132-5.

[224] A.B. Sieval, M. Thanou, A.F. Kotze´, J.C. Verhoef, J. Brussee, H.E. Junginger, Preparation and NMR characterization of highly substitutedN-trimethyl chitosan chloride, Carbohydr Polym 36 (1998) 157–165. https://doi.org/10.1016/S0144-8617(98)00009-5.

[225] Ö.V. Rúnarsson, J. Holappa, C. Malainer, H. Steinsson, M. Hjálmarsdóttir, T. Nevalainen, M. Másson, Antibacterial activity of N-quaternary chitosan derivatives: Synthesis, characterization and structure activity relationship (SAR)

investigations, Eur Polym J 46 (2010) 1251–1267.
https://doi.org/10.1016/j.eurpolymj.2010.03.001.

# Original Publications

# Paper I

# Paper II

# Paper III

# Paper IV